A SUPERELASTIC HELICOTOME

FOR CAPSULORHEXIS

by

Matthew Stephen Cavilla

A thesis submitted to the faculty of
The University of Utah
in partial fulfillment of the requirements for the degree of

Master of Science

Department of Mechanical Engineering

The University of Utah

May 2016

The University of Utah Graduate School

STATEMENT OF THESIS APPROVAL

The thesis of **Matthew Stephen Cavilla**

has been approved by the following supervisory committee members:

Bart Raeymaekers	, Chair	**2/7/2015**
		Date Approved
Jake Abbott	, Member	**2/11/2015**
		Date Approved
Balamurali Ambati	, Member	**2/7/2015**
		Date Approved

and by **Tim Ameel** , Chair/Dean of

the Department/College/School of **Mechanical Engineering**

and by David B. Kieda, Dean of The Graduate School.

ABSTRACT

We design and characterize a novel, single-use device to perform capsulorhexis, a critical step during cataract surgery, during which a 5 mm diameter incision is made in the anterior lens capsule. This device, the Helicotome, is a handheld tool based on a superelastic shape-memory-alloy blade to perform the circular incision in the lens capsule. The blade deploys into a helix shape within the eye through a cannula that is inserted into a small incision in the cornea. When pressed into the anterior lens capsule and retracted, the blade produces a nearly circular incision in the lens capsule.

The cut diameter and circularity of the prototype Helicotome capsulorhexis excisions are compared against manual and laser excisions performed in published studies. The prototype Helicotome deviates from a target excision diameter of 5 mm by 0.17 mm +/- 0.34 mm (mean +/- standard deviation) for 17 bovine capsulorhexis procedures, compared to the manual lens capsule excisions that deviate from the specified diameter of 5 mm by 0.337 mm +/- 0.258 mm for 18 manual procedures, and the laser-excised lens capsules that deviate from a specified diameter of 4.6 mm by 0.029 mm +/- 0.026 mm for 39 laser procedures. The prototype Helicotome produces a mean circularity of 0.83 +/- 0.06, the manual method achieves a mean circularity of 0.80 +/- 0.15, and the laser capsulorhexis procedures achieve a mean circularity of 0.94 +/- 0.15. The average procedure duration for all experiments performed with the prototype Helicotome blade is nearly 75% shorter than the average procedure duration of 120 seconds using the currently

available manual method. The prototype Helicotome yields a success rate of 30% in creating a full 360° capsulorhexis, and incomplete cuts can be completed manually.

The results obtained with the Helicotome are comparable to those provided by currently available methods, but the device is easier to use and reduces the time required to perform the procedure. However, future prototypes of the Helicotome should be scaled down to be deployed within the anterior chamber of the eye without contacting the posterior of the cornea, and should be modified to improve repeatability.

TABLE OF CONTENTS

LIST OF TABLES

ACKNOWLEDGEMENTS

The research team would like to extend their deepest appreciation and respect to the members of our advisory committee, Dr. Jake Abbott, Dr. Bart Raeymaekers, and Dr. Balamurali Ambati. Their dedication to scholarship and research will serve as an example to us for all of our future endeavors. Without their continual guidance and devotion this research would not have been possible.

We would also like to extend our sincere gratitude to Dr. Tomasz Petelenz, Dr. Robert Hitchcock, and Dan Wright, whose contributions included comprehensive instruction in the field of regulatory affairs, countless hours of encouragement, brainstorming, and design ideation, as well as providing us with a full laboratory and education on the many machines and processes made available to us. Again, this research would not have been possible without their participation.

Our families also deserve our heartfelt gratitude and affection for their support through the many long hours spent on this research. Their unfailing encouragement sustained us through the tough times and allowed us to see this project through to completion.

Finally, we would like to thank the University of Utah Technology and Commercialization Office for the financial support they provided.

CHAPTER 1

INTRODUCTION

Cataracts are the most common visual impairment and account for approximately 42% of all blindness worldwide. More than 50% of the population above the age of 80 is afflicted with cataracts [1]. There are approximately eleven million cataract surgeries performed each year around the world, roughly 3.5 million of which are completed in the United States [2]. As a result, cataract removal is one of the most common procedures performed today [3]. Figure 1.1 illustrates a cataract in a human eye. It is a clouding and discoloration of the lens that results in blurred vision. A cataract can be caused by adverse living conditions such as smoking, diabetes, or poor diet [2]. However, the most common cause for cataracts is simply the aging of the lens.

Figure 1.1: Comparison between a healthy eye (right) and one inflicted with cataract (left). Image modified from [4].

1.1 Anatomy of the Eye

Figure 1.2 displays the anatomy of the human eye. Incident light passes through the cornea into the anterior chamber. The iris dilates to control the amount of light allowed into the lens [5]. The lens is an ellipsoidal-shaped mass of water and proteins that focuses the incident light and projects the image on the posterior portion of the eye, which contains the sensory organs (i.e., the retina), which in turn detect and transmit the information to the brain for processing. The lens capsule is a small, bag-like membrane that ensconces the lens, and is primarily composed of a three-dimensional (3D) meshwork of triple-helix type IV collagen [6, 7, 8], shown in Fig. 1.3. The importance of the lens capsule is a topic of ongoing debate among the ophthalmological community due to its critical role in cataract removal [7].

The capsule, like most biological tissues, exhibits nonlinear, viscoelastic behavior [6]. At birth, the lens capsule is highly elastic and has a thickness of approximately 11 μm.

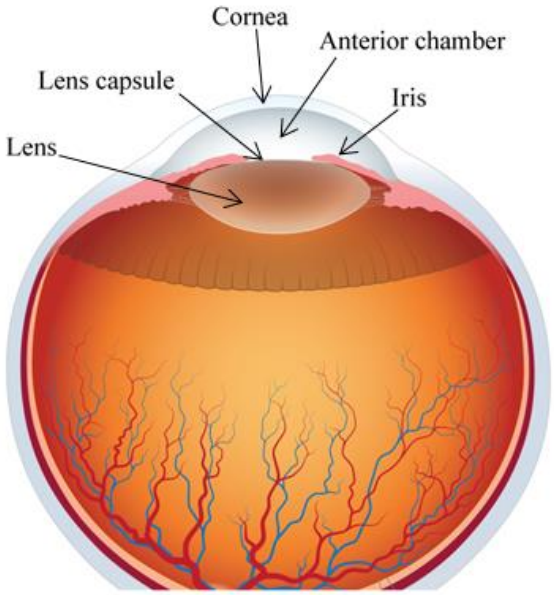

Figure 1.2: Anatomy of the anterior portion of the human eye. Image modified from [5].

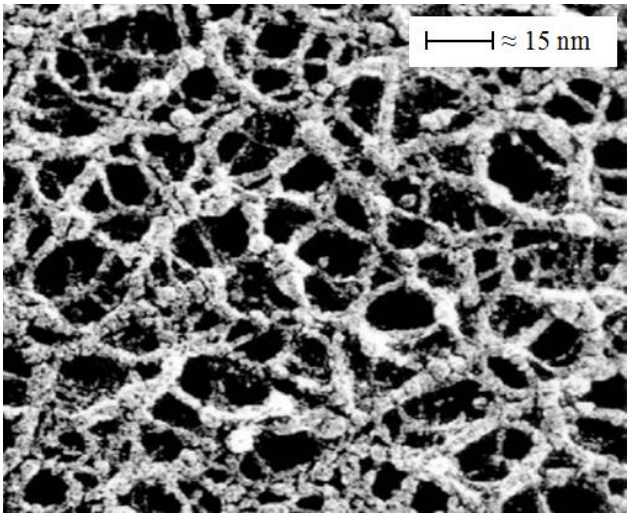

Figure 1.3: 3D meshwork of triple-helix, type IV collagen found in the lens capsule.
Image modified from [6].

With increasing age, the collagen in the body loses elasticity [6-8]. As a result, the lens capsule becomes less able to cope with mechanical stress, and the body compensates by increasing the capsule thickness. The capsule can grow as thick as 33 μm [6].

Figure 1.4 shows the age-dependence of the mechanical properties of the lens; Figure 1.4 A shows the load-deformation curve, and Fig. 1.4 B shows the stress-strain curve [6]. From Fig. 1.4, we observe that the relationship between load and deformation of the lens capsule is nonlinear and age-dependent. The deformation of the lens capsule for a constant load decreases with increasing age, because the lens capsule thickness increases. Thus, the use of linear-elastic models to interpret the mechanical response of the lens capsule tissue is likely not accurate.

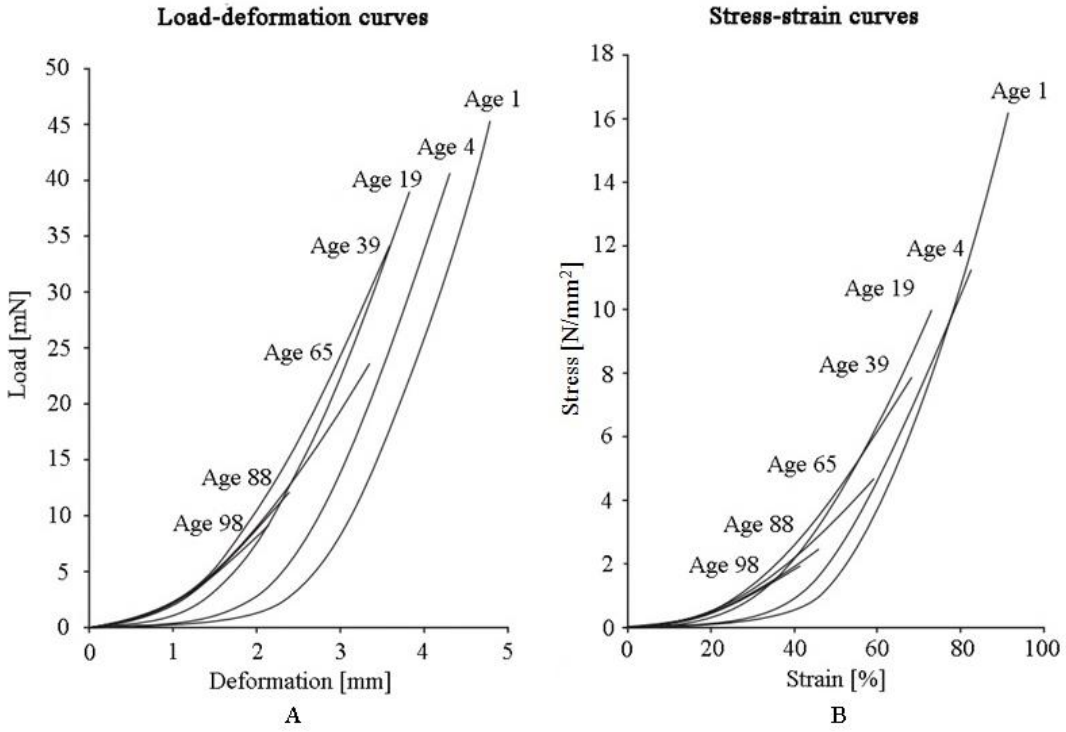

Figure 1.4: Age-dependence of the mechanical properties of the human lens capsule. Image modified from [6]; (A) load-deformation curve, (B) stress-strain curve.

1.2 The Capsulorhexis Procedure

Cataract extraction requires three critical steps: (1) accessing the cataract-afflicted lens, (2) removing the cataract from the eye, and (3) implanting the new, artificial intraocular lens in place of the cataract. Figure 1.5 shows the steps required to perform cataract surgery. To access the cataract, the iris is dilated, a small incision is made in the side of the cornea (Fig. 1.5 A), and the anterior portion of the lens capsule is removed (Fig. 1.5 B and C). To remove the cataract, a suction device is inserted into the incision in the cornea, and sucks out the cataract (Fig. 1.5 D, E, and F). Once the cataract is removed, an insertion tube is placed into the incision, and the new, artificial intraocular lens is implanted in place of the cataract-stricken lens (Fig, 1.5 G, H, and I). It is typically asserted that the

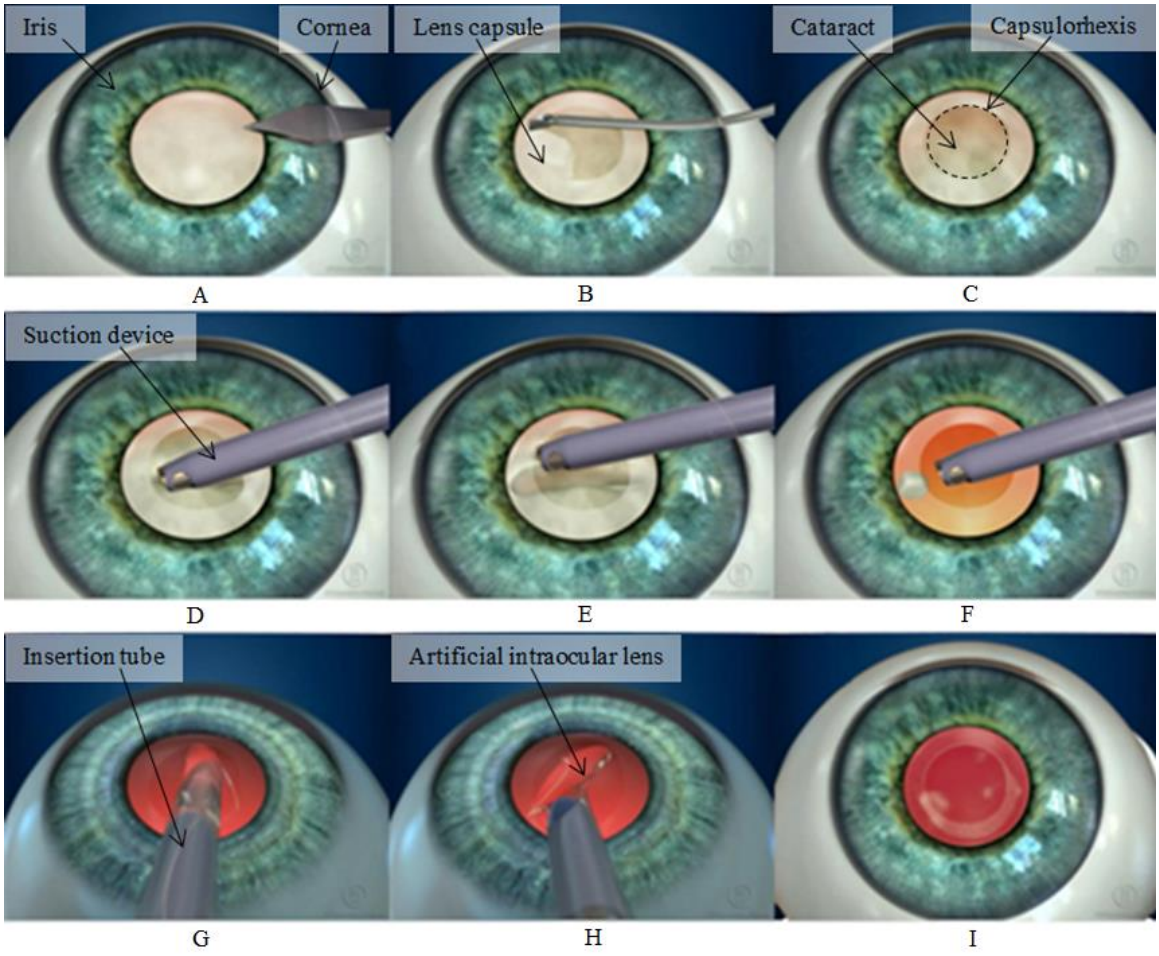

Figure 1.5: Cataract surgery steps. Image modified from [10].

portion of cataract surgery that proves to be most difficult is accessing the cataract [9], commonly referred to as capsulorhexis. Capsulorhexis is the process of making a circular cut, with a diameter of approximately five millimeters, in the anterior portion of the lens capsule, and removing the excised tissue (Fig. 1.5 B and C). This portion of the surgery is the most difficult due to the unstable structure of the lens capsule, and the high level of precision required to perform a successful capsulorhexis.

The lens capsule is tensioned in its in-vivo state, so a circular incision provides maximum stability for the remaining portion of the capsule. Additionally, making a 5- mm circle in the capsule gives sufficient room for safe implantation of the new, artificial lens

without compromising the remainder of the lens capsule. The variability of the mechanical properties of the lens capsule adds difficulty to the already challenging cataract removal procedure. Only two methods for cataract extraction are currently used in clinical practice, and the more common of the two methods involves a surgeon manually performing the incisions necessary to access the cataract, which we refer to here as the standard method. This method requires a skilled hand and can occasionally lead to excessive scarring, or tearing of the lens capsule due to an incomplete, or out-of-round circular cut. Such complications result in procedural failure and may render the lens capsule useless. Figure 1.6 shows examples of one successful (Fig. 1.6 A) and several common failed capsulorhexis procedures. The latter include a radial tear (Fig. 1.6 B), a spiral tear (Fig. 1.6 C), and an extended tangential tear (Fig. 1.6 D). Although complications are rare, only the more skilled ophthalmologists can perform this procedure. The average cost of a standard cataract surgery in the US in 2011 was $3,522 per eye [3].

The second clinical method does not involve a scalpel (i.e., "bladeless"), but rather, utilizes a laser to generate precise, near-perfect cuts. This method requires high-tech equipment that is expensive to acquire and operate. In addition, adverse side effects, such as scarring surrounding the cuts, or a lack of adhesion of the lens capsule to the artificial lens, can complicate the surgery. The average cost of laser-assisted cataract extraction in the US in 2011 was $4,587 per eye [3]. The difference in cost compared to the standard surgery may seem negligible, but the patient incurs a much greater cost for laser-assisted cataract surgery. According to the Department of Health and Human Services (Laser-Assisted Cataract Surgery and CMS Rulings 05-01 and 1536-R): "While traditional cataract surgery is fully covered by most private medical insurance and Medicare, bladeless

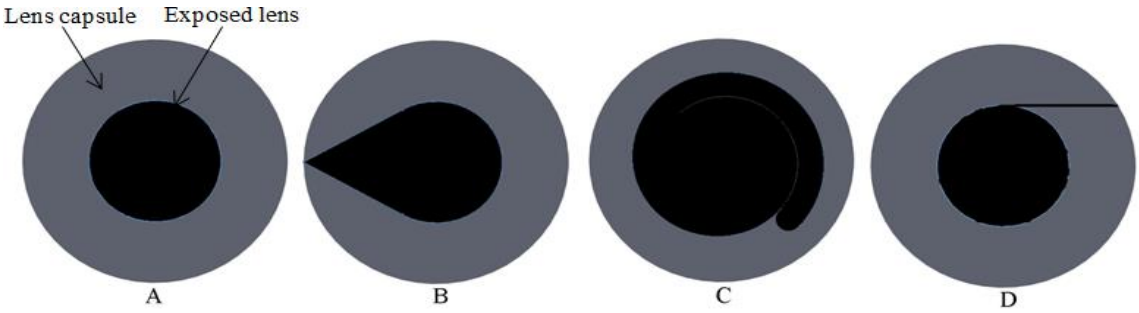

Figure 1.6: A successful capsulorhexis (A), a capsulorhexis with a radial tear (B), a capsulorhexis with a spiral tear (C), and a capsulorhexis with an extended tangential tear (D).

cataract surgery requires patients to pay out-of-pocket for the portion of the procedure that insurance does not cover." Hence, only a small subset of the population has access to bladeless cataract extraction. Additionally, since the majority of those afflicted with cataracts reside in developing nations, often coincident with poor living conditions and substandard healthcare, the cost of the laser and supporting equipment make access to this technology very difficult to obtain.

1.3 Problem Statement

The current methods used in cataract removal surgeries are optimal neither in terms of accessibility nor patient outcomes. The need for a safer, more effective, less expensive, and more accessible cataract removal method is of interest to the ophthalmological community. In particular, capsulorhexis, or removal of the anterior lens capsule, is a tedious and intricate procedure. The development of a manually operated, handheld cutting device specifically designed to produce circular incisions in the lens capsule of the eye could create a paradigm shift in the capsulorhexis portion of cataract surgery, providing quality and reproducibility comparable to laser-assisted surgery, while maintaining the efficiency and cost of standard surgery.

1.4 Proposed Solution

The proposed solution is to produce a device to minimize the risk and improve the accuracy of capsulorhexis in cataract removal surgeries. The device will consist of a handheld deployment tool, a shape-memory alloy blade, a manual actuator to deploy the blade, and a small cannula through which the blade will be deployed and retracted. The cannula will be inserted into the corneal incision and the blade will be deployed within the eye. Once fully deployed, the blade will be brought into contact with the lens capsule and, upon retraction of the blade, trace out a near-perfect, repeatable, circular cut into the anterior lens capsule. This innovative design, which utilizes both the shape-memory and superelastic properties of Nitinol, will enable the 5 mm diameter circular blade to be inserted and removed from the 2 to 3 mm corneal wound. This will not only make the procedure more effective and easier to perform, but also reduce the time required to perform the capsulorhexis. Because the capsulorhexis is currently one of the most difficult portions of a cataract surgery, the device described in this thesis will enable less-skilled surgeons to perform the procedure with outcomes similar to their more-skilled colleagues. This will enable more of the world's population to receive high-quality medical care.

1.5 Thesis Outline

The remainder of this thesis is structured as follows. In Chapter 2, we give an overview of devices used for capsulorhexis. This overview includes both devices currently used in clinical practice, as well as several proposed devices not used in clinical practice. Accompanying each device is a description of how the device performs capsulorhexis, how the device is made, and potential concerns with the device. In Chapter 3, we detail the concept design of our own device, the Helicotome. This includes user needs, concept

design, and device operation. Chapter 4 provides information on Nitinol, including the shape-memory effect, superelasticity, shape-setting, outer-fiber strain, and biocompatibility. Chapter 5 discusses surgical blades and the concept of "sharpness" in both qualitative and quantitative senses. A general overview of the terminology used in describing sharpness is provided, as well as details on sharpening and qualifying sharpness. Chapter 6, Device Design, includes the design specifications and the final tool geometry and dimensions. Chapter 7 details the manufacturing of the Helicotome. Chapter 8 consists of verification testing of the device, experimental results, and validation. We conclude in Chapter 9, and provide recommendations for future research.

1.6 References

[1] "Johns Hopkins Medicine, Department of Ophthalmology," 2013, from http://www.hopkinsmedicine.org/wilmer/conditions/cataracts.html

[2] "National Institute of Health, National Eye Institute Facts about Cataract," 2013, from http://www.nei.nih.gov/health/cataract/cataract_facts.asp

[3] Abell, R.G., and Vote, B.J., 2014, "Cost-Effectiveness of Femtosecond Laser-Assisted Cataract Surgery versus Phacoemulsification Cataract Surgery," American Academy of Ophthalmology, **121**(1), pp. 10-16.

[4] Horton, J.C., "University of California, San Francisco, Laboratory for Visual Neuroscience," 2012, from http://vision.ucsf.edu/horton/ResearchProgram.html

[5] "Vision Insights," 2013, from http://128.248.91.60/visioninsights/?page_id=1044

[6] Krag, S., and Andreassen, T.T., 2003, "Mechanical Properties of the Human Lens Capsule," Progress in Retinal and Eye Research, **22**, pp. 749-767.

[7] Krag, S., Olsen, T., and Andreassen, T.T., 1997, "Biomechanical Characteristics of the Human Anterior Lens Capsule in Relation to Age," Investigative Ophthalmology & Visual Science, **38**(2), pp. 357-363.

[8] Bailey, A.J., Sims, T.J., Avery N.C. and Miles C.A., 1993, "Chemistry of Collagen Cross-links: Glucose-mediated Covalent Cross-linking of Type-IV Collagen in Lens Capsules," Biochemistry Journal, **296,** pp. 489-496.

[9] Ambati, B.K., 2012, Professor of Ophthalmology and Visual Sciences at the University of Utah, U.S., private communication.

[10] “Benjamin Eye Institute,” 2011, from http://benjamineye.com/en/cataract/surgery-options/phacoemulsification

CHAPTER 2

DEVICES FOR CAPSULORHEXIS

The goal of every capsulorhexis is to remove a circular section of the anterior lens capsule to access the cataract. The unique constraints imposed by ocular anatomy complicate improving the efficiency, repeatability, and accuracy of the capsulorhexis procedure. This section describes several existing devices for performing capsulorhexis.

2.1 Devices Used in Clinical Practice

Two primary methods exist in clinical practice for performing capsulorhexis. The most common method involves using a sharp tool to puncture and tear a five-millimeter circle in the anterior lens capsule, and then manually remove the tissue. Phacoemulsification, i.e., ultrasonically breaking the cataract into quadrants, is subsequently used to section the cataract into small pieces. The broken cataract is evacuated from the eye using a suction device. The second commonly used method for capsulorhexis employs a femtosecond laser to burn the desired circular geometry into the anterior lens capsule, and breaks down the cataract into sections using the energy from the laser in place of phacoemulsification used in conjunction with the first capsulorhexis method.

2.1.1 Manual Capsulorhexis with Forceps or Bent Needle

Most surgeons employ cystotome forceps to perform capsulorhexis. These are small, tweezer-like tools with sharp, pointy tips [11]. Figure 2.1 shows cystotome forceps. However, other surgeons prefer a bent needle to perform the procedure [12], as shown in Fig. 2.2. During capsulorhexis, the anterior chamber of the eye is filled with a viscoelastic material such as a 1% solution of sodium hyaluronate to aid in flattening the lens and improving control while tearing the capsule. Also, the viscoelastic filler material increases pressure in the anterior chamber of the eye, which expands the chamber and increases the workspace for the surgeon. Figure 2.3 illustrates the manual capsulorhexis process. The surgeon will first use the forceps or bent needle to make the initial penetration of the lens capsule near the center of the intended capsulorhexis. Then, the surgeon will grasp the capsule with forceps and create a circumferential tear around the initial penetration point (Fig. 2.3 A). Depending on surgeon preference, the tear in the capsule is either pushed away from or pulled toward the surgeon to propagate the tear into a circular shape. The process is repeated on the opposite side of the capsule in the opposing direction to continue the circle (Fig. 2.3 B).

Figure 2.1: Capsulorhexis forceps. Inset shows close-up view of forceps tips. Image modified from [11].

Figure 2.2: Surgeon-bent cystotome needle. Image modified from [12].

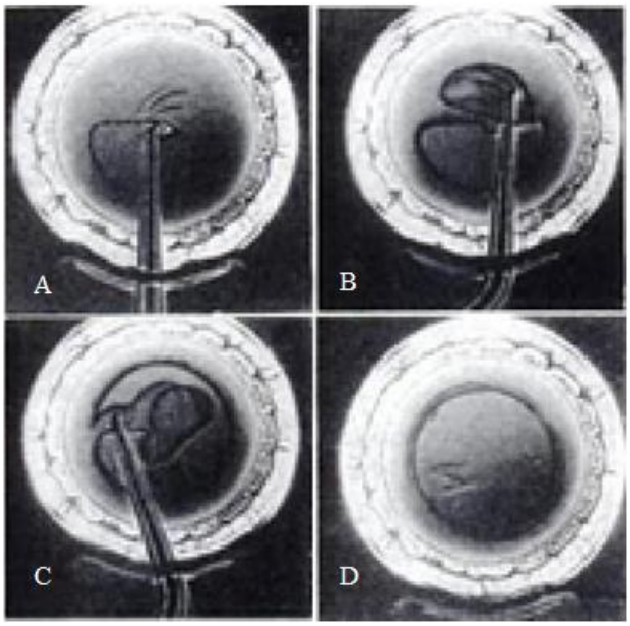

Figure 2.3: Manual capsulorhexis: tear is initiated (A) continued on opposing side of the lens capsule (B), tear is completed (C) then removed (D). Image modified from [13].

The process of grasping, tearing, and repositioning can be repeated several times, since keeping a firm grasp close to the tear itself maximizes control over the outcome, substantially improving the results (Fig. 2.3 C). The circle is then completed and the excised portion of the capsule is removed [13] (Fig. 2.3 D). Although this method is less expensive than many available alternatives, it is difficult to perform and prone to complications and errors, which affect the outcome for the patient.

2.1.2 Laser-assisted Capsulorhexis

Figure 2.4 shows the equipment to perform laser-assisted capsulorhexis [15]. The device consists of a femtosecond laser, a power supply, and a user interface. In a small percentage of patients, the heat generated by the laser can permanently damage the surrounding tissue and can possibly lead to the formation of additional scar tissue. Advantages of the laser-assisted method include reduced healing time, reduced scarring in the majority of patients, and better centration of the artificial intraocular lens as a result of the increased accuracy of the capsulorhexis [14]. Whereas the incisions necessary for a manual capsulorhexis rely on small intraocular blades, laser-assisted capsulorhexis is entirely blade-free. A femtosecond laser can accurately inscribe a circular capsulorhexis, and even break up the cataract for removal. This method eliminates the need for phacoemulsification of the cataract prior to removal, as it is accomplished with the energy from the laser.

Figure 2.4: Alcon Surgical LenSx femtosecond laser for refractive cataract surgery. Image modified from [15].

A protective shroud encapsulates the patient's eye (Fig. 2.5 A), the interior of the eye is scanned, and the parameters of the laser are adjusted based on the patient's particular ocular anatomy [15] (Fig. 2.5 B). The laser will first make the incisions in the cornea necessary for intraocular lens implantation. Then, it performs the capsulorhexis with extreme precision and accuracy, and dissolves the cataract into quadrants for easy removal through suction. Only the suction tube for removing the cataract and the introducer tube for implanting the artificial intraocular lens actually make contact with the inside of the eye, which minimizes scarring and the potential for complications.

2.2 Previously Disclosed Devices Not Currently Used in Clinical Practice

Many devices have been designed to perform capsulorhexis. The following are examples of devices not currently used in clinical practice for various reasons.

2.2.1 US Patent # 6,551,326 - Capsulorhexis Device

This device consists of a shape-memory-alloy wire, a blade, attachment mechanism, and an insertion tube [16] (Fig. 2.6 A and B). A Nitinol wire is formed into a

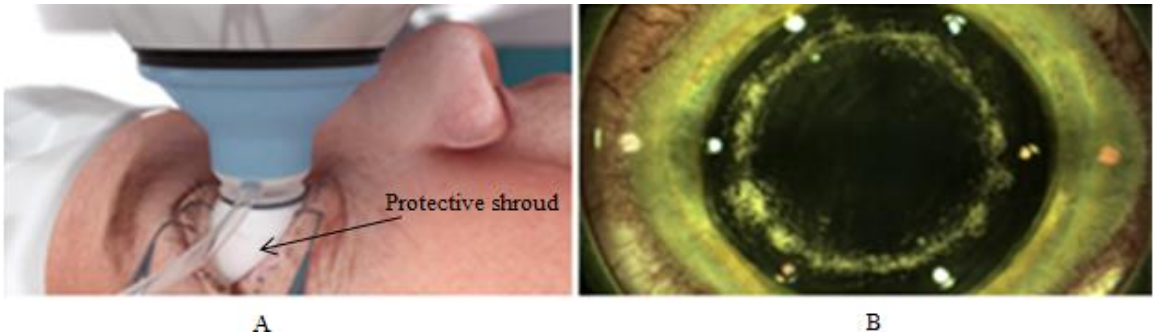

Figure 2.5: Protective ocular shroud (A) and user interface display of laser capsulorhexis (B). Image modified from [15].

circle of desired diameter using thermal shape setting. A blade is attached to the distal end of the shape-set wire using an attachment mechanism. The superelastic properties of Nitinol enable retraction of the wire into a straight tube and redeployment into its original shape without incurring any permanent deformation. The properties of Nitinol are discussed further in Chapter 4. To perform capsulorhexis, the Nitinol wire is retracted within the tube (Fig. 2.6 C). After the corneal incision is made and viscoelastic material is injected into the anterior chamber, the tube is inserted into the eye through the incision (Fig. 2.6 D). The blade attached to the Nitinol wire is deployed from the tube and the wire regains its circular shape (Fig. 2.6 E and F). The blade is placed in contact with the lens capsule and, upon retraction of the wire, traces and cuts the circular path (Fig. 2.6 G and H). After the cut is performed, the tube is removed from the cornea and the flap of tissue is removed using forceps (Fig. 2.6 I).

A critical problem of this design is that if the blade does not cut immediately upon retraction of the wire, the method results in an incomplete cut. It also may be difficult to cut a full 360° circle without the cut extending beyond the inscribed circle, since the blade will eventually complete the circular path and begin travelling along a straight path; this will leave a small flap and result in a radial tear in the lens capsule, which could complicate the implantation of the artificial lens. The assumption that the blade will follow the intended circular path of the wire could be substantially violated once a load is applied to the blade, resulting in the wire deforming from its circular shape upon retraction. Finally, there is a potential risk of the blade or attachment mechanism detaching from the Nitinol wire.

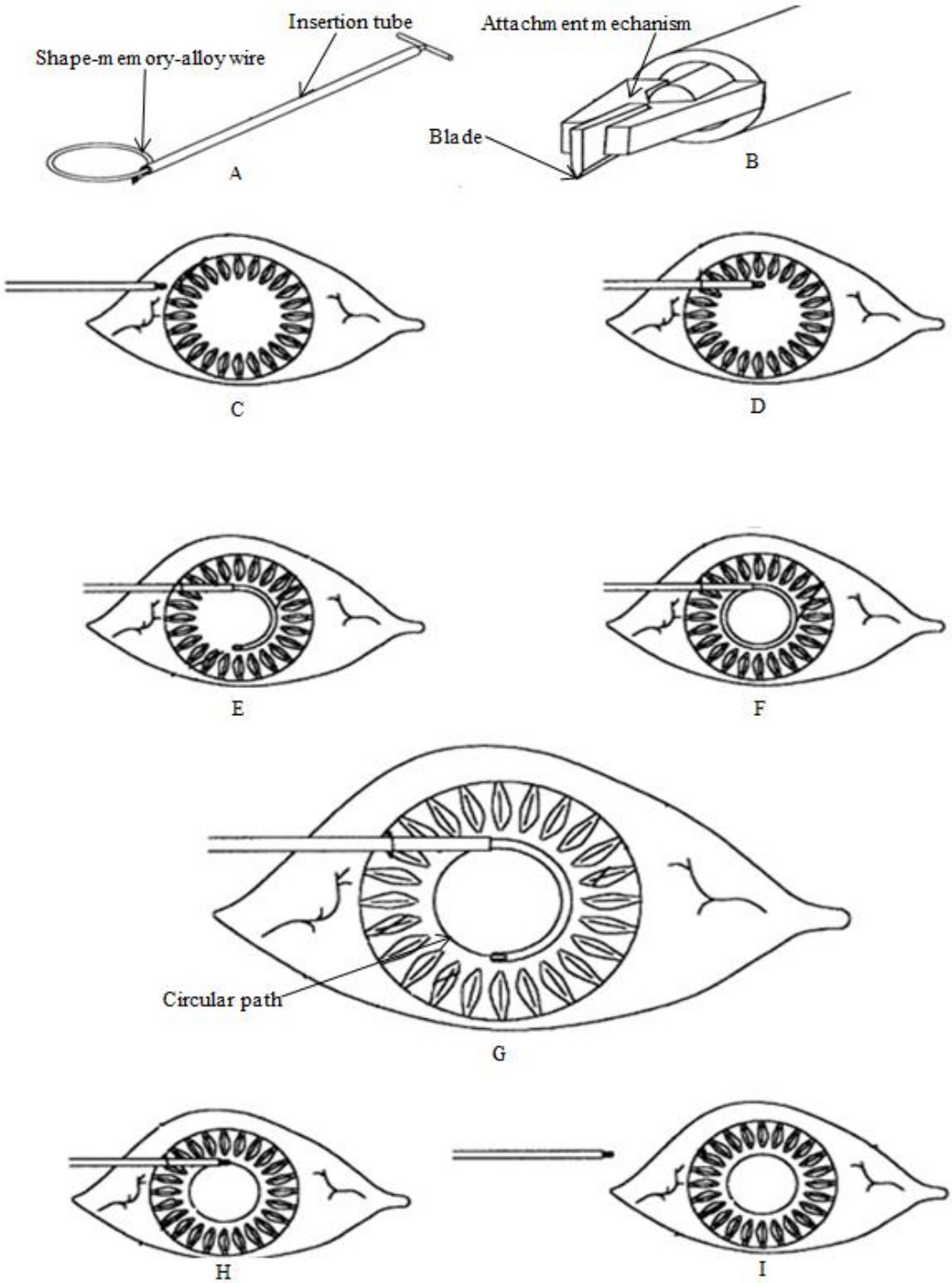

Figure 2.6: Capsulorhexis device operation. Fully deployed (A) and close up of the bladed tip (B). Device being inserted into the eye (C), and deployed to form a circular loop (D-F). Device is retracted, and the lens capsule is cut (G-H), then the device is removed from the eye (I). Image modified from [16].

2.2.2 US Patent # 5,269,787 - Apparatus and Method for Capsulorhexis

This device is comprised of a flexible ring made of superelastic shape-memory alloy, a shaft, and a fastener [17] (Fig. 2.7 A). The ring is sharpened on the side that makes contact with the lens capsule. The shaft connects to the ring in two places to provide flexural support and rigidity to the ring. On the other end of the shaft a fastener is attached to an ultrasonic power source. The device is inserted into the cornea after the anterior chamber is filled with viscoelastic material. The device is then put into contact with the lens capsule (Fig. 2.7 B), and the ultrasonic power source is energized. Ultrasonic energy is transmitted via the blade to the lens capsule to complete the cut. The device designers claim that because of the continuous nature of the circular cut, the tissue will scar symmetrically, improving adherence of the implanted artificial lens to the lens capsule, thus prolonging centration of the new lens.

The superelastic material used for the ring cannot sustain unlimited elastic strain without incurring permanent plastic deformation. Hence, inserting this device into the eye requires a corneal incision that is larger than that which is currently done in practice. If the ring is made such that it fits within a standard 2 to 3 mm incision without exceeding the maximum elastic strain that can be sustained by the superelastic material, the circular cut will be too small for artificial intraocular lens implantation. Also, since the lens capsule lies beneath the plane of the corneal incision, the straight shaft of this device may prohibit making flush contact with the lens capsule, which would result in uneven application of cutting force. Achieving a full, circular cut in the lens capsule without damaging the surrounding tissue requires the application of force solely on the lens capsule, which this device cannot achieve in its current configuration.

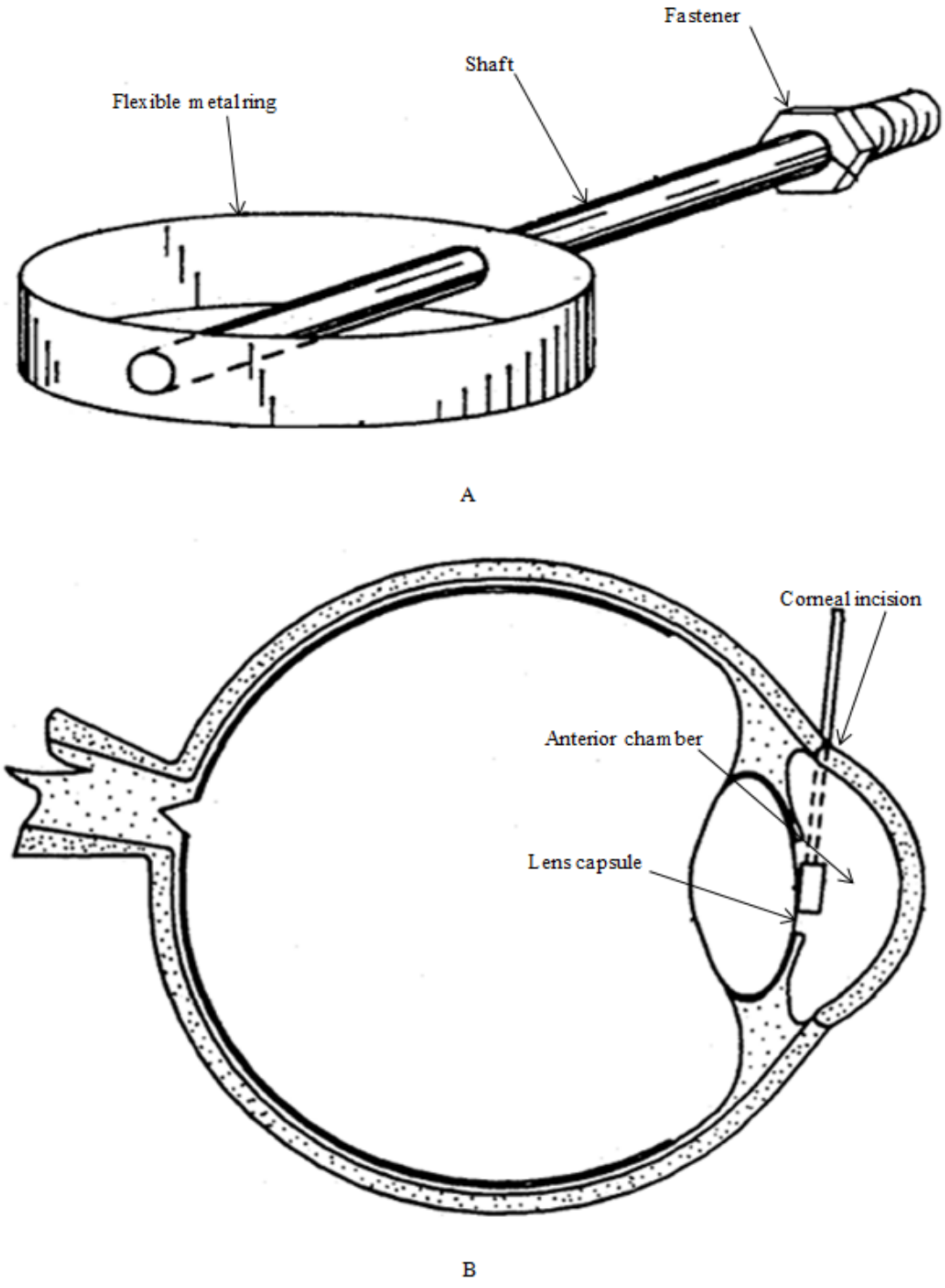

Figure 2.7: Apparatus for capsulorhexis. The device (A) and ocular insertion of the device for capsulorhexis (B). Image modified from [17].

2.2.3 US Patent # 5,728,117 - Retractable Capsulorhexis Instrument

This device includes a flexible ring attached to a plunger, which can be retracted into an introducer tube [18] (Fig. 2.8). The flexible ring may consist of any material capable of being sharpened and displays a sharp and a blunt side. Upon retraction into the tube, it will elastically deform into an elliptical shape. After ejection from the tube, the ring will resume its circular form. The introducer tube fits within the standard 2 to 3 mm corneal incision. After the anterior chamber of the eye is filled with viscoelastic material, the tube is inserted into the incision and the ring-shaped blade will be ejected from the tube, taking on its circular form (Fig. 2.8 A). The blade is then pressed onto the lens capsule to perform the capsulorhexis (Fig. 2.8 B), after which it is retracted back into the introducer tube, and the tube is removed from the corneal incision (Fig. 2.8 C).

The thickness of the flexible ring must be small to avoid plastic deformation upon retraction in the injector tube. This thickness may be too small to maintain sufficient rigidity and withstand the cutting force during capsulorhexis. Indeed, the size of the introducer tube is limited by the maximum allowable corneal incision size.

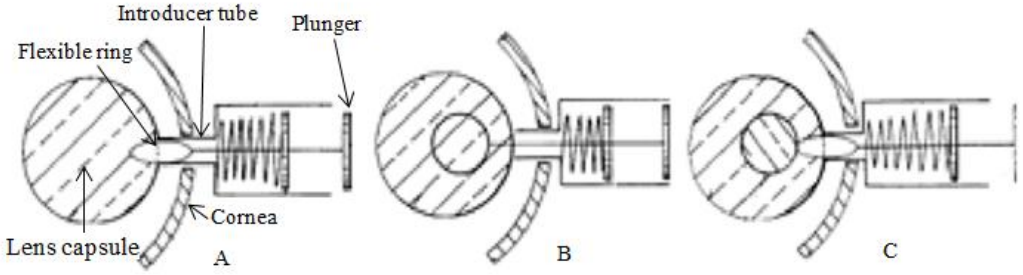

Figure 2.8: The retractable capsulorhexis instrument. The device deployed within the eye (A), depressed onto the lens capsule, performing capsulorhexis (B), and retracted back into the cannula (C). Image modified from [18].

2.2.4 WO 2009 Patent Application # 153,550 – Surgical Cutting Implement

The device consists of a superelastic ring-shaped Nitinol shape-memory-alloy blade. This blade has several serrations superimposed on the cutting edge to facilitate penetration of the lens capsule, using only a force oriented normal to the lens. No force tangential to the lens capsule, like that used in a sawing motion, is applied. The Nitinol blade is formed into a loop using thermal shape-setting. The blade is retracted into a cannula for insertion into the eye through a standard corneal incision. The cannula has a small protrusion along the top side of its distal end. When the blade is fully deployed, this protrusion provides flexural rigidity to the blade during the capsulorhexis. The cannula is attached to a handle with a sliding mechanism to retract and deploy the blade [19] (Fig. 2.9). Some variations of the tool also contain a device for injecting a viscoelastic medium or other lubricating fluid into the eye; this is accomplished via a connector for a syringe, or housing in which to insert a syringe containing viscoelastic material. The blade is deployed from the cannula. A normal force is applied to perforate the lens capsule with the serrations. Upon continued application of force, the perforations join to complete a full circular cut. The blade is then retracted into the cannula and removed from the corneal incision. The flap of tissue is evacuated from the anterior chamber using forceps.

We attempted to emulate this design in our laboratory. However, in experiments with bovine eyes, a consistent flaw was evident throughout. Regardless of the blade sharpness and the number, shape, and accuracy of the serrations, the normal force required to penetrate the lens capsule compromised the structural integrity of the lens capsule, i.e., the lens capsule ruptured before the blade completed the capsulorhexis.

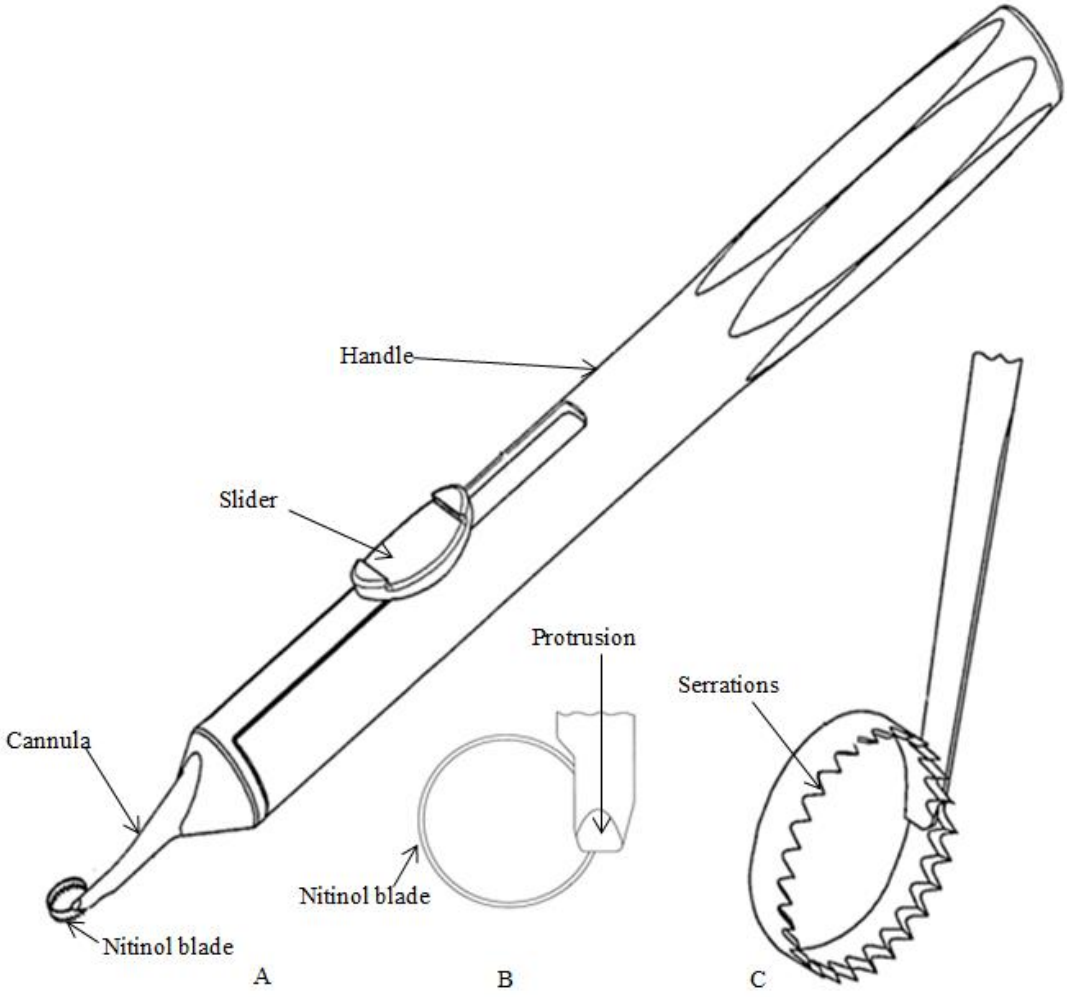

Figure 2.9: Surgical Cutting Implement. The device (A) with close-ups of the protrusion (B) and the blade (C). Image modified from [19].

2.2.5 US 2010 Patent Application # 0274272 - Instrument and Method for Creating a Controlled Capsulorhexis for Cataract Surgery

The device consists of an S-shaped, or mirrored S-shaped, serrated cutting band attached to a support rod [20] (Fig. 2.10 A). The support rod attaches proximally and distally to the cutting band, where it joins with a long handle (Fig. 2.10 B). The device is inserted into the eye through a corneal incision after the anterior chamber is filled with viscoelastic material. The cutting band is pressed onto the lens capsule, which cuts the S-

shaped or mirrored S-shaped pattern into the capsule. The tool is lifted off the capsular bag and evacuated from the corneal incision. The surgeon subsequently grasps one of the two tabs created by the device with forceps and tears out half of the circle (Fig. 2.10 C). The surgeon repeats the process on the other tab until the entire circle of tissue is removed.

The cutting band of this device is too small to make the necessary size of cut in the lens capsule for artificial lens implantation. Also, without the use of a protective sheath, it is difficult to insert the device into the corneal incision without damaging the surrounding tissue of the eye. This device provides little advantage over the standard manual method with forceps or a bent needle, since the lens capsule must still be torn out manually. As a result, neither the safety of the patient, nor the efficiency and accuracy of the procedure seems to be improved with this device.

2.2.6 US Patent # 8,157,797 - Capsulorhexis Device with Retractable Bipolar Electrodes

This device includes two layers of superelastic Nitinol material separated by an insulating layer such as Parylene [21] (Fig. 2.11 A). These layers are formed into a loop of 5 mm diameter by thermal shape-setting. The layers continue beyond the loop and into an insertion cartridge. Two electrical connectors on the proximal end of the device are attached to each of the two conducting layers of Nitinol, and are connected to a power supply. The superelastic properties of Nitinol enable retracting and deploying the loop into and from the introducer without incurring any permanent deformation. The insertion cartridge is positioned into the corneal incision (Fig. 2.11 B). The loop is deployed within the anterior chamber (Fig. 2.11 C), and positioned onto the anterior portion of the lens capsule (Fig. 2.11 D). A radio-frequency power supply is then energized, which generates

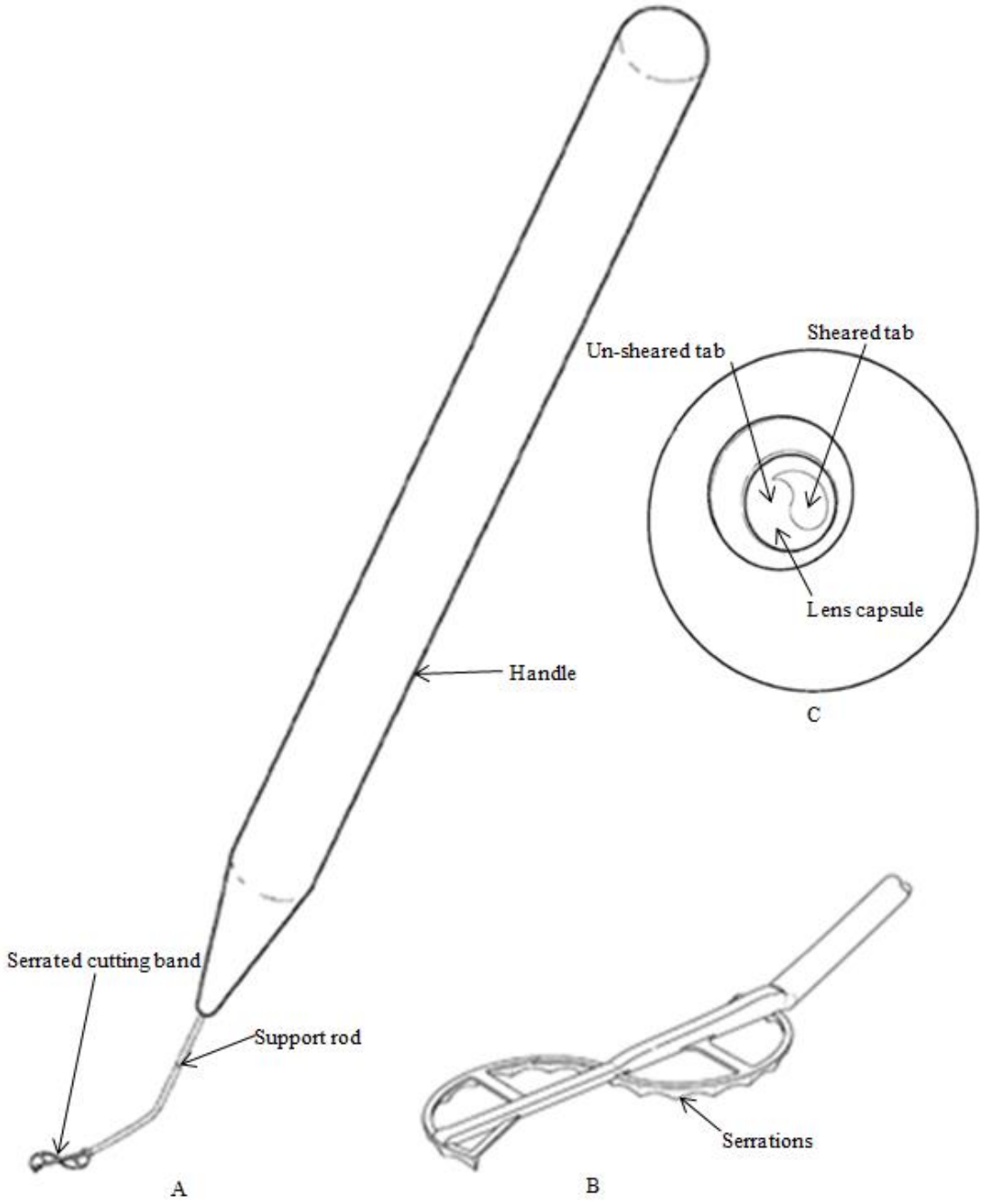

Figure 2.10: Instrument for creating a controlled capsulorhexis for cataract surgery. The device (A), a close-up of the blade tip (B) and reverse S-shaped pattern cut into the lens capsule with one tab removed (C). Image modified from [20].

electrical current between the two layers of Nitinol, causing rapid resistive heating of the loop. The heat is used to perform the capsulorhexis. The loop is then retracted into the insertion cartridge and removed from the eye (Fig. 2.11 E).

Although it is not specified that the device is to be used in the presence of a viscoelastic material, it would likely be advisable to do so. Unintended burning of the underside of the cornea could cause further damage and exacerbate the patient's impaired vision. It is also evident that it is difficult to perfectly form a complete circle, as the two ends of the loop cannot meet to avoid an electrical short circuit. Hence, this device is likely to create an incomplete cut.

2.2.7 US 2010 Patent Application # 0312252 - Capsulorhexis Device with Flexible Heating Element Having an Angled Transitional Neck

The device is comprised of a superelastic, shape-memory-alloy wire that has been thermally shape-set into a loop [22] (Fig. 2.12 A). A kink at the proximal end of the loop positions the plane of the loop slightly below that of the rest of the tool (Fig. 2.12 B). The wire runs into an insertion sleeve attached to the handle of the tool. An insulating layer separates the two ends of the conductive wire, which is connected to a power supply at the rear end of the handle. The superelastic nature of the loop enables retracting and deploying it into the insertion sleeve without permanently deforming. The loop forms its circular shape after it is deployed from the insertion sleeve. It is positioned onto the anterior portion of the lens capsule and the power supply is activated. The wire rapidly heats when subject to an electric current as a result of the high electrical resistivity of the Nitinol material. After completing the capsulorhexis, the loop is retracted into the insertion sleeve and

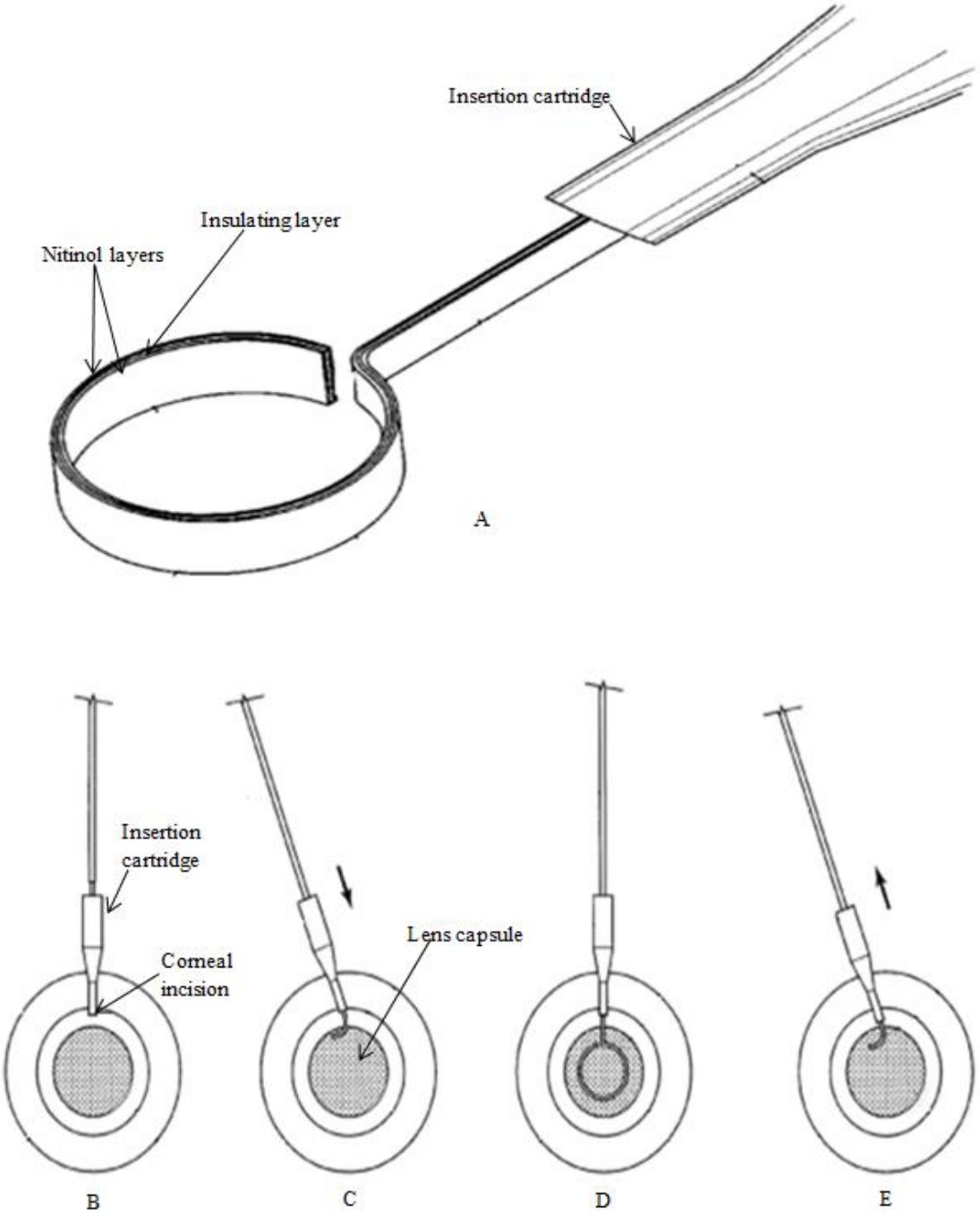

Figure 2.11: Capsulorhexis device with retractable bipolar electrodes. The device (A) is inserted into the eye (B), and deployed (C). Then, the tool burns a circle into the lens capsule (D) and is retracted back into the insertion cartridge (E).
Image modified from [21].

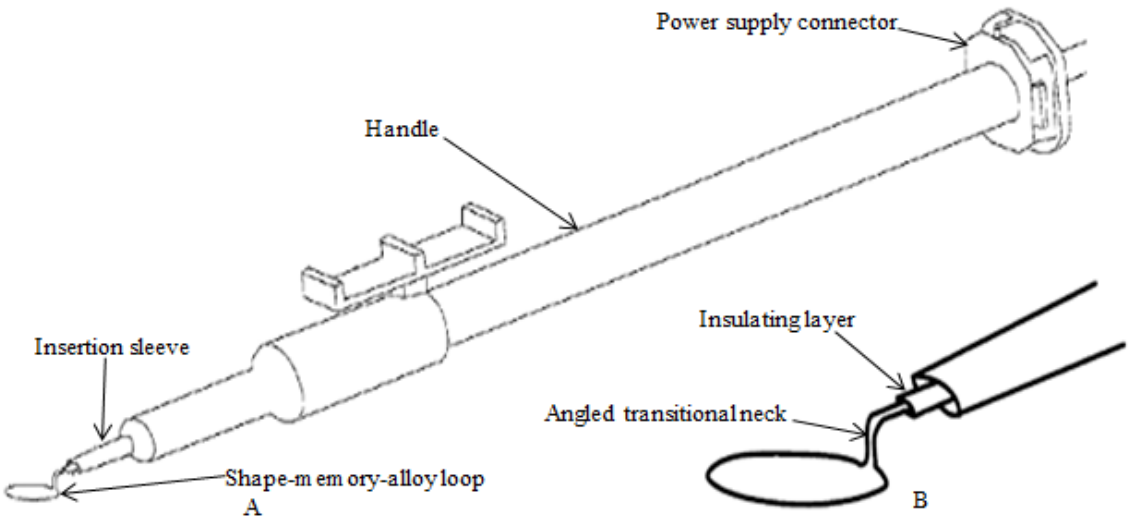

Figure 2.12: Capsulorhexis device with flexible heating element having an angled transitional neck (A) and close up of the heating element tip (B).
Image modified from [22].

removed from the corneal incision.

It is not specified that this device should be used in the presence of a viscoelastic filler material. However, in the presence of a potentially harmful heating element within the eye, it is advisable to maximize the workspace. This mitigates the risk of the heating element touching a surface unintentionally and causing further impairment to the patient's vision. As with the previous heating device, the cutting loop does not form a complete circle, which may result in an incomplete capsulorhexis.

2.3 References

[11] "Katalyst Surgical, LLC.," 2014, from http://www.katalystsurgical.com/instruments/ophthalmic/ capsulorhexis-forceps-cystotome-teeth

[12] "Boston University School of Medicine, Department of Ophthalmology," 2014, from http://www.bu.edu/eye/phacoprimer/capsulorrhexis/

[13] Mahipal, S.S., and Tanuj, D., 2003, *A Practical Guide to Phacoemulsification*, Lordson Publishers, New Delhi, pp. 60.

[14] National Eye Institute, 2014, from https://www.nei.nih.gov/health/cataract/cataract_facts.asp

[15] "Valley Eye Surgical Center", n.d., from http://www.valleyeyesurgical.com/cataract_laser_physicians.html

[16] Van Heugten, A.Y., Van Heugten, S.L. and Van Heugten, C.J., 2003, "Capsulorhexis Device," U.S. Patent 6551326.

[17] Cozean, C.H. Jr., and Cozean, C.H. III, 1993, "Apparatus and Method for Capsulorhexis," U.S. Patent 5269787.

[18] Lash, R.S., 1998, "Retractable Capsulorhexis Instrument," U.S. Patent 5728117.

[19] Gibbs, R.A., and Stokes, J.D., 2009, "Surgical Cutting Implement," International Application Publication Number WO 2009/153550.

[20] Medina, R., 2010, "Instrument and Method For Creating a Controlled Capsulorhexis for Cataract Surgery," U.S. Patent Application 0274272 A1.

[21] Boukhny, M., and Chon, J., 2012, "Capsulorhexis Device with Retractable Bipolar Electrodes," U.S. Patent 8157797.

[22] Jia, G., and Sussman, G.R., 2010, "Capsulorhexis Device with Flexible Heating Element Having an Angled Transitional Neck," U.S. Patent Application 0312252.

CHAPTER 3

DEVICE CONCEPT

This chapter describes the design concept of the Helicotome. Requirements for the device are derived from user needs. We also describe the intended use of the design concept. Quantitative design specification are provided and discussed in Chapter 6.

3.1 User Needs

The medical advisor for this project, Ophthalmologist and Cataract Surgeon Balamurali Ambati, M.D., presented the research team with the needs that this device must fulfill. The device must be used in conjunction with standard ophthalmic procedures for performing a small-incision capsulorhexis, which includes entering the anterior chamber of the eye through a 2 to 3 mm-wide corneal incision. The device must be handheld, actuated with the index finger and disposable after a single use. The device needs to cut a continuous, 5 to 6 mm-diameter circle in the anterior lens capsule of the human eye. The circular cut must be complete and close to a "perfect" circle, as discussed in Chapter 1, to perform a successful capsulorhexis, and compete with the accuracy of existing laser-based systems for capsulorhexis. The device must be inexpensive and improve upon the current method for performing a manual capsulorhexis [23], described in Chapters 1 and 2.

Although our customers and users of the device will be ophthalmologists, the

regulations set forth by the Food and Drug Administration (FDA) must be taken into account when considering user needs. According to the Code of Federal Regulations (CFR) Title 21 (Food and Drug Administration Department of Health and Human Services), subchapter H (Medical Devices), part 886 (Ophthalmic Devices), subpart E (Surgical Devices), section 886.4350 (Manual ophthalmic surgical instrument): "A manual ophthalmic surgical instrument is a non-powered, handheld device intended to aid or perform ophthalmic surgical procedures." As such, this is considered a Class-I device, which is subject to general controls only (see CFR Title 21, Section 820), and therefore is exempt from restrictions imposed by a premarket notification. This regulatory pathway greatly reduces the requirements for the device to be brought into clinical practice. Above all, as with all medical devices, the device must exhibit safety and efficacy when performing its intended task.

3.2 Design Concept

To keep the design of this device as simple as possible, and to avoid any device classification complications imposed by the FDA, we are designing a manual ophthalmic surgical instrument. To insert a 5 mm diameter circular blade into a 2 to 3 mm wide incision (1.27 to 1.91 mm diameter when opened) is challenging. Our solution to this "keyhole" problem, which is found in the designs of many predicate devices discussed in Chapter 2, is to deploy a Nitinol shape-memory-alloy component from a cannula into the eye. Figure 3.1 shows the proposed blade concept. It comprises a Nitinol element that is shape-set into a helix-shape with at least two complete turns on its distal end. The helix has the same diameter as the intended capsulorhexis, and has minimal pitch, such that it is tightly wound.

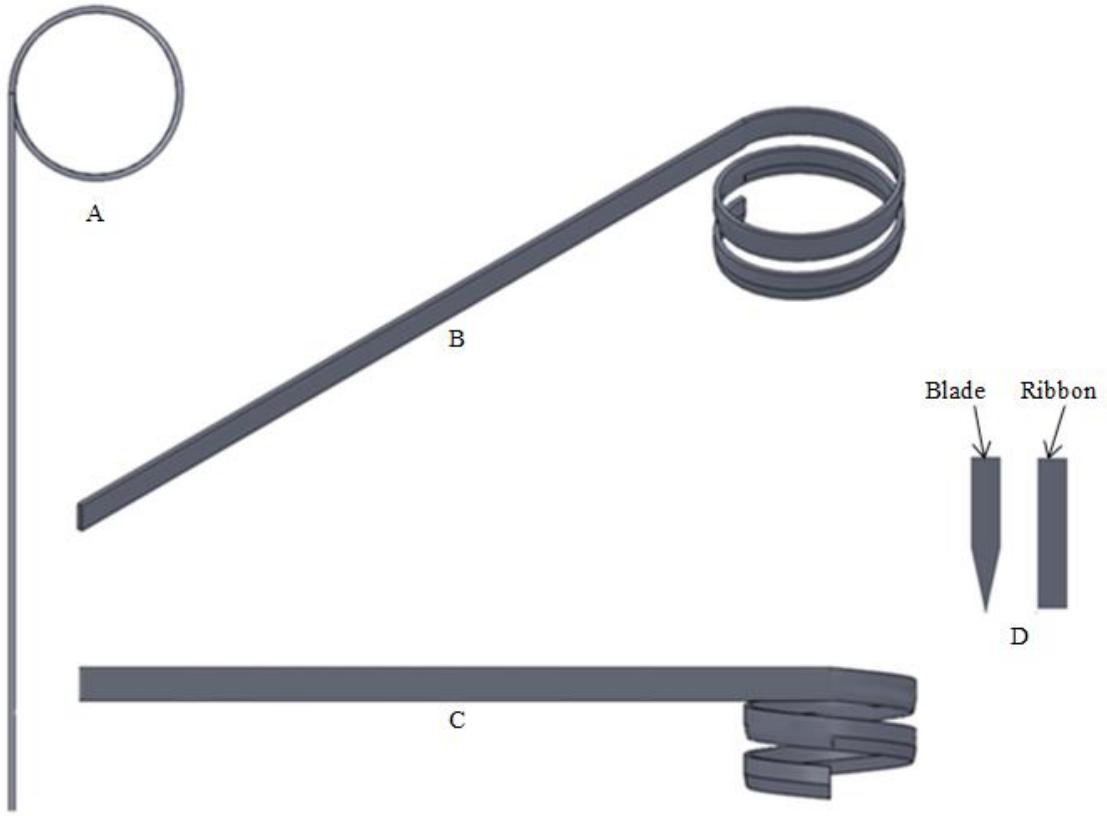

Figure 3.1: Helical blade concept design. (A) Top, (B) isometric, (C) and side view of blade concept design. Inset (D) shows an enlarged view of the cross-section of the Nitinol ribbon with and without the machined blade.

The Nitinol element is sharpened into a blade on the underside of the final complete turn of the helix (360°). Figure 3.2 illustrates the concept of the device in a step-by-step fashion. The Nitinol element is completely housed within a cannula as the cannula is inserted into the anterior chamber of the eye through the corneal incision, and the blade element is then deployed within the anterior chamber of the eye.

To perform the capsulorhexis, the blade is pressed down onto the lens capsule, and the Nitinol element is retracted into the cannula, causing the blade to rotate in an approximately circular path, causing a slicing motion on a segment of a circular arc. Once the capsulorhexis is complete, the blade is lifted up and away from the lens capsule, the

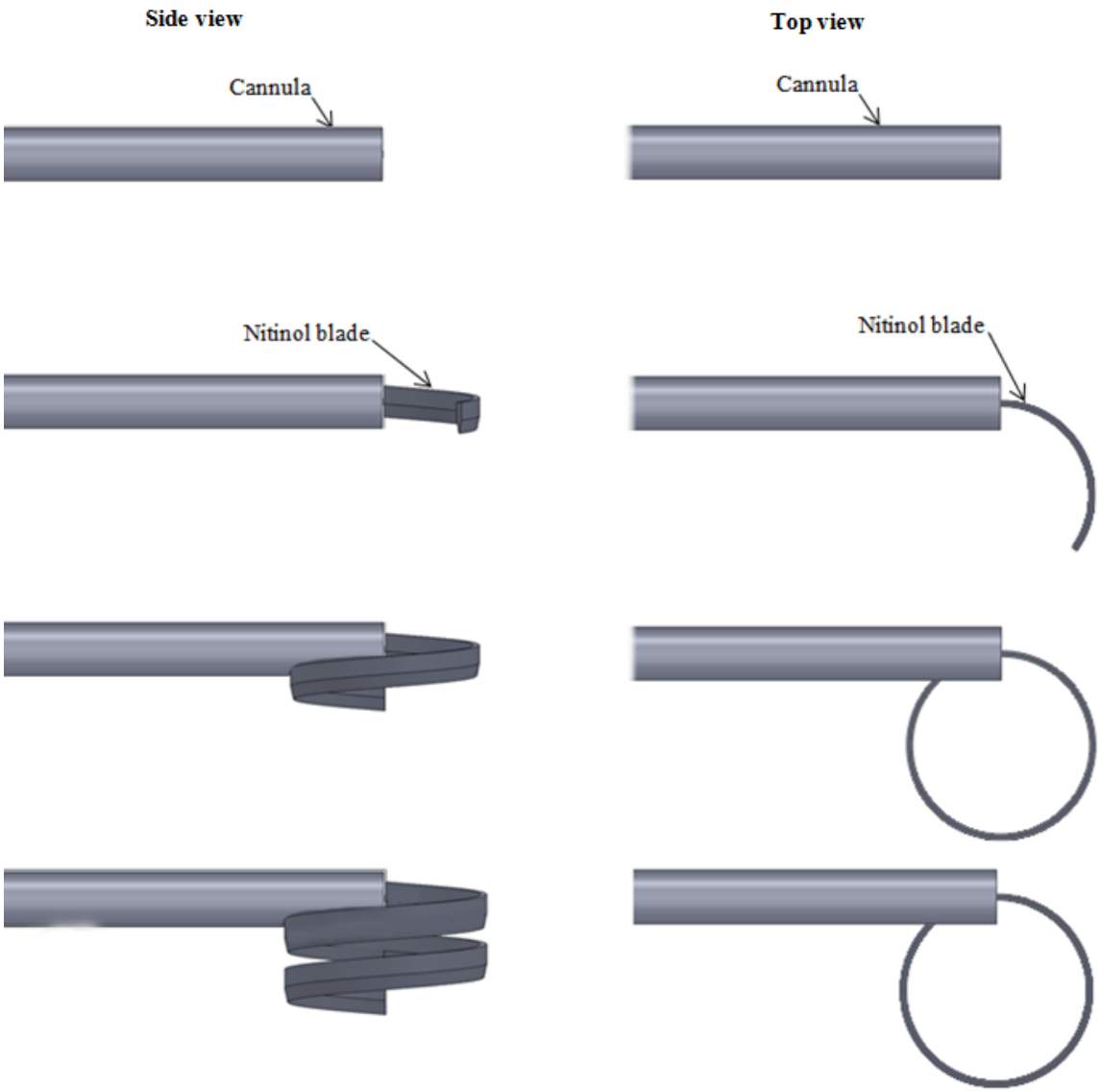

Figure 3.2: Deployment of the helical Nitinol element.

remainder of the Nitinol element is retracted into the cannula, and the cannula is withdrawn from the eye. A number of considerations motivated this concept. The Nitinol element is ultimately designed as a two-turn helix sharpened into a blade for a number of reasons: First, the design mitigates the risk of an incomplete capsulorhexis since the blade traces over its own path (at least approximately) while being retracted, avoiding the requirement that cutting start immediately upon retraction. Cutting need only begin before

the first complete helical turn has been retracted, providing time for the surgeon to ensure that the blade is engaging with the lens capsule. Second, once cutting has begun, it will rapidly occur along the arc of intended circle, leading to completion of the capsulorhexis with minimal retraction of the Nitinol element. Third, when depressed onto the lens capsule, the upper loop of the Nitinol element will press against the lower loop, providing additional support and rigidity during the initial stages of cutting. Because of the small dimensions of the Nitinol element that must be used to ensure that the Nitinol not undergo plastic deformation, we found during prototype development that overall compliance in the device was a significant limiting factor in making a successful cut, and this additional rigidity contributed to the success of the working prototype. This need for rigidity in the vertical direction is also the reason that our design uses a tall Nitinol ribbon, as opposed to a Nitinol wire. Fourth, the complete circular cut can be completed with the blade in its intended circular shape, such that the blade can be lifted off of the lens capsule before it returns to a straight shape as it re-enters the cannula. Fifth, the helix helps account for the vertical drop that must occur from the cannula insertion at the cornea to the anterior surface of the lens capsule through the dilated pupil.

Figure 3.3 shows the assembled device (with the blade fully deployed), which comprises an injection-molded plastic handle, a nylon slider, a knob, a cannula, and a helix-shaped Nitinol blade. In our prototype, the body of the tool (i.e., the plastic handle, nylon slider, and knob) is simply a modified Malyugin Ring Injector. Modifications to the injector include an extended slider path and a stainless-steel cannula to facilitate the housing and deployment of the Nitinol blade, as discussed in Chapter 7. The device shown is designed for right-handed use, but a simple modification can be made to make the tool left-handed.

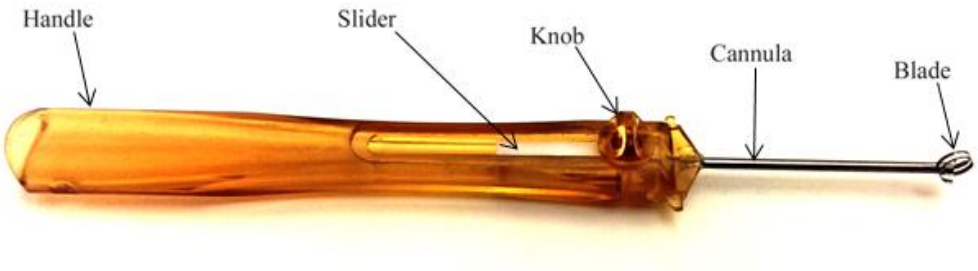

Figure 3.3: Prototype of the Helicotome.

The concept is similar to the predicate device described in Section 2.2.1 (Capsulorhexis Device) in that a Nitinol element is deployed to form a circle and then capsulorhexis is performed by a slicing action upon retraction of the element [24]. However, our design has two key differences that significantly change the functionality of the blade. First, the Nitinol itself is the blade, rather than affixing a blade to the end of the Nitinol loop. This choice facilitates instantaneous cutting along an entire segment of a circular arc rather than cutting at a point, and it eliminates the potential risk of the blade detaching from the Nitinol and remaining inside the eye. Second, rather than attempting to achieve a complete circle upon deployment of the blade, our intent is to achieve a helix with at least two complete turns but with a blade only on the most distal complete turn. It is our conjecture that these two design differences will lead to the many benefits discussed previously. Our concept is also similar to the predicate device of Section 2.2.4 (Surgical Cutting Implement) in that the blade is fabricated directly into the Nitinol element [25]. However, there are no serrations on our blade, and rather than punching out the circle by applying a downward force that is orthogonal to the lens capsule, our concept is designed to slice tissue by cutting upon retraction of the blade.

3.3 Device Operation

Our device is intended to replace cystotome forceps [26], a bent needle [27], or any manually-operated device for capsulorhexis. After the anterior chamber of the eye is filled with a viscoelastic material, the cannula, with the blade fully retracted, is inserted into the eye through the corneal incision. The blade is deployed from the cannula into the anterior chamber of the eye, such that the sharpened edge faces down toward the lens capsule and the helical element passes through the dilated pupil. Once the Nitinol element is fully deployed within the eye, the sharpened edge is lowered onto the lens capsule. To perform capsulorhexis, the blade is pressed onto the capsule with moderate pressure and retracted. As the blade is being retracted, it traces out a near-perfect circular cut in the anterior lens capsule. The compliance of the lens capsule, combined with the compliance of the helix, will result in an arc segment of the circular blade engaging with the lens capsule, rather than just the most distal portion of the blade, with the length of the arc segment growing with applied pressure. Too much pressure should be avoided since it will result in deformation of the compliant Nitinol element that causes the blade to deviate from its intended circular path. Once the capsulorhexis is complete, the blade is immediately lifted up and away from the lens capsule, and the Nitinol element is then fully retracted into the cannula, taking care not to further cut the lens capsule or the iris. The cannula is withdrawn from the corneal incision, and the excised portion of the lens capsule can be retrieved from the eye. In the event that an incomplete cut is made, forceps are used to complete the capsulorhexis, as in the standard manual method, before removing the excised portion of the lens capsule from the eye. Due to the temperature dependence of Nitinol, our device should neither be used nor stored in extreme temperatures (i.e., below 10°C or above 50°C).

3.4 References

[23] Ambati, B.K., 2012, Professor of Ophthalmology and Visual Sciences at the University of Utah, U.S., private communication.

[24] Van Heugten, A.Y., Van Heugten, S.L., and Van Heugten, C.J., 2003, "Capsulorhexis Device," U.S. Patent 6551326.

[25] Gibbs, R.A., and Stokes, J.D., 2009, "Surgical Cutting Implement," International Application Publication Number WO 2009/153550.

[26] "Katalyst Surgical, LLC.," 2014, from http://www.katalystsurgical.com/instruments/ophthalmic/ capsulorhexis-forceps-cystotome-teeth

[27] "Boston University School of Medicine, Department of Ophthalmology," 2014, from http://www.bu.edu/eye/phacoprimer/capsulorrhexis/

CHAPTER 4

NITINOL

Nitinol is a shape-memory alloy consisting of nickel and titanium. It has become an increasingly popular material for design of biomedical devices due to its unique shape-memory and superelastic properties, in combination with its exceptional biocompatibility [28, 29]. This chapter describes its basic properties and its application to this work.

4.1 Properties of Nitinol

The unusual physical properties of Nitinol stem from its crystal lattice structure differing in shape and orientation depending on which phase it occupies. This is caused by a diffusionless phase transformation between the austenitic phase, which ensues at higher temperatures, and the martensitic phase, occurring at lower temperatures [30]. Transitions between the shape-memory and superelastic behavior occur after the material has fully transformed from the martensitic phase to the austenitic phase and vice versa [30]. Due to thermal hysteresis, the temperature at which austenite transforms to martensite is not the same temperature at which martensite forms into austenite [31], giving rise to a transformation temperature range [31]. Figure 4.1 shows the austenite fraction in a particular Nitinol alloy as a function of temperature, illustrating the thermal hysteresis at the transition from martensite to austenite and back to martensite.

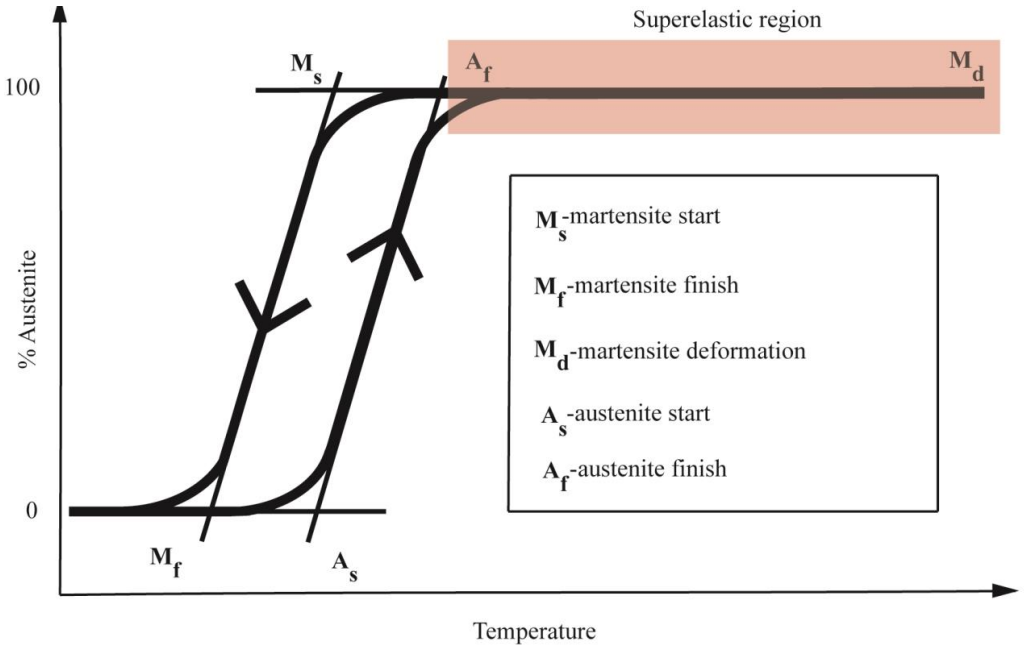

Figure 4.1: Austenite fraction of Nitinol as a function of temperature, showing thermal hysteresis between the martensite and austenite phases. Image modified from [31].

The temperature range over which the phase transformation takes place, known as the transition temperature, is a function of the composition of the Nitinol alloy. For instance, the most commonly used Nitinol alloy, which is composed of 50.8 atomic percentage (at%) nickel and 49.2 at% titanium, has a phase transformation that occurs between 22°C and 40°C [30]. Figure 4.2 shows the Nitinol transition temperature as a function of Nickel content in the Nitinol alloy [30]. Small changes in Nickel content correlate to large differences in phase transformation temperature. A 1% shift in the quantity of either of Nitinol's constituent materials will produce an approximately 100°C change in the phase transformation temperature [30]. In addition to changing the composition of the alloy, thermomechanical processing can be used to fine-tune the transformation temperature, enabling tailoring the alloy to specific applications [30].

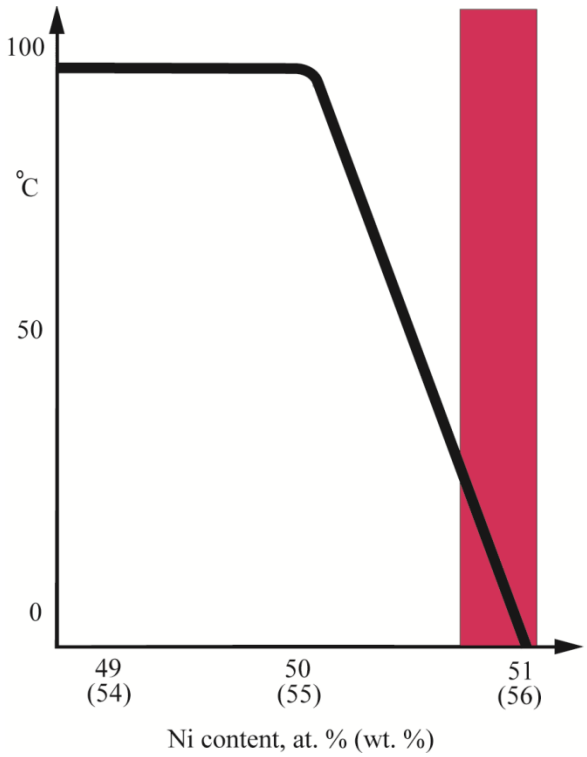

Figure 4.2: Phase-transformation temperature versus nickel content of Nitinol. The red shaded area denotes the region occupied by typical superelastic Nitinol. Image modified from [30].

4.2 The Shape-Memory Effect

Figure 4.3 illustrates the shape-memory effect. This occurs when a shape-memory alloy, such as Nitinol, is mechanically deformed in its martensitic phase, i.e., at a temperature below its transitional temperature range. Nitinol deforms into a shape imparted by the applied external loading (Fig. 4.3 A), appearing to deform plastically (Fig. 4.3 B). However, once the material is heated beyond its transformation temperature (Fig. 4.3 C), it will revert back to its original shape (Fig. 4.3 D) [32]. Figure 4.4 illustrates this process in more detail. A Nitinol alloy consisting of approximately equal parts nickel and titanium existing in its austenitic phase has a crystal lattice that is organized as a B2 body-centered cubic structure [33]. Upon cooling to the martensitic phase, the lattice becomes a heavily

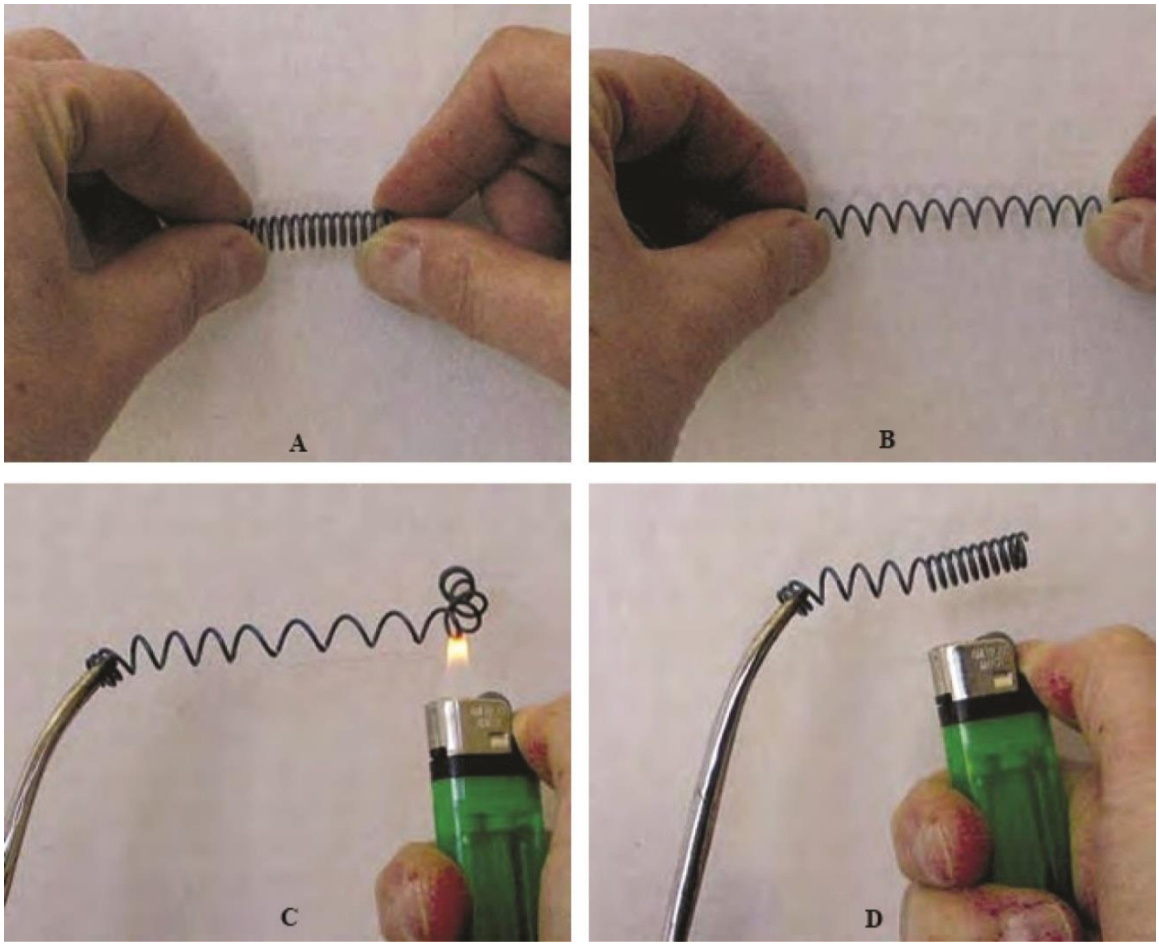

Figure 4.3: Nitinol shape-memory effect. Image modified from [32]. (A) Undeformed Nitinol in its martensitic phase. (B) Nitinol is readily plastically deformed under external loading. (C) Heating Nitinol above its phase-transformation temperature returns it to its original shape. (D) Allowed to cool, Nitinol reverts back to its martensitic phase.

twinned B19' structure [31 and 33]. In this phase, Nitinol can be deformed with an externally applied load, allowing the crystal lattice to bend significantly without severing the interatomic bonds. The process of deforming Nitinol in its martensitic phase (known as detwinning) causes the lattice structure to transform into a stretched, single-crystal orientation. Upon heating the material from this state to a temperature above its phase-transition temperature, the alloy reverts back to the initial body-centered B2 cubic structure (austenite) returning the deformed Nitinol to its original configuration [30, 31].

4.3 Superelasticity

Superelasticity (or pseudoelasticity) is the capability of certain shape-memory alloys, in a narrow temperature range slightly above the transformation temperature between martensite and austenite, to revert back to their original shape, after experiencing "substantial mechanical deformation" [31]. Figure 4.4 illustrates this phenomenon. Similar to the shape-memory regime, superelasticity is a fully reversible diffusionless phase transformation. However, the effect occurs when the material is deformed with an applied

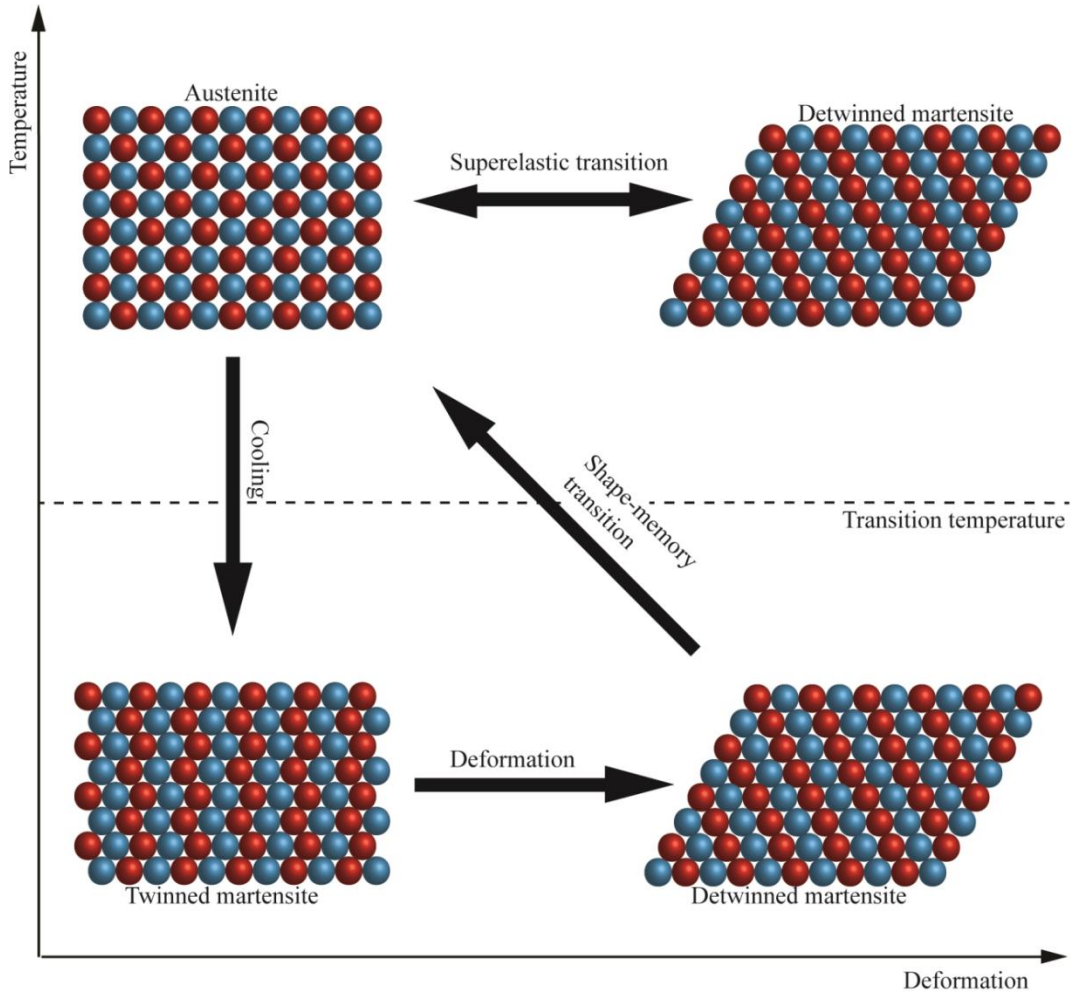

Figure 4.4: Nitinol shape-memory and superelastic phase changes as a function of temperature versus deformation.

of strain-induced martensite by virtue of the detwinning process [34]. When the material is subsequently unloaded, the strain-induced martensite immediately reverts back to the austenitic phase, causing the metal to "spring" back into its original shape [31]. Donahue [32] documented that superelastic Nitinol can absorb up to 8% strain with full elastic recovery to its initial shape, as shown in Fig. 4.5. Stoeckel and Yu [31] found that, in general, superelastic alloys can absorb ten times more strain than "ordinary" linear elastic spring materials without experiencing plastic deformation. Outer-fiber strain describes the maximum strain a superelastic alloy can withstand before plastically deforming from its initial shape. Figure 4.6 illustrates this schematically for the case of pure bending. When a Nitinol wire is bent into a circular arc as a result of bending moment *M*, the outer-fiber strain ε is computed as the ratio of half the Nitinol's thickness *r* to the radius of curvature of the arc to which it is being bent *R* [35]. Thus,

$$\varepsilon = r/R \tag{4.1}$$

The recoverable maximum outer-fiber strains of "up to 8%" typically attributed to Nitinol are limited to tensile strains because Nitinol exhibits anisotropic mechanical properties with respect to tension and compression [36]. To illustrate this, Nitinol manufacturers Johnson Matthey and NDC state that compressive strains of 3% to 4% can lead to plastic deformation, depending on the Nitinol alloy [34, 35, 37]. Our own experience suggests that for a Nitinol alloy with composition of 50.8 at% nickel and 49.2 at% titanium, plastic deformation occurs under pure bending for compressive outer-fiber strain as low as 3.5%. These results are in line with experiments performed by Saigal and Fontes, whose strain-controlled compression testing of a superelastic Nitinol wire show that the onset of plastic deformation occurs at a similar compressive strain of 3.5% [38].

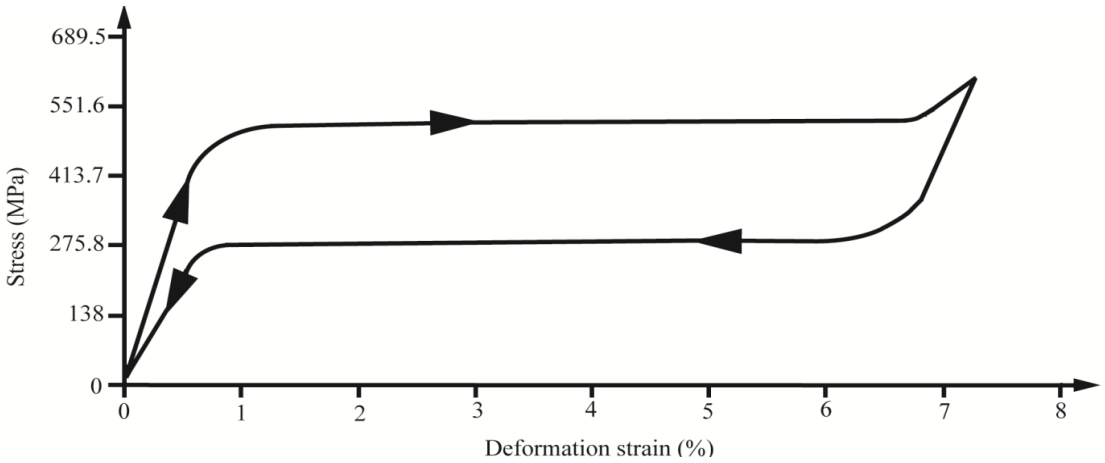

Figure 4.5: Stress as a function of strain during loading and unloading for a typical superelastic Nitinol alloy. Image modified from [34].

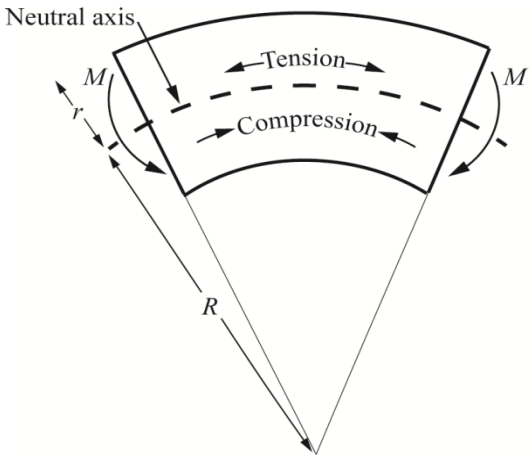

Figure 4.6: Schematic of a section of a Nitinol element subject to pure bending.

4.4 Shape-Setting

The temperature at which the shape of a Nitinol component can be permanently set is defined as the shape-set temperature, and ranges between 450°C and 550°C for any Nitinol alloy, depending to some extent on thermomechanical processing, such as cold working or annealing [30, 32, 24]. The shape-setting procedure involves deforming and constraining the Nitinol to the desired shape, and then applying heat at least until the entire cross-section of the material reaches the shape-set temperature. Pelton et al. [30]

documented that holding the temperature for longer periods, or heating to higher temperatures, results in a more permanent or robust shape-set, i.e., the shape-set Nitinol will be able to better withstand repeated external loading without deterioration to the superelastic properties, compared to when the material is heated to a lower temperature, or for a shorter period of time. However, when the material is shape-set at a higher temperature or for a longer period of time than prescribed by the manufacturer, annealing will occur, which deteriorates the superelastic properties. After the completion of the shape-set, the material must be rapidly cooled, preferably with a cold-water quench [30].

4.5 Biocompatibility

Biocompatibility refers to the severity of foreign-body reaction that occurs when a foreign material comes into contact with living tissue [28, 39]. A foreign-body reaction causes acute and chronic inflammation and infection, the magnitude of which varies with respect to the surface area and toxicity of the foreign contaminant, the degree of injury to the tissue, and to a certain extent, the physical properties of the tissue under consideration [39]. All foreign materials produce some reaction, but the intensity of that reaction depends largely on the corrosion behavior of the foreign material and its tendency to release potential toxins. The primary reason for the classification of Nitinol as a highly biocompatible material is its capability of forming a passive titanium-oxide (TiO_2) layer upon its outer surface when exposed to air. This layer acts to minimize corrosion, to the extent that surface toxicity is significantly reduced [28]. Rhyanen [28] measured the soft-tissue response to the implantation of Nitinol throughout several 26-week-long, in-vitro, soft-tissue experiments, showing no discernable toxicity and very little inflammation,

outperforming both Titanium alloy (Ti-6Al-4V) and stainless steel, two of the materials most commonly used in the biomedical field. Thus, in spite of the apparent difficulty involved in its manufacture and high associated production costs, Nitinol has become ubiquitous in the biomedical industry over the last two decades, appearing in endovascular stents, cardiovascular stents, vena cava filters, endoscopic equipment, orthodontics, ophthalmology, optometry, and many other highly specialized applications.

4.6 References

[28] Ryhanen, J., "Biocompatibility Evaluation of Nickel Titanium Shape Memory Alloy," 1999, Academic Dissertation, University of Oulu, Oulu, Finland.

[29] Duerig, T., Pelton, A., and Stockel, D., 1999, "An Overview of Nitinol Medical Applications," Materials Science and Engineering, **A273-275**, pp. 149-160.

[30] Pelton, A.R., Russell, S.M., and DiCello, J., 2003, "The Physical Metallurgy of Nitinol for Medical Applications," Journal of Metals, pp. 33-37.

[31] Stoeckel, D., and Yu, W., 1991, "Superelastic NiTi Wire," Wire Journal International, pp. 45-50.

[32] Donahue, B., 2009, "Developing a Good Memory: Nitinol Shape Memory Alloy," Today's Machining World, **March,** pp. 42-48.

[33] "B2 Martensite," 2006, from http://www.phys.shimane-u.ac.jp/ohba_lab/English/strcture1.htm

[34] "How Does it Work? All about Nitinol Shape Memory and Superelasticity," 2014, from http://jmmedical.com/resources/122/How-Does-Nitinol-Work%3F-All-About-Nitinol-Shape-Memory-and-Superelasticity.html

[35] "Surface Strains in Wire, Ribbon, and Sheet," 2014, from http://jmmedical.com/resources/271/Surface-Strains-in-Nitinol-Wire--Ribbon-and-Sheet.html

[36] Pelton, A.R., Fino-Decker, J., Vien, L., Bonsignore, C., Saffari, P., Launey, M., Mitchell, M.R., 2013, "Rotary-Bending Fatigue Characteristics of Medical-Grade Nitinol Wire," Journal of Mechanical Behavior of Biomedical Materials, **27**, pp. 19-32.

[37] "Nitinol Facts," 2014, from http://www.nitinol.com/nitinol-university/nitinol-facts

[38] Saigal, A., and Fonte, M., 2011, "Solid, Shape Recovered "Bulk" Nitinol: Part I—Tension–Compression Asymmetry," Materials Science and Engineering, **528**(16–17), pp. 5536–5550.

[39] Anderson, J.M., Rodriguez, A., and Chang, D.T., 2008, "Foreign Body Reaction to Biomaterials," Semin Immunol, **20**(2), pp. 86-100.

CHAPTER 5

SURGICAL BLADES AND SHARPNESS

Surgical blades are extremely sharp, compact blades designed specifically for the excision of biological soft tissue. These blades are often referred to as scalpels or scalpel blades, and are available in a large assortment of shapes and sizes depending on their intended function. Regardless of their particular geometry, surgical blades are constructed using the same fundamental sharpening techniques as those employed to produce any cutting instrument.

5.1 Terminology

Figure 5.1 shows the basic geometry of a cutting blade. Blade thickness refers to the width of the unsharpened portion of the blade. This is an important parameter with respect to its ability to withstand the mechanical stress and deflection imposed by the sharpening process, which is critical to achieve accurate blade geometry. The primary angle refers to the initial angle ground into the blade [40-42], and is also referred to as the primary bevel or alpha angle. The included primary angle is defined as twice the primary angle. This angle has a significant influence on the sharpness and the strength and stiffness of the blade. The strength and stiffness of the blade increase with increasing primary angle because it increases the cross-sectional area of the blade. The force required to cut increases

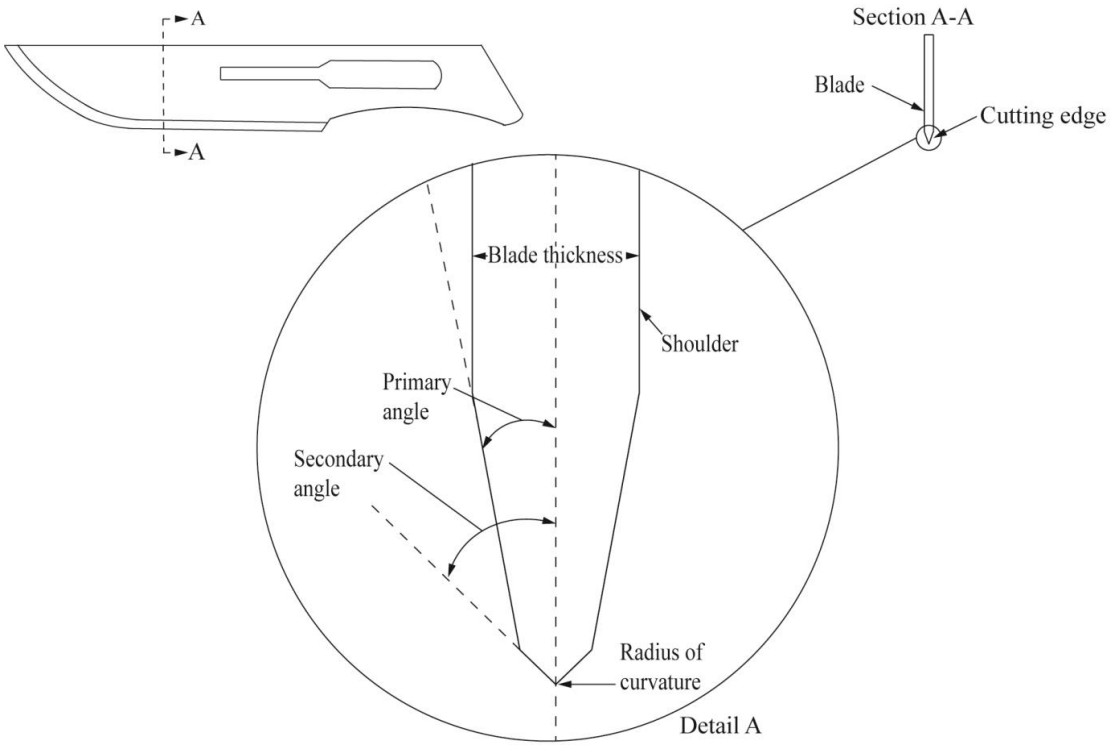

Figure 5.1: Schematic of a blade, illustrating the terminology.

with increasing primary angle because the blade is less sharp, and increased friction force is experienced during cutting [40-42]. The secondary angle is always larger than the primary angle, and is imposed along the cutting edge of the blade after the primary angle has been established. Its purpose is to increase the strength and stiffness of the blade edge, while allowing a shallow primary angle to reduce friction along the blade surface [43]. When a large primary angle is used, a secondary angle is not needed.

The radius of curvature describes the radius of the cutting edge at the termination of the edge of the blade. Similar to the primary angle, this feature has a significant influence on the sharpness of the blade [40, 42, 44]. The minimum achievable radius of curvature is dependent on the yield stress and hardness of the blade material [41, 42, 44]. Figure 5.2 illustrates the formation of the radius of curvature on the cutting edge. When yielding of

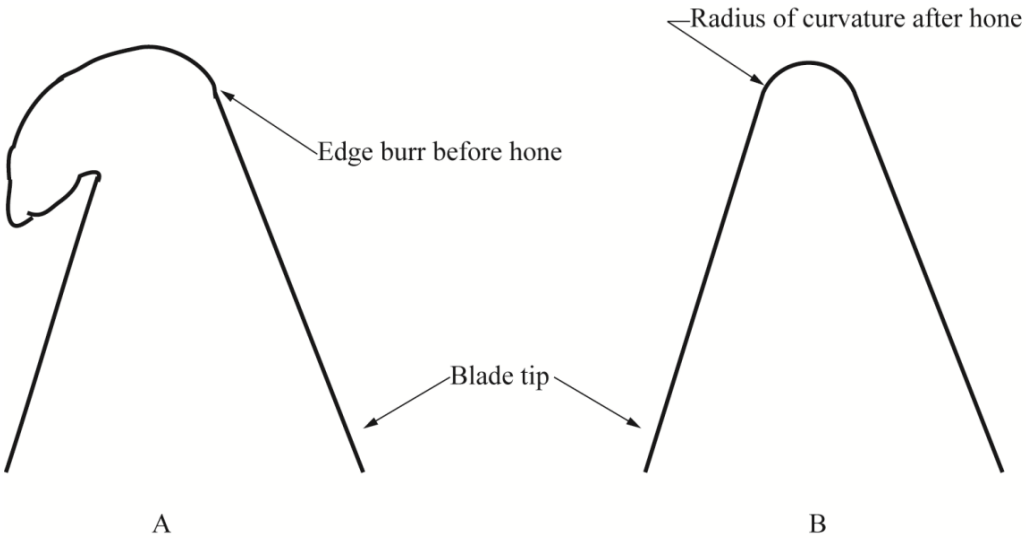

Figure 5.2: Burr formation induced from grinding the primary or secondary blade angle. (A) Edge burr. (B) Radius of curvature (equal to half the edge width). Image modified from [42].

the blade edge occurs during sharpening, the blade deforms plastically and forms a burr [42] (Fig. 5.2 A). A honing process then removes the burr, resulting in a distinctive rounding of the blade edge (Fig. 5.2 B) [42], defined as the radius of curvature.

5.2 Sharpness

No single standard definition, measurement, or protocol seems to exist to define sharpness in quantifiable terms. Instead, several different methods exist that are subject to ambiguous interpretation. One such method is based on measuring the radius of curvature of the blade edge [40, 41, 44]. Komanduri et al. [45], among others, demonstrated that the force required to penetrate a blade through a test specimen decreases with decreasing radius of curvature. Others have assumed a direct relationship between decreasing radius of curvature and blade sharpness [45-49]. However, there are other factors that affect sharpness and are not accounted for in this assessment, including the magnitude of the

primary angle, the blade thickness, and the surface finish of the blade, all of which affect the friction force experienced by the blade during cutting. In addition, the material of the blade also plays a role because it determines the resistance of the edge of the blade against deflection, thus imposing a limit on the achievable radius of curvature [42, 44, 45]. A potential complication when defining sharpness as a function of the radius of curvature is the difficulty of obtaining a precise measurement of this feature. Indeed, the radius of curvature of sharp blades is on the order of micrometers, and in some cases, tenths of micrometers. The scale of this parameter may require the use of a scanning electron microscope (SEM) to obtain a reliable measurement [43, 44, 46].

A second method commonly used to define sharpness of a blade is based on measuring, under controlled laboratory conditions, the force required to penetrate a solid material with known mechanical properties [40, 42, 44]. Although this may be a more practical alternative than the first method, it requires a large number of tests to provide meaningful statistical data [40, 41]. Gilchrist et al. [40] showed that this method is only useful for blades that are sharpened with a well-defined, repeatable manufacturing process. In their experiments, the cutting force required for factory-sharpened surgical blades to penetrate a known solid was compared to the cutting force required for the same blades artificially dulled along the cutting edge with 180-grit silica paper. Figure 5.3 A shows the load-deflection curves of three factory-sharpened surgical blades (penetration tests 1 through 3), and Fig. 5.3 B displays the load-deflection curves of the dulled blades (penetration tests 1 through 3 with a factory-sharpened blade included for comparison). The load and displacement at the point where the blades penetrate the solid material are indicated on each figure. An average blade thickness of 0.4 mm, a primary angle of 12.5°,

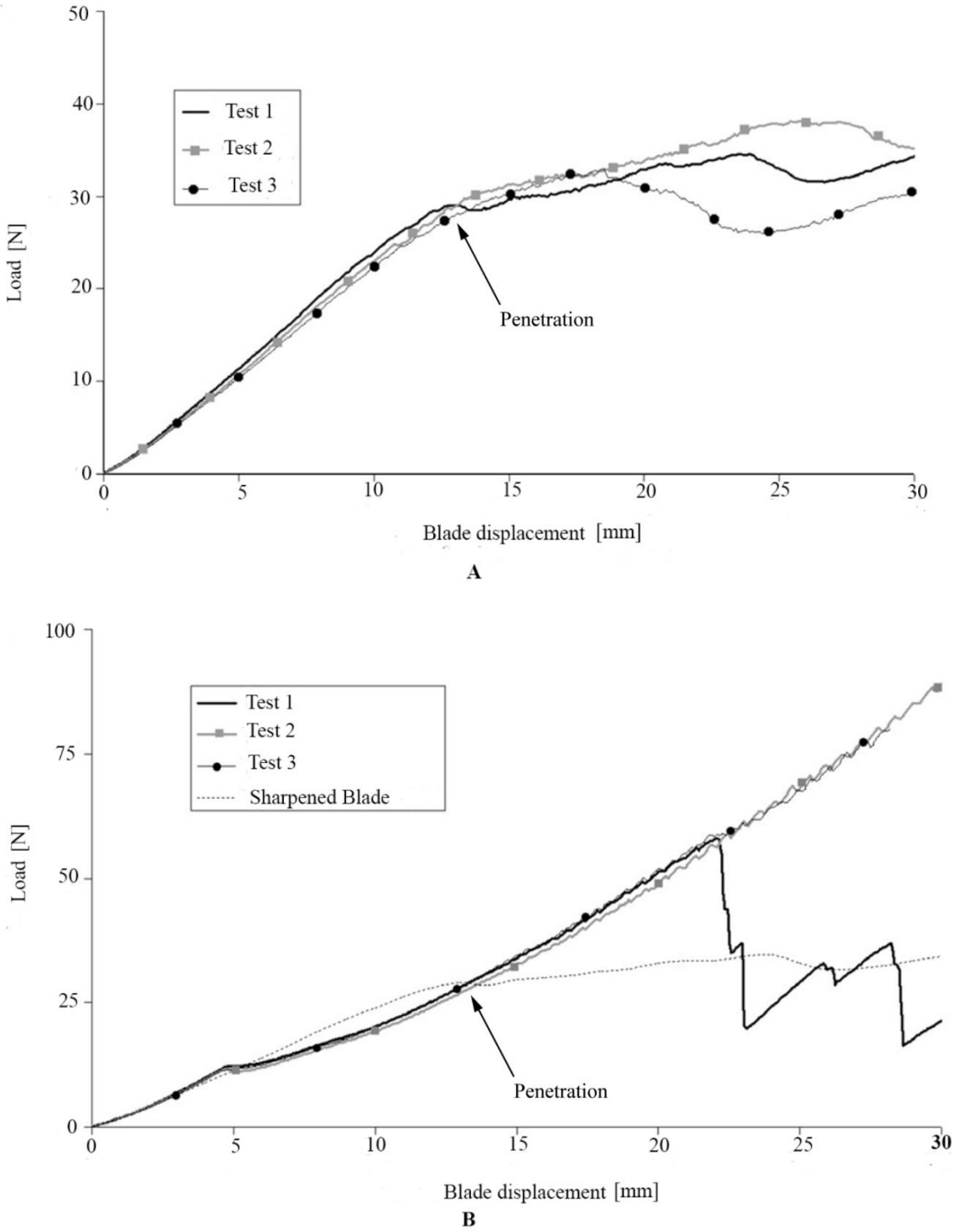

Figure 5.3: Load-deflection curves of indentation cutting with three Swann-Morton size-16 surgical blades. Images modified from [40]. (A) Factory-sharpened blades. (B) Artificially dulled blades with sharpened blade curve for comparison.

and an approximate radius of curvature of 1 micron were indicated as the principal blade-sharpness parameters. These parameters were determined using calipers and high-resolution optical microscopy. No secondary angle was imposed on the blades. The solid material was a 2.25 mm thick polyurethane sheet, chosen because it closely resembles the constitutive properties of many soft bio-solids. The authors found that the artificially dulled blades required over twice the force to penetrate the solid material than the factory sharpened blades, supporting their contention that sharpness can be defined by the amount of force required to penetrate a substance [40, 41].

Another viable method of qualifying the sharpness of a cutting instrument is to compare specific parameters of a newly designed blade to those of a blade of "known" sharpness, such as a common surgical scalpel blade or commercial razor blade [40, 41, 42]. Commercial razor blades are ubiquitous and approximately equivalent in terms of sharpness (in spite of an apparent lack of available manufacturing standards), so any commercially available razor blade should suffice for comparison. General-use scalpel blades are categorized in accordance with a numbering system based on size and shape [50]. The #20 is larger than the #10, but otherwise identical.

Consequently, a comparison of the sharpness parameters of a #10 or #20 surgical scalpel blade to those of a common household razor blade should enable the definition of a benchmark that can be used to characterize the sharpness of a blade for which sharpness is unknown or undefined. The sharpness parameters in question (namely the blade thickness, the primary and secondary blade angles, and the radius of curvature), can be closely approximated from high-resolution micrographs and/or SEM images to facilitate a comparison and thus establish a qualitative or comparative measure of sharpness for any

blade of unknown sharpness. Figure 5.4 A shows an SEM image of the cutting edge of a commercially available razor blade, and Fig. 5.4 B represents a #20 surgical scalpel blade edge for comparison. Table 5.1 summarizes the measurements of the sharpness parameters obtained for the blades shown in Fig. 5.4.

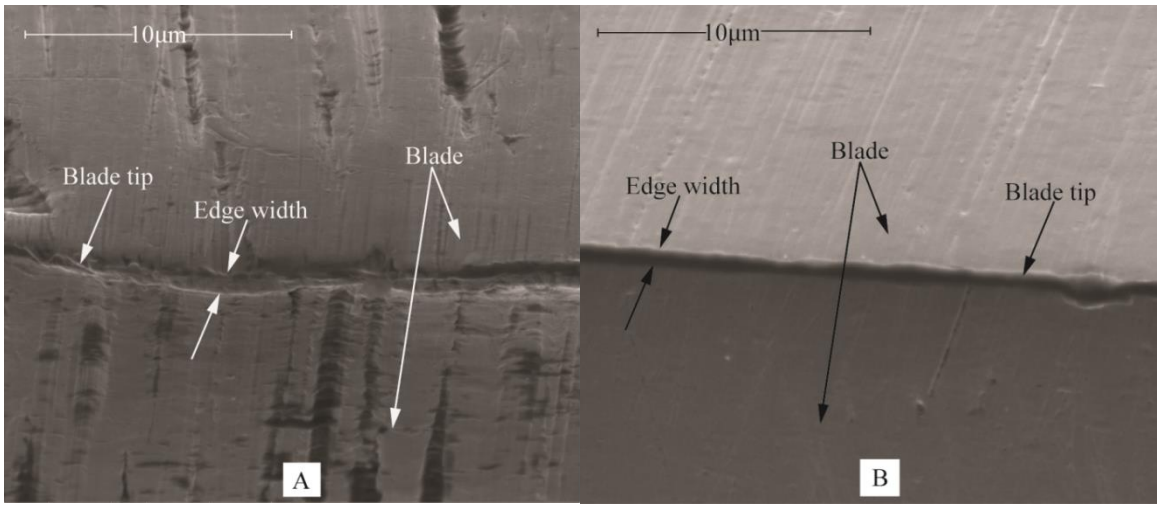

Figure 5.4: SEM images of blades. (A) SEM image of a commercial razor blade. (B) SEM image of a # 20 scalpel blade.

Table 5.1: Sharpness parameters of a #20 surgical scalpel blade and commercial razor blade.

Blade type	**Blade thickness [mm]**	**Primary angle [°]**	**Secondary angle [°]**	**Radius of curvature [µm]**
Commercial razor blade	0.400	12.0	17.0	0.765
#20 Scalpel blade	0.400	12.5	N/A	0.677

5.3 Mechanics of Sharpening

Imparting a sharp edge to any object requires material removal from the object being sharpened. This can be accomplished through a variety of means, such as chemical etching, laser etching, electrical discharge machining (EDM), and water jet cutting [51]. However, the most common method to remove material for sharpening processes involves the use of natural and man-made abrasives [46]. The material removal rate and the surface finish quality depend on the size and hardness of the abrasive particles. Coarse abrasive particles result in a high material removal rate but leave a rough surface finish, whereas fine abrasive particles result in a slow material removal rate but create a smooth surface finish [46]. The abrasives most often used in sharpening processes are grinding wheels (Fig. 5.5 A), and grinding stones (Fig. 5.5 B), in addition to various honing and polishing compounds.

Grinding stones and wheels come in a wide variety of shapes and sizes depending on the intended application. They are composed of a matrix of coarse particles embedded in a soft bonding agent [51]. The decomposition rate determines how many abrasive particles detach from the matrix, thus defining the rate at which new, unworn abrasive particles are exposed [46, 51]. The most common type of bonding agent is a vitreous ceramic compound composed predominantly of clay and feldspar [51]. Other bonding agents include silicates, resins, rubber, metals, and other compounds. The coarse particles embedded in the soft matrix determine the hardness of the abrasive. These include silicon carbide, aluminum oxide, boron nitride, sandstone, diamond, and ceramic particles [51]. Grain size and grain particle density also play a role in the wear rate of the grinding stone and surface finish of the ground cutting edge. Ascending grain size (grit) number

Figure 5.5: Grinding tools common to the sharpening process. Images modified from [52, 53]; (A) grinding wheels, (B) grinding stones.

corresponds to decreasing particle diameter (μm). Available grain sizes for grinding tools range from #8 (coarsest) to #1200 (finest), corresponding to particle diameters of 2,800 μm and 3 ± 0.4 μm, respectively. The particle density, often referred to as the grain ratio, reflects the ratio of the volume of embedded particles to the total volume of the grinding wheel. This value is represented on a unitless scale ranging from 0 to 15 (most to least dense) [54]. Figure 5.6 shows the grain matrix of three common grinding stones at high magnification, illustrating the difference in grain size and density. Figure 5.6 A, B, and C show an Arkansas stone at 1800x magnification, an aluminum-oxide stone at 1000x magnification, and a silicon-carbide stone at 1000x magnification, respectively [46]. Honing and polishing compounds are predominantly used for surface finishing after the primary and secondary angles have been ground into a tool [46]. These compounds mainly

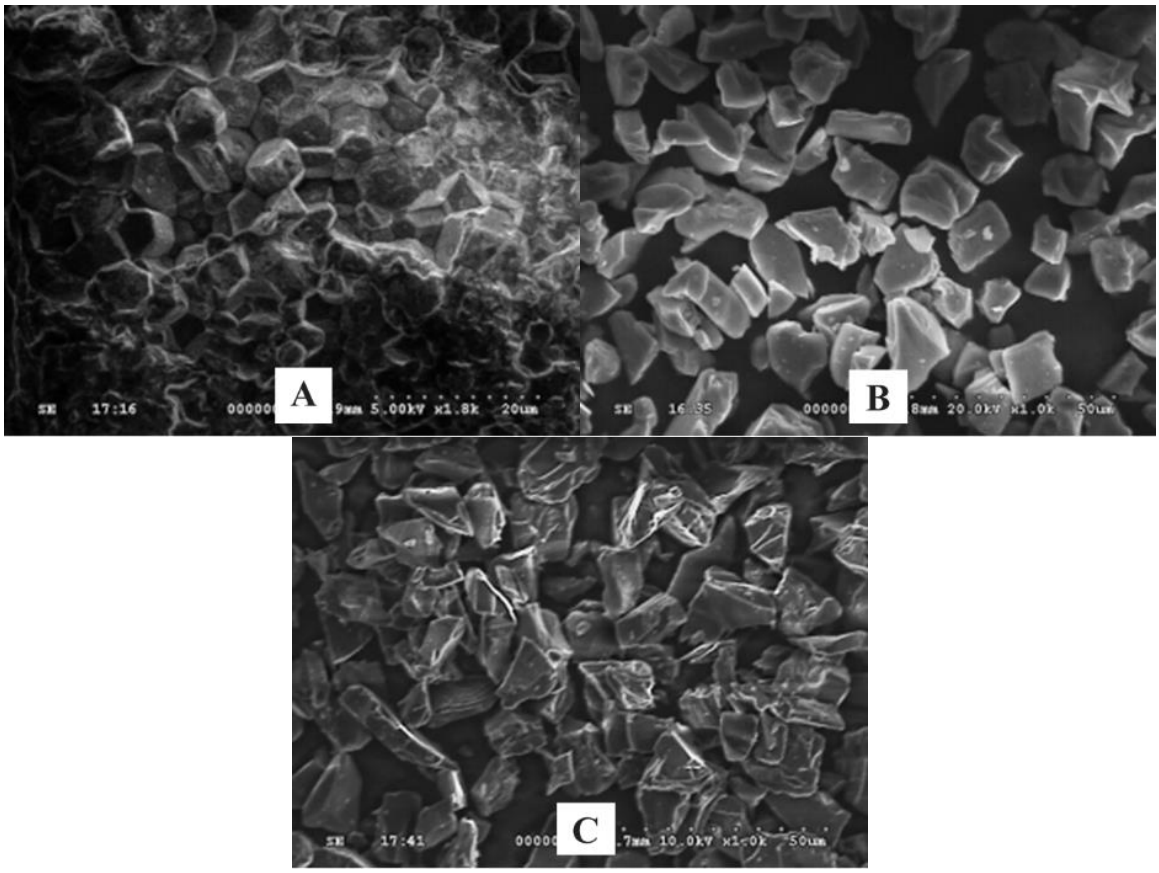

Figure 5.6: Grain images of selected grinding stones. Images modified from [46]; (A) Arkansas stone at 1800x magnification, (B) Aluminum-oxide stone at 1000x magnification, (C) Silicon-carbide stone at 1000x magnification.

consist of aluminum oxide or chromium oxide suspended in a wax bonding agent. As with grinding tools, the particle grain size and density determine the degree of the compound's abrasiveness.

Any object can be sharpened, assuming that the object used to perform the material removal is harder than the object being sharpened. Assuming a large enough hardness difference between the two, the object being sharpened can theoretically achieve a radius of curvature of zero, resulting in infinite sharpness [44]. Harder, stronger materials can be sharpened to a greater extent than softer, weaker materials because sharpening induces mechanical stress and deflection towards the sharpened edge [40-42, 44]. The harder and

stronger the material, the smaller the cross-sectional area of the blade tip that is needed to sustain the mechanical stress generated by the material removal process [44, 45]. Serrations are a special type of sharpening that are defined as a series of small, tooth-like projections imposed along the edge of cutting blades to facilitate the cutting process [55]. Figure 5.7 illustrates a typical set of serrations on the cutting edge of a blade. Serrations are desirable when attempting to cut materials that exhibit tough, fibrous, or low-friction surface characteristics, such as bone, plastics, woods, and textiles [55]. They are effective because they provide a reduced contact-area along the blade surface, causing an increase in contact pressure between the serrations on the blade and the specimen that is cut [55]. As with other sharpening procedures, serrations are most often established using an abrasive material-removal tool, usually a specialized grinding stone or wheel that has been formed with the negative of the desired serration profile embedded into its surface [55], illustrated in Fig. 5.7.

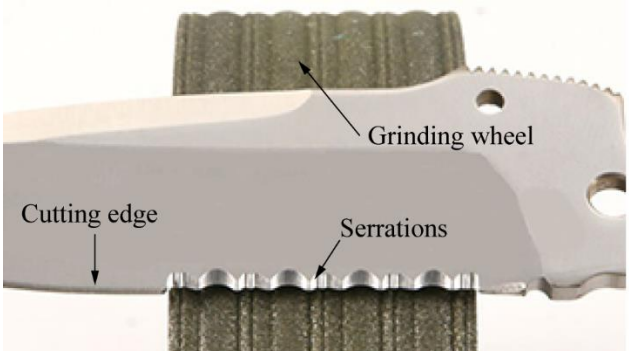

Figure 5.7: Use of a specialized serrating wheel to establish serrations on a knife. Image modified from [55].

5.4 References

[40] Gilchrist, M.D., Hussey, M., and McCarthy, C.T., 2007, "On the Sharpness of Straight Edge Blades in Cutting Soft Solids: Part I - Indentation Experiments," Engineering Fracture Mechanics, **74**(14), pp. 2205-2224.

[41] Gilchrist, M.D., Annaidh, N.A., and McCarthy, C.T., 2010, "On the Sharpness of Straight Edge Blades in Cutting Soft Solids: Part II - analysis of blade geometry," Engineering Fracture Mechanics, **77**(3), pp. 437-451.

[42] Verhoeven, J.D., "Experiments on Knife Sharpening," 2004, Technical Report Iowa State Univ., Ames IA.

[43] "Sharpening Made Easy," 1996, from http://sharpeningmadeeasy.com/Juranitch1977Feb.htm

[44] Reilly, G.A., McCormack, B.A.O., and Taylor, D., 2004, "Cutting Sharpness Measurements: a Critical Review," Journal of Materials Processing Technology, **153-154**, pp. 261-267.

[45] Komanduri, R., Chandrasekaran, N., and Raff, L.M., 1998, "Effect of Tool Geometry in Nanometric Cutting: A Molecular Dynamics Simulation Approach," Wear, **219**, pp. 84-97.

[46] Lee, L., 1995, The Complete Guide to Sharpening, Taunton Press, Newtown CT, Chap. 1,3,4,5, and 8.

[47] Yuan, J.J., Zhou, M., and Dong, S., 1996, "Effect of Diamond Tool Sharpness on Minimum Cutting Thickness and Cutting Surface Integrity in Ultraprecision Machining," Journal of Materials Processing Technology, **62**(4), pp. 327-30.

[48] Meehan, R.R., Kumar, J., Earl, M., Svenson, E., and Burns, S.J., 1999, "Role of Blade Sharpness in Cutting Instabilities of Polyethylene Terephthalate," Journal of Material Science Letters, **18**(2), pp. 93-95.

[49] Goh, S.M., Charalambides, M.N., and Williams, J.G., 2005, "On the Mechanics of Wire Cutting of Cheese," Engineering Fracture Mechanics, **72**(6), pp. 931–46.

[50] "Classification of Surgical Blades," 2004, from http://www.apexmed.eu/indeling-van-chirurgische-mesjes.html

[51] "Manufacturing Processes - Non-traditional Machining," 2004, from http://www.engineershandbook.com/MfgMethods/nontraditionalmachining.htm

[52] "Grinding Stones with Open Structures for Cooler Operation" 2014, from http://news.thomasnet.com/fullstory/Grinding-Wheels-have-open-structure-for-cooler-operation-8078

[53] “Crafts Supply U.S.A., Wood turner’s Catalog,” 2014, from http://www.woodturnerscatalog.com/t/97/Grinding-Wheels

[54] “Grinding Wheel Composition,” 2007, from http://www.keihin-kogyo.co.jp/en/products/006_toishi_kousei.html

[55] “Serrations and Sharpening on Modern, Handmade Knife Blades,” 1996, from http://www.jayfisher.com/Serrations.htm

CHAPTER 6

DEVICE DESIGN

This chapter describes the design of the Helicotome. Design specifications are generated based on the design concept and task requirements, and are used to determine the final device geometry and dimensions.

6.1 Design Specifications

Table 6.1 shows the specifications used in the design of this device, which are derived from the user needs and concept design. A description of each specification, including justification for the metrics used, and insight into how these metrics are verified during physical testing of the device, are discussed. The outcomes of the design can only be evaluated after the completion of a capsulorhexis, so they are only used to inform the concept design of the Helicotome, and do not directly influence the design parameters.

6.1.1 Blade Produces a 360° Circular Cut in the Anterior Lens Capsule

6.1.1.1 Cut Diameter

The average diameter of each excised lens capsule is measured to determine if the size of the capsulorhexis is within the allowable range. Though the excised lens capsules may not be perfect circles, the diameter of each cut will be calculated by computing the

Table 6.1: List of requirements and associated design specifications.

Requirement	Metric	Units	Limit values
Produce a circular cut in the anterior lens capsule (capsulorhexis quality)	Cut diameter	mm	4-6
	Cut completion angle (without tears)	degrees	≥350
	Circularity	Non-dimensional	>0.65
Blade deploys from cannula without plastic deformation	Outer-fiber strain	%	≤ 4
Cannula fits within corneal incision	Cannula diameter	mm	< 1.9
Blade fits within cannula	Blade height	mm	< 1.5
Blade is sharp	Radius of curvature	μm	< 5
	Included primary angle	degrees	< 30
Device reduces procedural time	Procedure duration	sec	< 120

area of the excision using image processing software and computing the diameter of a circle with the same area.

6.1.1.2 Cut Completion Angle

The cut completion angle is the angle over which the lens capsule is cut after using the Helicotome. While removing the lens capsule, the uncut portion of the full circle, which needs to be removed by tearing, is measured and subtracted from 360° to determine the cut completion angle. This is done by taking an image of the incomplete cut, marking the ends of the cut, and imposing an opaque protractor over the image to determine the angle. The cut must also be completed without creating any tears that compromise the structural integrity of the lens capsule (see Section 1.2).

6.1.1.3 Circularity

The minimum bounding circle (the smallest circle that can contain a closed shape) for an excision will be calculated by implementing an edge detection algorithm and determining the largest distance between points along the perimeter. Next, the area of the minimum bounding circle will be calculated. Finally, the circularity will be calculated as the area of the excision divided by the area of the minimum bounding circle. Note that a circularity of 1 represents a mathematically perfect circle.

6.1.2 Blade Deploys from Cannula without Plastic Deformation

6.1.2.1 Outer-fiber Strain

Outer-fiber strain is defined as the ratio half the Nitinol's thickness to the radius of curvature of the arc to which it is being bent (see Section 4.2). To exhibit superelastic behavior without incurring plastic deformation, the Nitinol blade must fall within the outer-fiber strain constraints. This is calculated to ensure the necessary constraints are met.

6.1.3 Cannula Fits within Corneal Incision

6.1.3.1 Cannula Diameter

The outer diameter of the cannula needs to be sufficiently small to fit within the 2 to 3 mm corneal incision, which results in a circular opening with a circumference of 4 to 6 mm and a diameter of 1.2 to 1.9 mm.

6.1.4 Blade Fits within Cannula

6.1.4.1 Blade Height

The cross-section of the blade is sufficiently small to fit within the cannula, i.e., the blade height must be smaller than the inner diameter of the cannula.

6.1.5 Blade is Sharp

6.1.5.1 Radius of Curvature of the Cutting Edge

Optical microscopy and/or scanning electron microscopy are used to measure the radius of curvature of the sharpened edge. This measurement is compared to that of other surgical blades to determine the sharpness of the Nitinol blades. The cutting edge of scalpels and other surgical blades typically has a radius of curvature on the order of 1 μm.

6.1.5.2 Included Primary Angle

The included primary angle of the blade is an important factor in determining its sharpness and is defined as twice the primary angle (see Section 5.1). This angle is set prior to sharpening, and is not further verified. Scalpels and other surgical blades used for cutting soft tissue typically have included primary angles of 12.5 degrees.

6.1.6 Device Reduces Procedural Time

6.1.6.1 Procedure Duration

To be financially advantageous, the use of this tool must reduce the time required to perform the capsulorhexis. The time between insertion of the tool and extraction of the excised tissue is recorded and compared with current methods.

6.2 Final Helicotome Design

The Helicotome consists of a 38 mm long cannula with an inner diameter of 1.22 mm and an outer diameter of 1.45 mm. This enables the cannula to be inserted into a standard 2 to 3 mm (1.27 to 1.91 mm diameter) corneal incision during the capsulorhexis procedure. The Helicotome is shown in Fig. 3.3 in Section 3.2.

The Nitinol element is 0.16 mm thick, 0.84 mm wide, and 79 mm long, with the most distal 32 mm formed into a helix. For these dimensions, the outer-fiber strain experienced by the blade is approximately 3.15%, which falls within the allowable range set by the design specifications. Of the portion formed into a helix, a blade is ground into the most distal 16 mm (approximate). The proximal 47 mm straight portion of the Nitinol element is affixed to the slider and knob.

The blade is formed into a 5 mm diameter helix with a 5° helix angle, corresponding to a 1.25 mm pitch. A schematic of the helical blade is shown in Fig. 3.1 of Section 3.2. The blade is ground with a 25° included primary angle and a 30° secondary angle. This is larger than typical surgical blades, but due to the lower hardness of Nitinol compared to 316 stainless steel, a larger angle is used to provide strength to the cutting edge of the blade. The secondary angle adds strength and stiffness along the blade edge and decreases friction between the blade and the soft tissue while cutting. It is speculated that an included primary angle as small as 12.5° could increase sharpness. However, our equipment and fixtures limit the angle to around 25°, which we empirically found to be sufficient. The final dimensions of the Helicotome fall within the allowable limits set by the design specifications, and are based on the concept design. The following chapter details the process used to fabricate the device.

CHAPTER 7

DEVICE FABRICATION

This chapter details the fabrication of the Helicotome prototype described in Chapters 3 and 6. The blade is sharpened, thermally shape-set, and assembled into the body of the tool.

7.1 Sharpening

The Nitinol blade is sharpened using the Tormek T-3 sharpening system shown in Fig. 7.1. The system utilizes a wet-stone grinding process with a wheel rotation frequency of approximately 2 Hz. Before use, the stone is leveled using the Tormek Truing Tool, shown in Fig. 7.2, to ensure that the grinding stone is flat, which facilitates consistent sharpening across the width of the stone. The truing tool, which consists of a tip of diamond grit embedded into a copper matrix, is mounted to the universal support and leveled with the highest point of the stone. The truing tool is then panned across the surface of the stone, taking approximately 90 seconds to go from one side of the stone to the other. The truing tool is lowered in increments of 0.13 mm, and the process is repeated until the grinding surface of the stone is level.

Ribbon-shaped Nitinol, with a transition temperate of approximately 10°C(approximately 50.65% nickel, 49.35% titanium (at%)), cold drawn with 30% cold

Figure 7.1: Tormek T-3 Sharpening System.

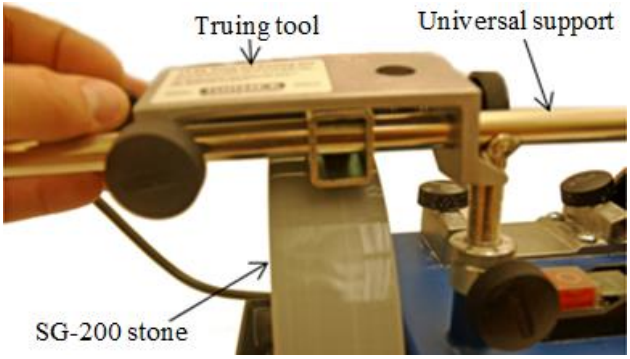

Figure 7.2: Truing the SG-200 stone.

work, is used. Figure 7.3 shows the geometry of the ribbon with dimensions 100 mm by 0.16 mm by 0.84 mm. The ribbon is mounted to the sharpening fixture shown in Fig. 7.4 and made from a 45 mm by 16 mm 20-gauge steel sheet (0.91 mm thick). The Nitinol ribbon is aligned with the edge of the fixture using clear adhesive tape, and then fixed in place using cyanoacrylate adhesive (CA) and CA accelerant (to ensure complete bonding). The adhesive is applied at the interface of the ribbon and the fixture using a stylus.

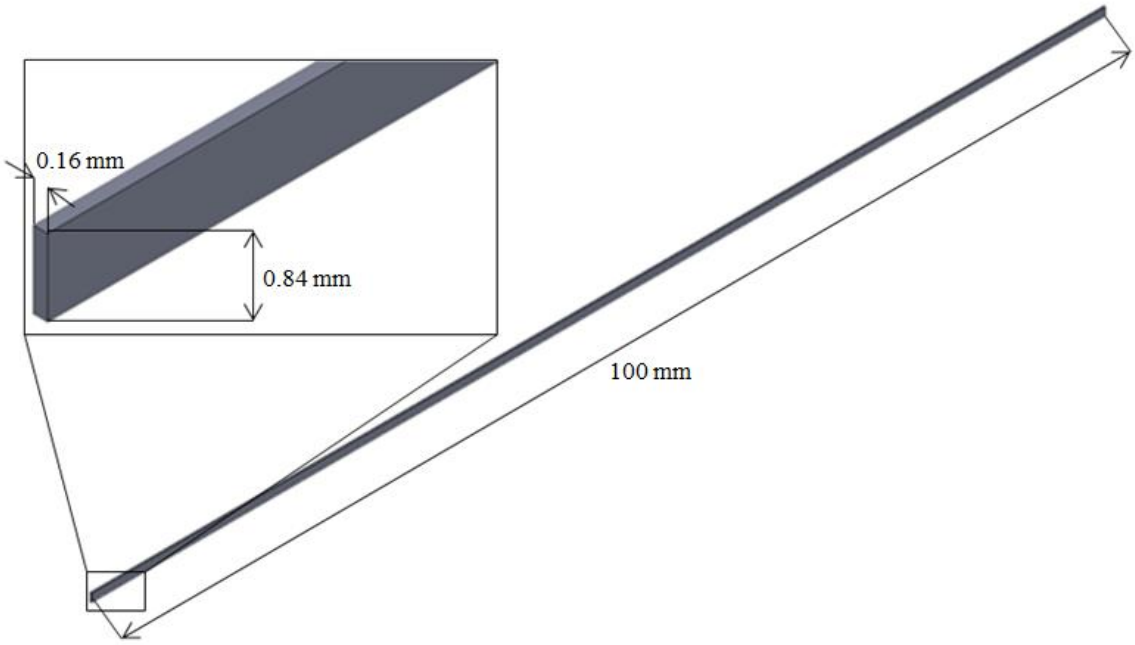

Figure 7.3: Schematic of the Nitinol ribbon with inset showing a magnified view of the ribbon cross-section.

The tape is removed and the adhesion process is repeated on the other side of the ribbon.

The sharpening fixture is mounted in the Tormek Knife Jig, such that the exposed portion of the fixture is constant across the width of the jig to ensure the blade makes even contact when placed on the grinding stone. The universal support is adjusted so that the blade is at a 12.5° primary angle with respect to the tangent of the contact point on the grinding stone; this will result in a 25° included primary angle after the ribbon has been sharpened on both sides. The angle is verified using the Tormek Angle Finder.

The Nitinol ribbon is then sharpened using the SG-200 200-grit grinding stone (Fig. 7.5). Each side of the ribbon is left in contact with the grinding stone for 60-90 seconds, under its own weight, which will establish the included primary angle of the blade. The knife jig is flipped over and the process is repeated on the other side of the ribbon. Upon

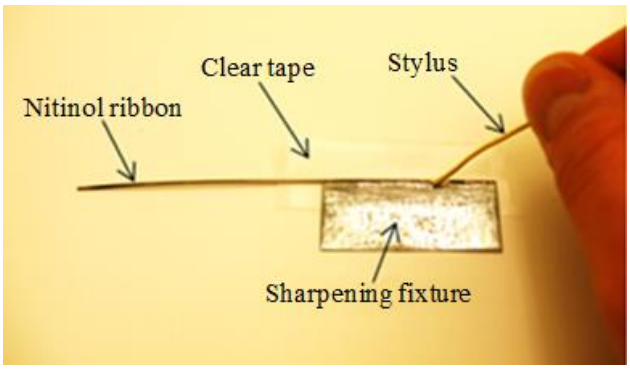

Figure 7.4: Alignment and adhesion of the Nitinol ribbon to the sharpening fixture.

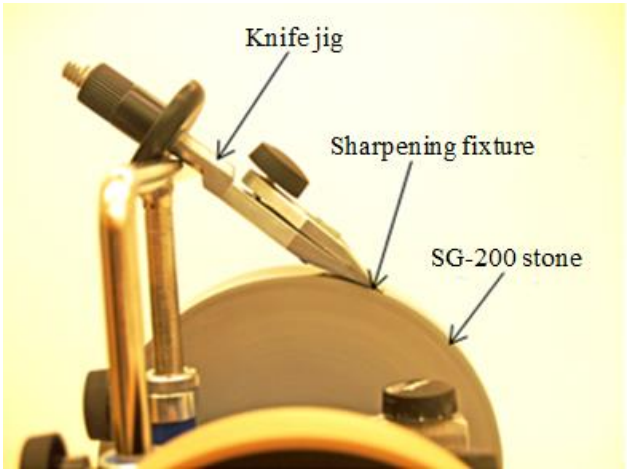

Figure 7.5: Sharpening on the 200-grit stone.

completion, the blade is inspected using an optical microscope to verify that a discernable burr exists on the sharpened edge (Fig. 7.6).

To further sharpen the cutting edge of the blade, and reduce the radius of curvature of the cutting edge, it is ground on progressively finer-grit stones. Figure 7.7 shows the Tormek Stone Grader pressed onto the SG-200 stone. Using different types of stone graders enables converting a 200-grit stone into finer grits. For instance, when pressing the fine side of the Tormek Stone grader for approximately 30 seconds with moderate pressure onto the 200-grit stone, the surface is converted to a much finer 1000-grit. Prior to sharpening

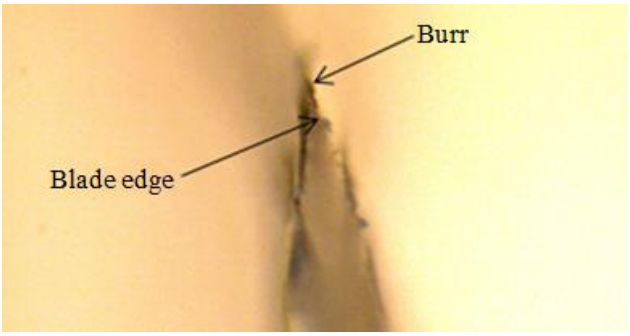

Figure 7.6: Optical inspection of the blade at 4.5x magnification after 200-grit sharpening.

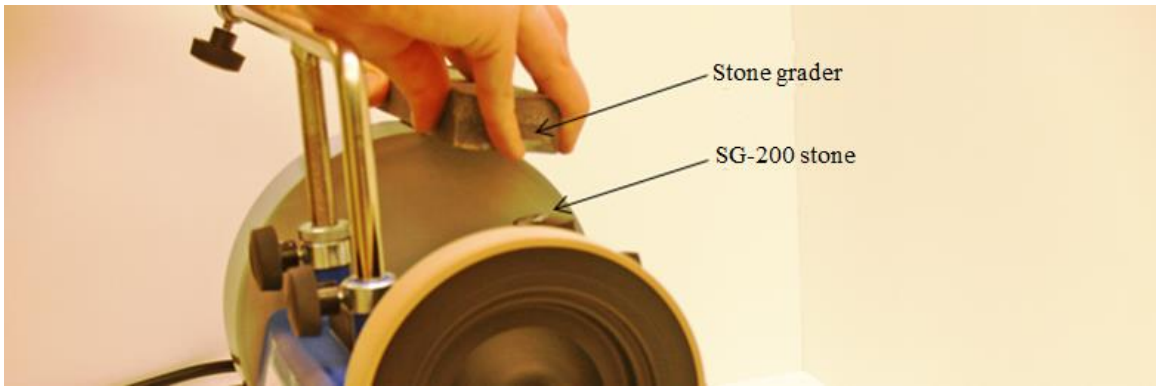

Figure 7.7: Grading the SG-200 stone to 1000-grit.

the blade on the 1000-grit stone, the ground surface of the blade is colored with a permanent marker to facilitate visual confirmation that the blade is being evenly sharpened. The knife jig is rested on the universal support at the same 12.5° primary angle, and the blade is sharpened on the 1000-grit stone for 30 seconds. The knife jig is flipped, and the other side of the blade is sharpened. After sharpening, the blade is optically inspected (Fig. 7.8).

Although the surface finish and sharpness of the blade is greatly improved after using the 1000-grit stone, the radius of curvature of the blade edge is still too large to yield sufficient sharpness. The radius of curvature is further reduced by sharpening the blade on the SJ-200 4000-grit Tormek Japanese Waterstone, shown in Fig. 7.9. After truing the

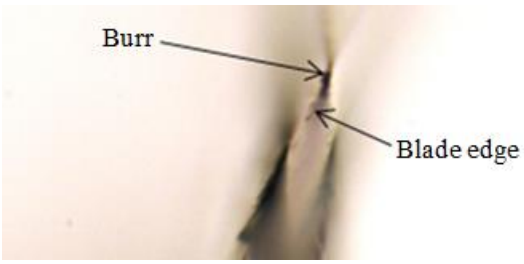

Figure 7.8: Optical inspection of the blade at 4.5x magnification after 1000-grit sharpening.

stone, the blade is colored again with a permanent marker and set at a 15° angle to the stone; this will create a 30° included secondary angle in addition to the existing 25° included primary angle. The blade is sharpened on the Waterstone for 30 seconds per side. Some additional light pressure may be utilized to ensure even sharpening of the blade.

Next, the blade is honed using the leather Tormek Honing Wheel, shown in Fig. 7.10, which is conditioned with light machine oil and impregnated with the Tormek Honing Compound. The knife jig is placed on the honing wheel at a 15° angle such that the wheel is rotating away from the blade edge. The blade is panned across the wheel at a rate of approximately 100 mm per minute. This is done five to seven times to ensure complete honing of the blade edge. The knife jig is flipped over, and the other side of the blade is honed. After honing, the blade is buffed by hand using a buffing wheel rotated away from the blade edge to remove any remaining particles or honing compound (Fig. 7.11). The final optical inspection of the blade is performed to verify the quality of the blade edge (Fig. 7.12).

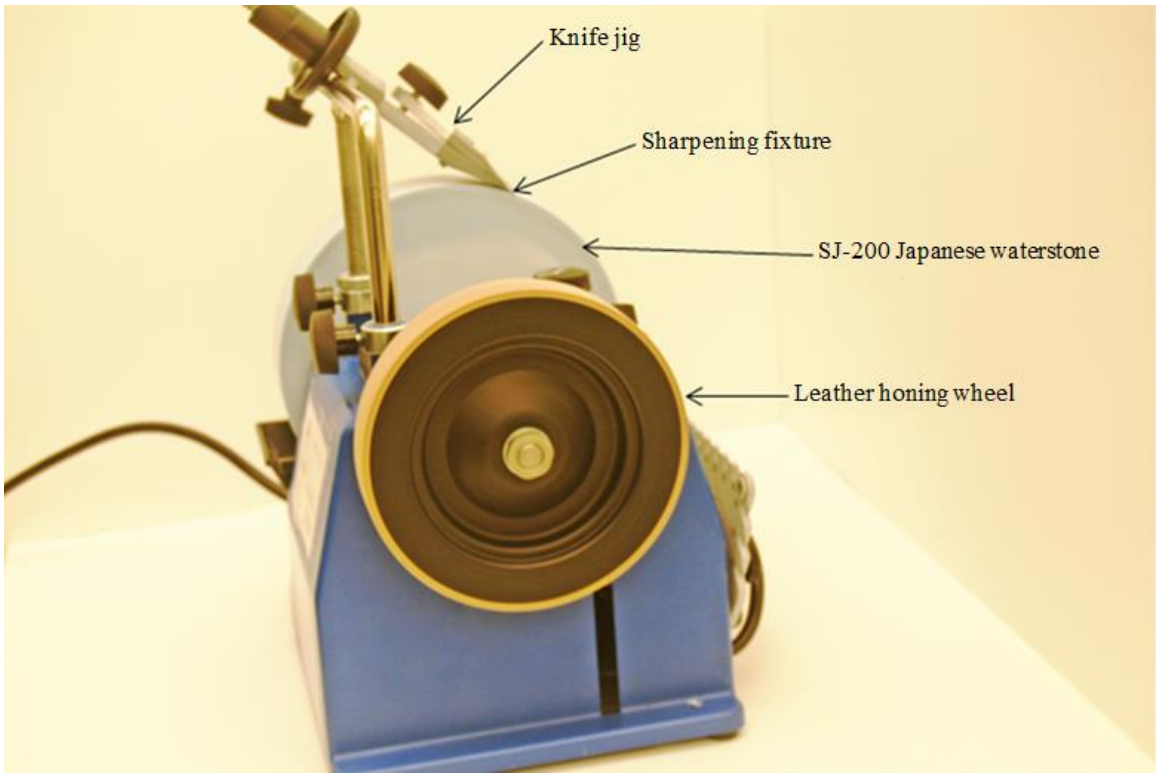

Figure 7.9: Sharpening on the 4000-grit Japanese Waterstone.

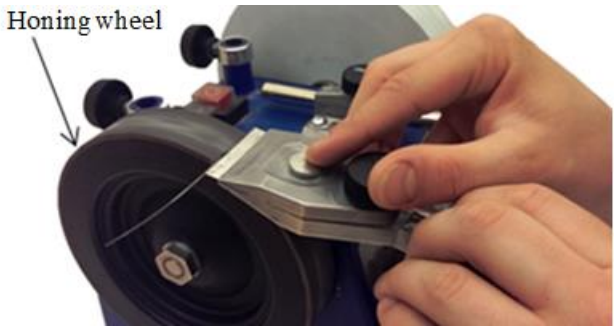

Figure 7.10: Honing the blade on the leather honing wheel.

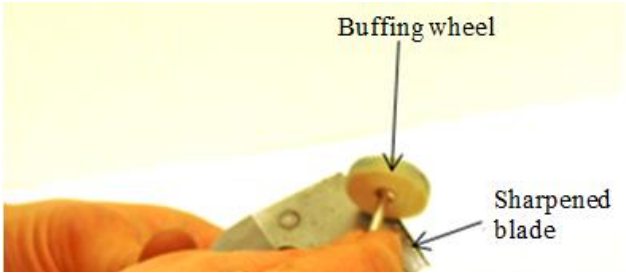

Figure 7.11: Buffing the blade after sharpening.

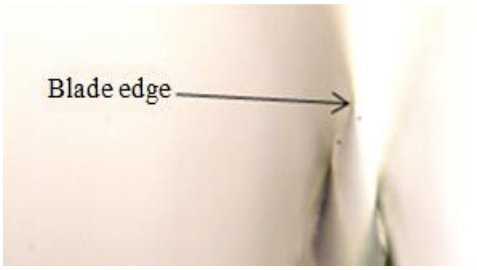

Figure 7.12: Post-buffing inspection of the blade at 4.5x magnification.

7.2 Shape-setting

To obtain the desired helix shape of the blade (see Chapter 3), it is thermally shape-set. The shape-set process includes forming the blade into the desired shape, securing it, and heating the material to the shape-set temperature of the Nitinol alloy. The duration of heating depends on the size of its cross-section, as one must ensure that the entirety of the material is heated. For the alloy and ribbon dimensions used in this work, the shape-set temperature is 550°C, maintained for 15 minutes. Figure 7.13 shows the shape-set device we have designed to form and secure the blade into the desired geometry. The sharpened blade is inserted into a through-hole in the shape-set device, such that the blade edge is facing down toward the short end of the spindle. The blade and spindle are inserted into a hollow cylindrical tube (winder) and secured in a vice, such that the blade extends out of a channel cut in the winder (Fig. 7.14). The spindle is rotated clockwise and the blade is drawn into the cylinder, where it will form the desired helical shape. The blade is wound three full rotations into the cylinder, such that there is a 5° helix angle, which corresponds to a 1.25 mm pitch (per revolution of the helix). Figure 7.15 shows the assembled shape-set fixture being inserted into a tube furnace for the heat treatment.

Once the Nitinol has been shape-set, the fixture and Nitinol blade are rapidly

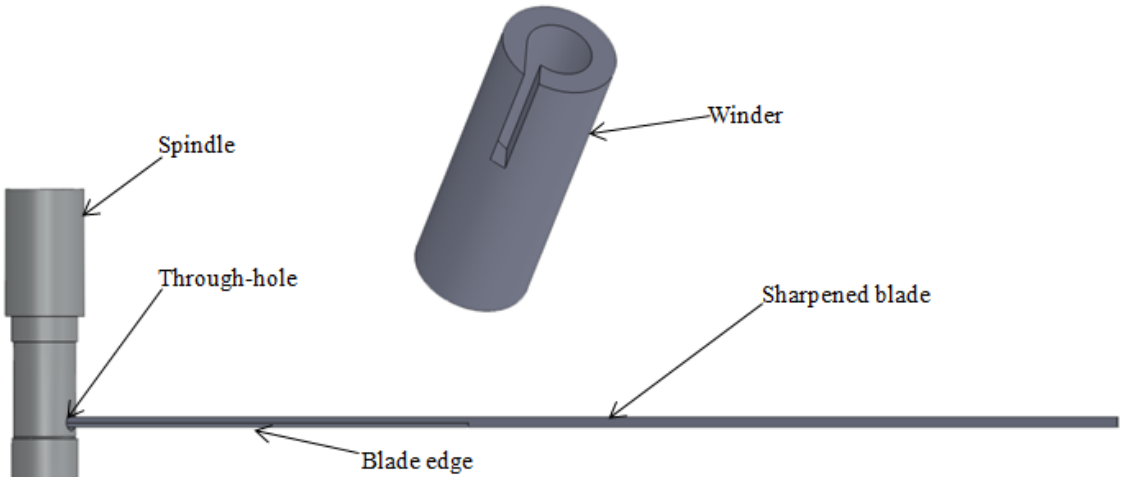

Figure 7.13: Sharpened blade inserted into the shape-set spindle.

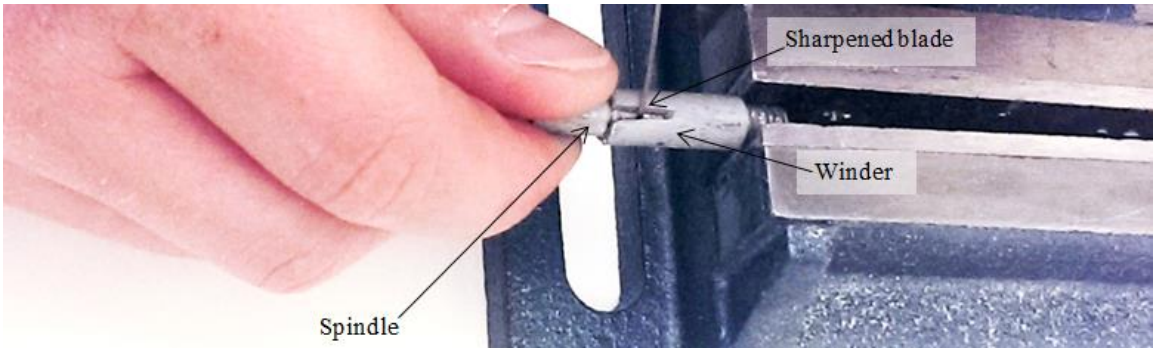

Figure 7.14: Winding the blade into the shape-set fixture.

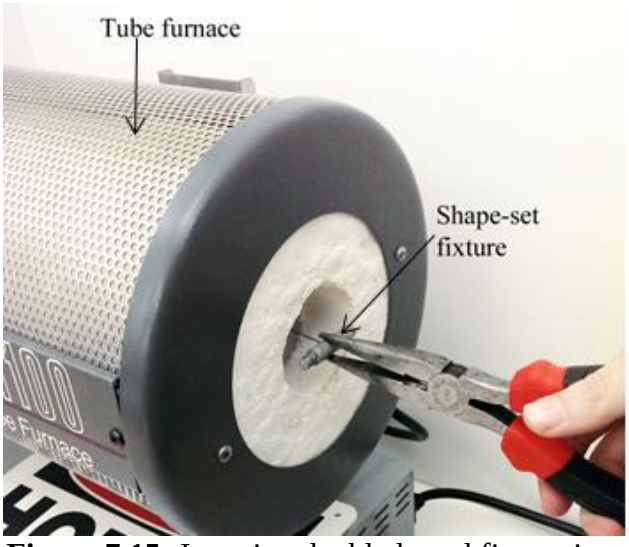

Figure 7.15: Inserting the blade and fixture into the furnace for shape-setting.

quenched in cold water to preserve the new shape. The shape-set blade is then removed from the shape-set device. Due to the insertion of the blade into the through-hole of the spindle, there is an undesired portion at the end of the blade that is trimmed using a pair of wire-cutters, such that the remaining helix wraps two full turns (720°), as shown in Fig. 7.16.

7.3 Tool Assembly

The body of the Helicotome prototype is built upon an existing disposable eye-surgery tool, the Malyugin-Ring injector. Figure 7.17 shows the disassembled injector. The plastic portion of the tool containing the cannula is pulled off using pliers, the knob and slider are removed from the handle, and the knob is removed from the slider. The following modifications are made. First, the cannula and ring-deployment mechanism are removed from the injector. Next, the original cannula is replaced by a 38 mm long stainless-steel hypodermic cannula with an inner diameter of 1.22 mm and an outer diameter of 1.45 mm. The cannula is secured in the plastic head of the tool using CA adhesive. The back 19 mm are cut off for ease of handling and ergonomics. Finally, the slider path is elongated to facilitate 32 mm of slider travel. After these modifications are complete, the final tool is assembled. The shape-set blade is inserted into the cannula with the helical portion exposed, and the proximal, non-sharpened portion of the Nitinol ribbon is trimmed level with the plastic head (Fig. 7.18).

The proximal end of the Nitinol ribbon is attached to the slider. The slider is inserted into the handle, and the tool head and handle are snapped into place. The proximal end of the blade is positioned in the opening at the tip of the slider, such that approximately 2.50

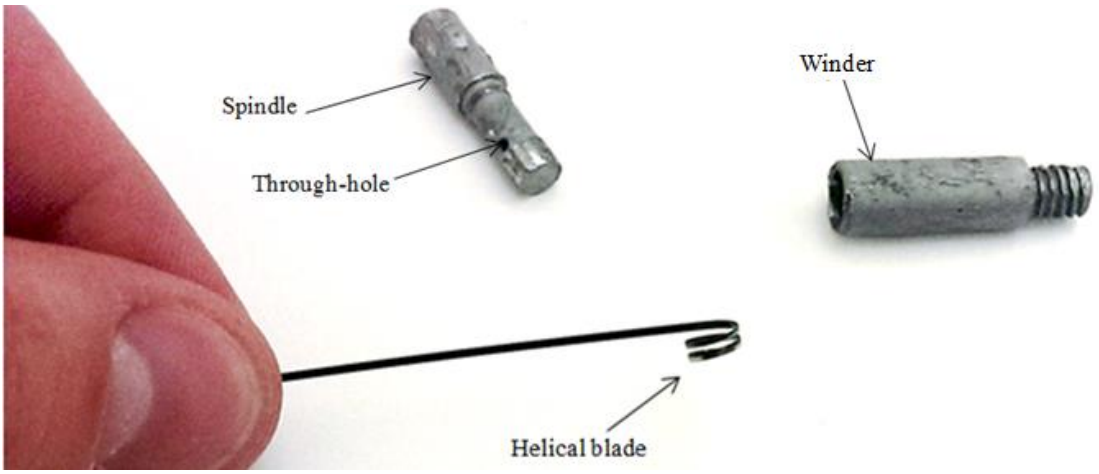

Figure 7.16: Completed, shape-set, helical blade.

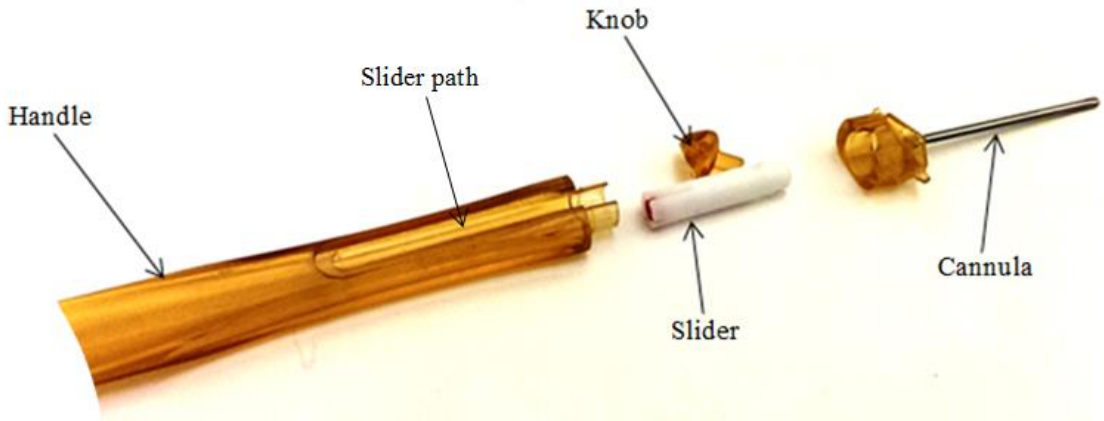

Figure 7.17: Disassembled Malyugin-Ring injector with modified cannula, shortened back end and extended slider path.

mm of the proximal end of the blade is exposed within the knob opening of the slider (Fig. 7.19) to ensure a robust connection. However, if too much of the ribbon is exposed within the knob opening, the ribbon will protrude out of the bottom of the opening and the end of the ribbon will scrape along the inside of the handle. This adds excessive friction to the system and can lead to damage of the handle or slider, or possibly disruption of the smooth action that is required by the surgeon during use.

Without retracting the blade or moving the slider, the knob is inserted into the

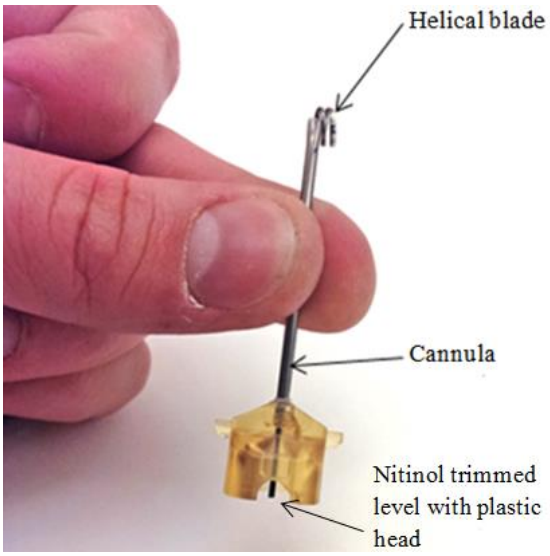

Figure 7.18: Insertion of the Nitinol ribbon into the cannula.

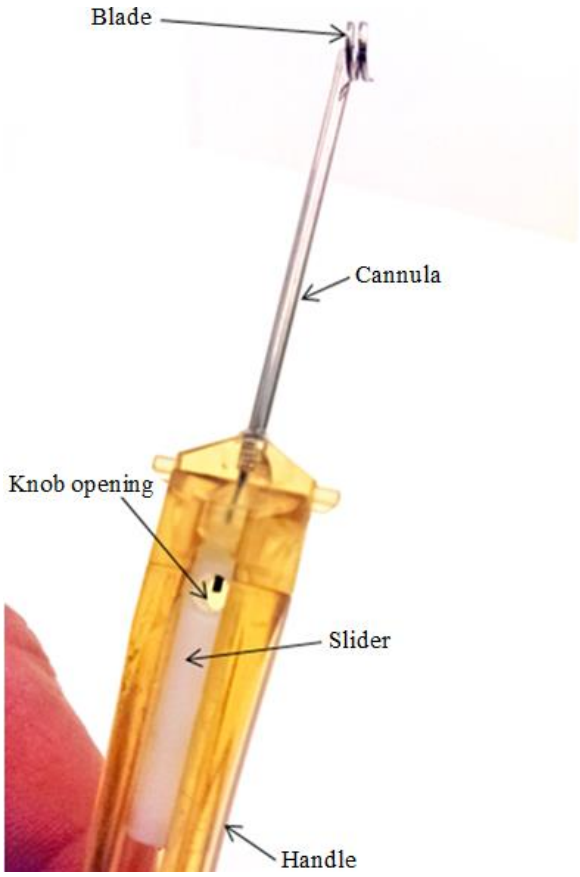

Figure 7.19: Assembly of the Nitinol element, cannula, handle, and slider.

opening in the slider and depressed fully with the thumb (Fig. 7.20). There is a groove in the portion of the knob that is inserted into the slider to facilitate proper insertion of the original mechanism of the Malyugin-Ring injector. However, to properly secure the Nitinol ribbon within the modified injector, the knob must be inserted into the slider with the groove facing away from the Nitinol ribbon (i.e., toward the handle end of the tool). Doing so provides a tight fit between the knob, Nitinol ribbon, and slider, which prevents the ribbon from slipping out of the slider.

Once the modified Malyugin-Ring injector is fully assembled, the tool can be prepared for use. To retract the tool, the handle is gripped with the right hand, placing the index finger on the knob (Fig. 7.21A). Next, the index finger is slid back toward the proximal end of the tool in a smooth, controlled motion (Fig. 7.21B). With the blade fully retracted within the cannula, the tool is ready to be safely transported, and used in a clinical setting (Fig. 7.21C).

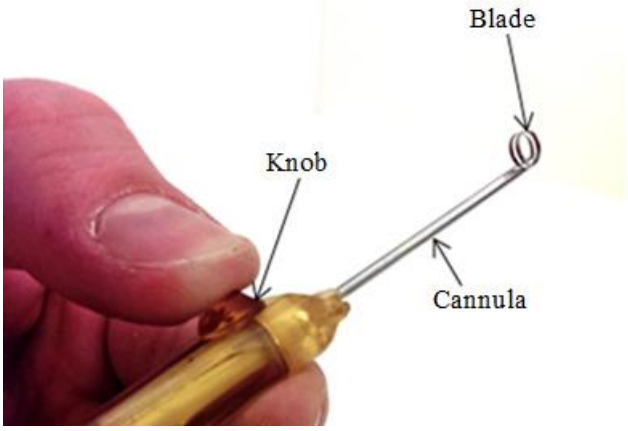

Figure 7.20: Securing the Nitinol element by inserting the knob.

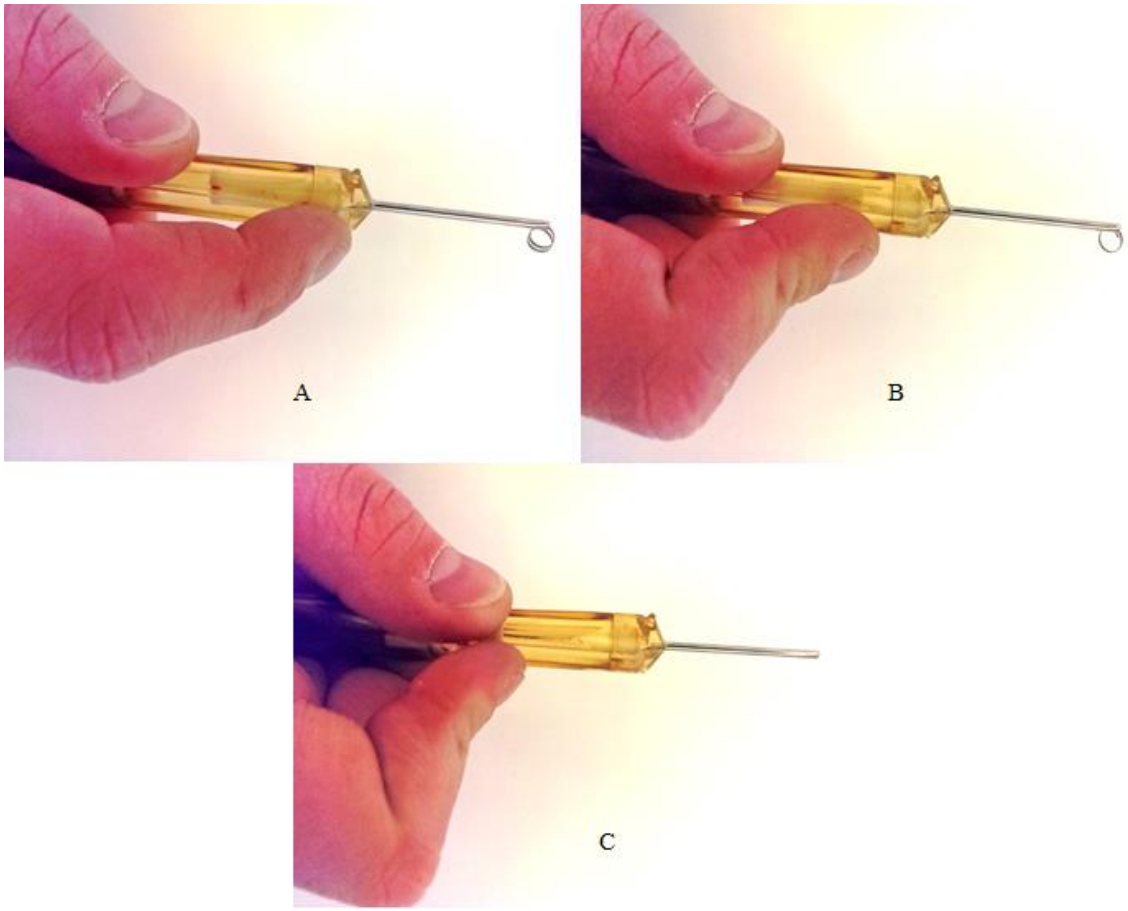

Figure 7.21: Deployment of the Helicotome, Blade fully deployed (A), being retracting (B), and fully retracted into the cannula (C).

CHAPTER 8

VERIFICATION AND RESULTS

Verification testing evaluates whether all design specifications have been satisfied [56]. It is performed on all newly designed devices, in accordance with the Code of Federal Regulations (CFR) Title 21 820.3. Its primary purpose is to ensure the safety of the patient on whom the device is used.

8.1 Verification Testing Criteria, Results, and Discussion

The verification testing criteria to characterize a potential blade design are derived from user needs, and translated into product specifications. These product specifications are described in detail in Chapter 6. Each verification testing criterion quantitatively verifies whether a product specification has been met. We have performed 17 bovine and three human capsulorhexis experiments to obtain the verification data. The capsulorhexis experiments are performed on cadaver eyes with the corneas removed, unlike a typical capsulorhexis where the procedure is performed through a small incision in the cornea. Removing the cornea facilitates retrieval and verification of the excised lens capsules. The Helicotome's ability to perform a standard capsulorhexis, i.e., with the cornea in place, is discussed in the Validation section of this chapter. The verification testing criteria are based on the following metrics and their respective tolerances.

8.1.1 Cut Diameter

According to Dr. Ambati, the diameter of each excised lens capsule must be within 4.00 mm to 6.00 mm to achieve an optimal visual outcome.

8.1.2 Cut Completion Angle

A successful cut requires a cut completion angle of 350° to 360º, because otherwise the surgeon must manually complete the cut, which (1) defeats the purpose of the Helicotome and (2) allows for complications to occur. Although a 360° cut is ideal, a 350º cut may be acceptable in a clinical environment, where the remainder of the circle can be manually removed with little to no adverse effect on the surrounding tissue, as in a traditional manual procedure. The cut must also be completed without creating any tears that compromise the structural integrity of the lens capsule (see Section 1.2).

8.1.3 Circularity

The circularity of the cut must be greater than 0.65 to exceed the lower limit of circularity produced by manual capsulorhexis [57]. This will ensure that the Helicotome produces excisions that are at least as circular as the manual method of capsulorhexis.

8.1.4 Outer-fiber Strain of the Nitinol Material

This value must be less than 4% to avoid plastic deformation of the Nitinol material during retraction of the blade into the cannula. See Section 4.2 for a detailed description.

8.1.5 Cannula Diameter

The outer diameter must be smaller than 1.9 mm to fit within the corneal incision.

8.1.6 Blade Height

The dimensions of the cross-section of the blade must be smaller than the inner diameter of the cannula (1.21 mm) to prevent damage to the blade inside the cannula.

8.1.7 Radius of Curvature

The radius of curvature of the blade edge (see Chapter 5) must be less than 5 μm, which is the maximum radius of curvature for a "sharp blade" [58].

8.1.8 Included Primary Angle

The angle imposed on the blade during the sharpening process must be less than 30º.

8.1.9 Procedure Duration

The use of this tool must reduce the time required to perform the capsulorhexis to less than 120 seconds which, according to Dr. Ambati, is the approximate time required to perform a manual capsulorhexis.

8.1.1 Cut Diameter

The cut diameter is approximated using an image-processing algorithm implemented in Matlab. The image of the lens capsule is converted into a black-and-white

image using a contrast threshold. Next, the area of the lens capsule in pixels is calculated and converted to mm^2 using the image size and scale bar within the image. This area is approximated as a circle, and the diameter of that circle is calculated [57]. The code used for this is presented in Appendix D. Figure 8.1 shows a lens capsule image converted to black and white. Figure 8.1 A shows the lens capsule excision with a scale of 16/64 inch in the frame where the lens capsule has been stained blue to increase visibility. Figure 8.1 B shows the black-and-white conversion.

Table 8.1 shows the measurements for excision area, the calculations for cut diameter, and whether any tears were observed while removing the lens capsule for the bovine capsulorhexis procedures. Table 8.1 shows that all 17 cut diameters are within the allowable range, resulting in a success rate of 100%. The variability of the reported cut diameters could result from imperfect surgical technique or a defect in the Helicotome's cutting ability.

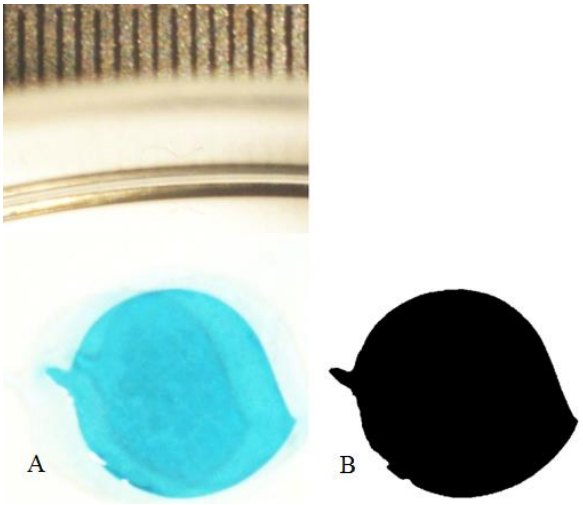

Figure 8.1: Bovine lens capsule excision with scale (A) and black-and-white conversion (B).

Table 8.1: Excision area measurements, cut diameter calculations, and tears for bovine capsulorhexis procedures.

Blade #	Excision area [mm^2]	Cut diameter [mm]
1	15.00	4.37
2	15.28	4.41
3	18.38	4.84
4	15.43	4.43
5	18.44	4.84
6	19.11	4.93
7	18.35	4.83
8	15.62	4.46
9	16.55	4.59
10	16.16	4.54
11	15.99	4.51
12	17.38	4.70
13	16.63	4.60
14	20.86	5.15
15	26.21	5.78
16	16.98	4.65
17	17.61	4.74

Table 8.2 shows the excision area, cut diameter, and observed tears obtained from capsulorhexis procedures for three human-cadaver eyes. Note that only two of the three human-cadaver experiments yield a measurable cut diameter, whereas the third experiment fails to produce results due to the fact that the third lens capsule, though fully excised, was retracted into the cannula along with the blade and could not be retrieved. Table 8.2 shows that two of the three experiments yield cut diameters within the allowable range. Hence, the success rate is at least 67%.

Table 8.2: Excision area measurements and cut diameter calculations for human capsulorhexis procedures.

Blade #	Excision area [mm^2]	Cut diameter [mm]
1	18.5	4.9
2	23.2	5.4
3	*	*

**The lens capsule could not be retrieved, so no data for the cut exists.*

8.1.2 Cut Completion Angle

The Helicotome must cut at least a 350° circular incision in the anterior lens capsule without tearing the remaining lens capsule. The cut completion angle is determined by marking the ends of the cut and overlaying a protractor on the image to approximate the angle of remaining tissue. Figure 8.2 shows the procedure. Figure 8.2 A shows an image of an incomplete excision of a bovine lens capsule. Figure 8.2 B highlights the non-excised tissue, and Fig. 8.2 C shows the image of a protractor imposed over the lens capsule to approximate the angle of the remaining tissue.

Table 8.3 summarizes the cut completion angle for the 17 bovine capsulorhexis procedures, and describes whether or not the excisions created tears in the remaining lens capsule. Five of the 17 blades produce a full, 360º cut in the lens capsule, and an additional seven blades produce a cut greater than or equal to 350º, none of which created tears in the lens capsule, resulting in a success rate of 70%. The blades' inability to produce a full cut may be attributed to variability in the cutting force applied by the user, and/or variability in blade quality. There is also a correlation between the lowest angles and lens capsule tears. When there is still a large portion of the lens capsule that needs to be torn out manually, the likelihood of destabilizing the remaining lens capsule with a tear increases. All excisions with a cut completion angle at or below 270° resulted in a tear. However, it should also be noted that each of these tear-inducing procedures was completed using only the microforceps to finish out the remainder of the capsulorhexis, as opposed to performing a more traditional manual procedure, which would have mitigated the risk of tears. Table 8.4 shows the cut completion angles for the human-cadaver procedures. The results show that only one blade out of three produced a cut completion angle of 360º in the human-

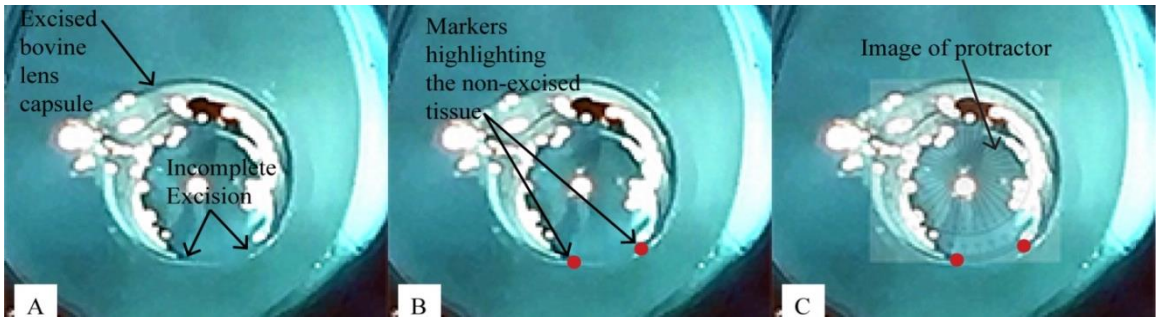

Figure 8.2: Cut completion angle of a bovine capsulorhexis. (A) incomplete excision of the lens capsule. (B) markers indicating leading edges of the non-excised tissue. (C) image of protractor imposed over lens capsule to approximate the angle of the remaining tissue.

Table 8.3: Cut completion angles and tears from bovine capsulorhexis procedures.

Blade #	Cut completion angle [°]	Tears [Y/N]
1	60	Y
2	355	N
3	360	N
4	360	N
5	355	N
6	270	Y
7	350	N
8	360	N
9	360	N
10	355	N
11	355	N
12	180	Y
13	220	Y
14	270	Y
15	350	N
16	360	N
17	355	N

Table 8.4: Experimental cut completion angles and tears from human-cadaver capsulorhexis procedures.

Blade #	Cut completion angle [°]	Tears [Y/N]
1	220	Y
2	270	Y
3	360	N

cadaver experiments without tearing the lens capsule, yielding a success rate of 33%. The remaining two blades produced cut completion angles substantially less than 360º, both of which resulted in a tear. The bovine lens capsules are approximately three times thicker than human ones. Although this enables using less force to cut human lens capsules, the human lens capsule is also less stiff and may rupture under a significantly smaller load than in the bovine experiments. Proper training and practice using the Helicotome may improve the success rate.

8.1.3 Circularity

Circularity is a quantitative measure of how round a shape is. Figure 8.3 graphically shows the steps to determine circularity. To determine circularity, the image of the lens capsule is imported into Matlab (Fig. 8.3 A) and converted into a black-and-white image based on a contrast threshold (Fig. 8.3 B). The area of the excision is calculated and converted into mm^2. Next, an edge-detection algorithm is used to locate the perimeter of the excised lens capsule. The diameter of the minimum bounding circle (the smallest circle that can contain a closed shape) is determined by finding the maximum distance between two points along the perimeter (Fig 8.3 C). This diameter is used to calculate the area of the minimum bounding circle. Next, the area of the excision is divided by the area of the minimum bounding circle to determine the normalized area, which is used as a measure of circularity [57].Note that a circularity of 1 represents a mathematically perfect circle.

Table 8.5 shows the excision area, the minimum bounding diameter, the minimum bounding circle area, and the circularity for bovine capsulorhexis experiments. All 17 of the bovine excisions exhibit circularity of greater than 0.65, yielding a success rate of100%.

Figure 8.3: Graphical steps to find circularity with (A) the excised lens capsule, (B) the black-and-white conversion, and (C) the perimeter and minimum bounding circle.

The variation in circularity is most likely attributed to the incomplete circular cuts discussed in the previous section. When only a portion of the circle is cut with the Helicotome, the remainder of the circle must be torn out. This is difficult to control and results in creating an out-of-round shape. For the Helicotomes that create full 360° cuts in the lens capsule, such as blades 3, 4, 8, 9, and 16 from the bovine experiments, the resulting excision is much more circular and results in greater circularity. Table 8.5 shows that blades 3, 4, 8, 9, and 16 have circularity of 0.86, 0.87, 0.91, 0.92, and 0.95, respectively.

Table 8.6 displays the excision area, the minimum bounding diameter, the minimum bounding circle area, and the circularity for human capsulorhexis. All measurable human lens capsule excisions exhibit a circularity greater than 0.65, yielding a success rate between 67% and 100%.

The variability of the circularity is likely the result of cut completion angles less than 360°. Cut completion angles equal to 360° do not tear the lens capsule, thus increasing the circularity as a result of a more controlled cut. Additionally, human lens capsules are thinner than bovine lens capsules, which renders tearing the capsule less controllable. This may account for the decreased circularity of the human compared to the bovine lens capsulorhexis procedures.

Table 8.5: Excision area, the minimum bounding diameter, the minimum bounding circle area, and the circularity for bovine capsulorhexis.

Blade #	Excision area [mm^2]	Minimum bounding diameter [mm]	Minimum bounding circle area [mm^2]	Circularity
1	15.00	5.26	21.70	0.69
2	15.28	4.77	17.90	0.85
3	18.38	5.21	21.35	0.86
4	15.43	4.76	17.76	0.87
5	18.44	5.26	21.75	0.85
6	19.11	5.37	22.66	0.84
7	18.35	5.39	22.81	0.80
8	15.62	4.68	17.20	0.91
9	16.55	4.78	17.92	0.92
10	16.16	4.95	19.22	0.84
11	15.99	5.14	20.77	0.77
12	17.38	5.28	21.92	0.79
13	16.63	5.10	20.39	0.82
14	20.86	6.03	28.53	0.73
15	26.21	6.39	32.08	0.82
16	16.98	4.77	17.83	0.95
17	17.61	5.14	20.77	0.85

Table 8.6: Excision area, the minimum bounding diameter, the minimum bounding circle area, and the circularity for human capsulorhexis.

Blade #	Excision area [mm^2]	Minimum bounding diameter [mm]	Minimum bounding circle area [mm^2]	Circularity
1	18.51	5.42	23.07	0.80
2	23.17	6.19	30.09	0.77
3	*	*	*	*

**The lens capsule could not be retrieved, so no data for the cut exists.*

8.1.4 Outer-Fiber Strain

Outer-fiber strain in excess of 4.0% causes the Helicotome blade to plastically deform when retracted in the cannula. Upon deployment, the plastic deformation results in a noncircular blade shape with a greater diameter than the limit allows. This metric is verified using the outer-fiber strain formula (Eq. (4.1) in Section 4.3). Figure 8.4 shows a Nitinol ribbon blade experiencing (outer-fiber) strain as a result of being wound around the shape-set spindle. Table 8.7 shows the blade thickness and outer-fiber strain for blades used in bovine capsulorhexis experiments, and Table 8.8 shows blade thickness and outer-fiber strain for blades used in human capsulorhexis experiments.

All Nitinol blades used in these experiments are fabricated from the same spool of Nitinol ribbon. The Nitinol ribbon, as specified by the manufacturer, does not exceed 0.16 mm in thickness, and the shape-set spindle has a diameter of 5 mm. The outer-fiber strain of all blades used in capsulorhexis experiments is calculated as 3.2% with Eq. (4.1), which does not exceed the limit of 4.0%, resulting in a 100% success rate. Thus, plastic deformation of the blade will not occur while it is retracted in the cannula.

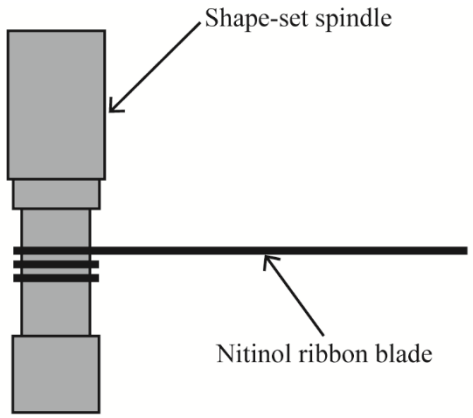

Figure 8.4: Schematic of a Nitinol ribbon blade experiencing (outer-fiber) strain as it is wound around the shape-set spindle.

Table 8.7: Blade thickness and outer-fiber strain of blades used in bovine capsulorhexis experiments.

Blade #	Blade thickness [mm]	Outer-fiber strain [%]
1	0.16	3.2
2	0.16	3.2
3	0.16	3.2
4	0.16	3.2
5	0.16	3.2
6	0.16	3.2
7	0.16	3.2
8	0.16	3.2
9	0.16	3.2
10	0.16	3.2
11	0.16	3.2
12	0.16	3.2
13	0.16	3.2
14	0.16	3.2
15	0.16	3.2
16	0.16	3.2
17	0.16	3.2

Table 8.8: Blade thickness and outer-fiber strain of blades used in human capsulorhexis experiments.

Blade #	Blade thickness [mm]	Outer-fiber strain [%]
1	0.16	3.2
2	0.16	3.2
3	0.16	3.2

8.1.5 Cannula Diameter

The outer diameter of the cannula must be smaller than 1.9 mm to fit within the corneal incision. Tearing to the corneal incision can occur if the fit between the incision and the cannula is too tight, i.e., if the cannula diameter exceeds the 1.9 mm limit. A tear in the corneal incision can cause scarring which could affect the patient's vision. Figure 8.5 shows a schematic of a cannula entering the corneal incision.

Tables 8.9 and 8.10 show the cannula outer diameter for all Helicotome blades used

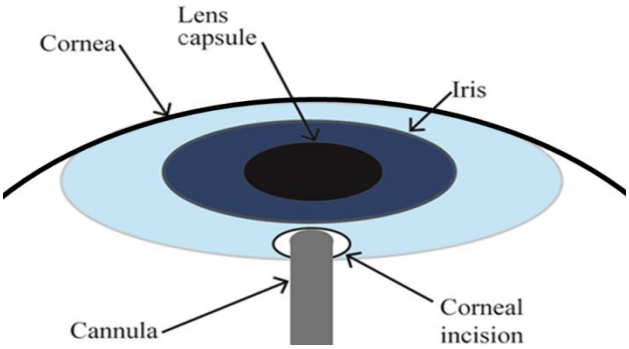

Figure 8.5: Schematic of a cannula entering the corneal incision, illustrating that the cannula outer diameter must be smaller than the maximum allowable diameter of the corneal incision.

Table 8.9: Cannula outer diameter for devices used in bovine capsulorhexis experiments.

Blade #	Cannula outer diameter [mm]
1	1.46
2	1.46
3	1.46
4	1.46
5	1.46
6	1.46
7	1.46
8	1.46
9	1.46
10	1.46
11	1.46
12	1.46
13	1.46
14	1.46
15	1.46
16	1.45
17	1.46

Table 8.10: Cannula outer diameter for devices used in human capsulorhexis experiments.

Blade #	Cannula outer diameter [mm]
1	1.46
2	1.45
3	1.46

in bovine and human capsulorhexis experiments, respectively. Tables 8.9 and 8.10 show that the diameter of all cannulas used in our experiments satisfy the Helicotome design specifications and will fit within a 3 mm corneal incision, which results in a 100% success rate, thus preventing excessive contact between the cannula and the corneal incision.

The maximum blade height is constrained by the inner diameter of the cannula through which the blade is deployed. Figure 8.6 shows a schematic of the Helicotome blade fully retracted within the cannula, demonstrating the need for the dimensions of the blade cross-section to be smaller than the inner diameter of the cannula.

8.1.6 Blade Height

Tables 8.11 and 8.12 show the cannula inner diameter and blade height for each Helicotome used in the bovine and human capsulorhexis experiments, respectively. From Tables 8.11 and 8.12 we verify that the Nitinol blade height is small enough to fit within the cannula without interference, resulting in a 100% success rate, preventing the blade from being damaged by contact with the cannula inner wall and facilitating smooth deployment and retraction of the blade.

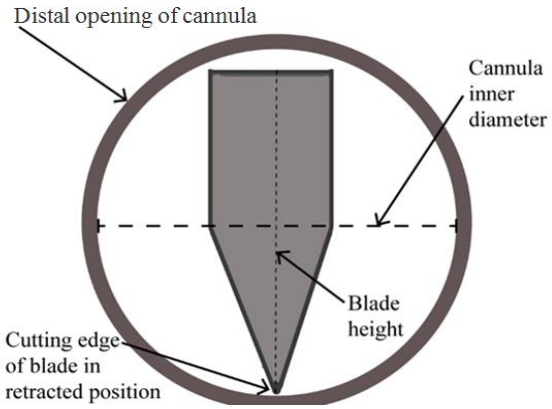

Figure 8.6: Schematic of the Helicotome blade in the fully retracted position. The blade

Table 8.11: Cannula inner diameter and blade height of Helicotomes used in bovine capsulorhexis experiments.

Blade #	Cannula inner diameter [mm]	Blade height [mm]
1	1.21	0.84
2	1.21	0.84
3	1.21	0.85
4	1.21	0.84
5	1.21	0.84
6	1.22	0.84
7	1.22	0.84
8	1.22	0.84
9	1.21	0.84
10	1.21	0.84
11	1.21	0.84
12	1.21	0.85
13	1.21	0.84
14	1.21	0.84
15	1.22	0.84
16	1.22	0.84
17	1.21	0.84

Table 8.12: Cannula inner diameter and blade height of Helicotomes used in human capsulorhexis experiments.

Blade #	Cannula inner diameter [mm]	Blade height [mm]
1	1.21	0.84
2	1.21	0.84
3	1.21	0.84

8.1.7 Radius of Curvature of the Blade Edge

There are two crucial metrics in defining the sharpness of a blade. The first is the radius of curvature of the blade edge (see Section 5.1). We use scanning electron microscopy (SEM) imaging to measure the radius of curvature of a clinical-use surgical blade of known sharpness for comparison with the radius of curvature of one Helicotome prototype blade. Figure 8.7 shows a comparison between a Helicotome and a clinical-use surgical blade. Figure 8.7 A shows the edge width of the Helicotome blade, and Fig. 8.7 B

shows the edge width of a clinical-use surgical blade. We are not able to measure the radius of curvature directly with SEM, but are able to calculate the radius of curvature by dividing the measured edge width by two (see Section 5.1).

The results of the SEM measurement of the Helicotome blade indicate a radius of curvature of 0.255 µm, significantly below the limit value of 5.00 µm. Based on the comparative measurements shown in Fig. 8.7, the Helicotome blade radius of curvature is 25% smaller than the surgical blade radius of curvature, meaning that the Helicotome is sharper than the surgical blade at the location where the measurement occurred. Because the prototype Helicotome blades are sharpened by hand, we expect some inconsistency in sharpness between various blades, as well as inconsistency in sharpness between various points along the same blade. These inconsistencies cannot be quantified for the Helicotome blades because only one blade was imaged using SEM at only a single point along its blade path. The principal outcome of this SEM experiment is the verification that it is in fact possible to sharpen a Nitinol blade to the specified sharpness.

8.1.8 Included Primary Angle

The included primary angle is the other critical metric associated with sharpness, and is set on the blade during the sharpening process. This angle is similar to the included primary angle found on most clinical-use surgical blades (25°). Angles larger than 30° are undesirable as sharpness increases with decreasing primary angle (see Section 5.1). Because the manufacturing of the Helicotome blades is done by hand, there is variation in the results, such that the reported value of 25° is approximate only. Figure 8.8 shows how the included primary angle is imposed on the blade during the sharpening process.

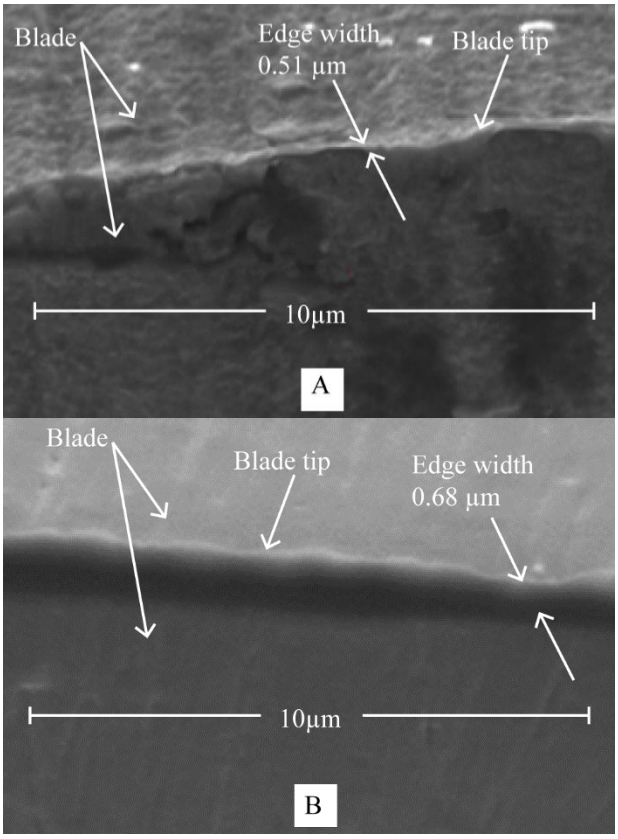

Figure 8.7: SEM image comparison of the edge widths of two blades. (A) Helicotome prototype, and (B) clinical-use surgical blade.

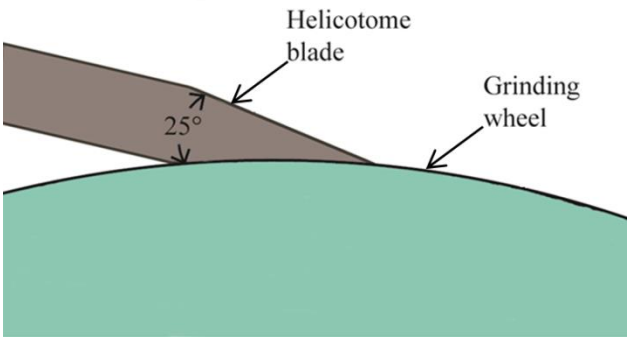

Figure 8.8: Included primary angle imposed on the Helicotome blade.

8.1.9 Procedure Duration

The procedure duration for capsulorhexis experiments performed with the Helicotome must be less than 120 seconds to be competitive with the other methods for performing capsulorhexis. Table 8.13 and Table 8.14 show the procedure duration from the bovine and human-cadaver capsulorhexis experiments.

The results show that all 17 bovine capsulorhexis procedures and all three human capsulorhexis procedures performed with the Helicotome have procedure durations under the limit value, resulting in a 100% success rate. The average procedure duration for all experiments performed with the Helicotome blade is nearly 75% shorter than the average procedure duration of 120 seconds using the currently available bent-needle method. Note that the procedure duration of 120 seconds for the bent-needle method is based on a successful capsulorhexis, whereas our data are based on the time required to make the attempt and remove the excised tissue, whether it is successful or not. However, the shortest procedure durations reported for bovine and human-cadaver experiments correspond directly to the Helicotome blades that achieved cut completion angles of 360°, indicating that successful lens capsule excisions result in shorter procedure duration.

8.1.10 Comparison of the Helicotome Blade to Other Techniques

Section 1.2 details the two most common methods of performing the capsulorhexis procedure currently in practice, i.e., a bent needle or cystotome forceps, or a femtosecond laser. The laser method produces exceptional results in terms of repeatability and circularity compared to the bent-needle technique. Friedman et al. [57] define circularity as a normalized ratio of the sample area to the area of a disk, with the diameter of the disk

Table 8.13: Procedure duration for bovine capsulorhexis.

Blade #	Procedure duration [s]
1	50
2	33
3	19
4	20
5	22
6	23
7	22
8	21
9	20
10	23
11	23
12	30
13	36
14	41
15	31
16	18
17	23

Table 8.14: Procedure duration for human-cadaver capsulorhexis

Blade #	Procedure duration [s]
1	34
2	46
3	23

corresponding to the maximum width of the sample. The laser capsulorhexis procedures they performed show a mean circularity of 0.94 with a standard deviation of 0.15 from the normalized ratio of an “ideal” circle (e.g., a circle with a normalized ratio equal to one). The bent-needle method achieves a mean circularity of 0.80 with a standard deviation of 0.15, indicating that the bent needle excisions are significantly less circular [57]. The Helicotome produces a mean circularity of 0.83 with a standard deviation of 0.06, which indicates that the Helicotome produces excisions that are consistently more circular than

the current manual method of performing capsulorhexis. Additionally, the procedure duration is on average 74% shorter for the Helicotome compared to the procedure duration of the bent needle, as described in Section 8.2.

Figure 8.9 shows excised lens capsules using the bent-needle method and the femtosecond laser method compared to lens capsules excised with the Helicotome. Figure 8.9 A shows the excised capsules from three bovine capsulorhexis procedures performed using the Helicotome. The most pronounced contour in the images is the lens capsule. The other contours are caused by a combination of shadows, reflection off of the petri dish, and bleeding of the blue stain from the lens capsule. Figure 8.9 B shows the excised capsules from three porcine manual capsulorhexis procedures performed using a bent needle [57]. Figure 8.9 C shows the excised capsules from three porcine capsulorhexis procedures using a femtosecond laser [57]. All excisions are stained blue to increase visibility.

According to Friedman et al. [57], the manual lens capsule excisions deviate from the specified diameter of 5 mm by 0.337 mm +/- 0.258 mm (mean +/- standard deviation) for the 18 manual procedures performed in the study [57]. The laser-excised lens capsules deviate from a specified diameter of 4.6 mm by 0.029 mm +/- 0.026 mm for the 39 laser procedures performed in the study [57]. The Helicotome deviates from a target diameter of 5 mm by 0.17 mm +/- 0.34 mm for 17 bovine procedures. These metrics show that the Helicotome, which is still in its development phase, provides results closer to the specified values than the bent-needle method.

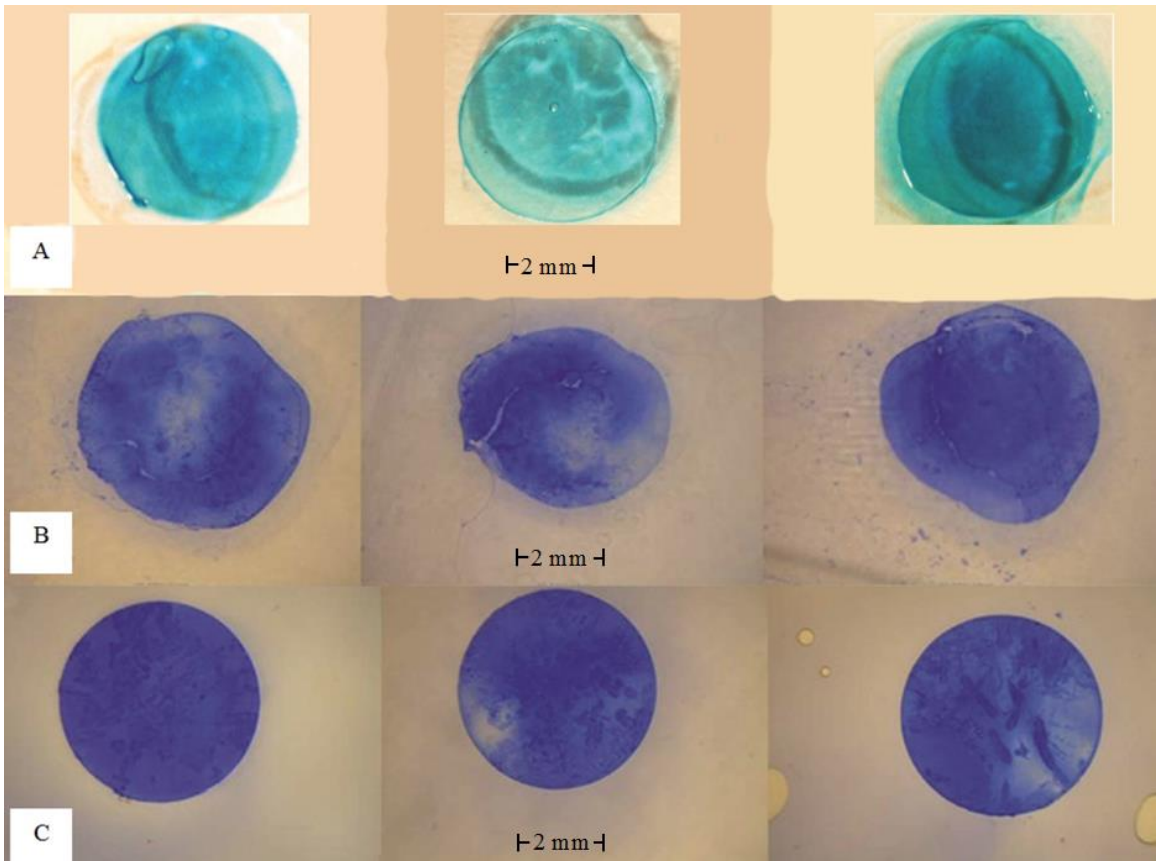

Figure 8.9: Lens capsule excision comparison. (A) bovine lens capsules excised with the Helicotome . (B) porcine lens capsules excised using a bent needle. Image modified from [57]. (C) porcine lens capsules excised using a femtosecond laser. Image modified from [57].

8.2 Validation

Validation of the final product design must be performed on all newly designed devices, in accordance with the Code of Federal Regulations (CFR) Title 21 820.3. The purpose of validation is to ensure that the device conforms to user needs and satisfies intended uses [56]. All experiments performed for device validation are done with the corneas intact (i.e., standard capsulorhexis). This is done to evaluate the performance of the device under actual clinical circumstances.

8.2.1 Ergonomic Design Considerations

This user need specifies that the device must be small, handheld, easily deployed and retracted with the index finger, and comfortable to use. Figure 8.10 illustrates the final design iteration incorporating the ergonomic user needs. After completing capsulorhexis procedures on human-cadaver and bovine eyes, Dr. Ambati reports that the ergonomics of the most recent iteration of the Helicotome device are satisfactory, including that the tool handle is appropriately small, comfortable to use, and that the tool deploys and retracts easily with his index finger, as specified by his original user needs.

8.2.2 Blade Must Not Contact the Posterior of the Cornea

This user need states that the blade cannot come into contact with the posterior surface of the cornea while being deployed within the anterior chamber of the eye. Figure 8.11 illustrates the location of the Helicotome blade deployed between the lens capsule and the posterior surface of the cornea.

The Helicotome used in the experiments fails to deploy above the anterior lens capsule without contacting and subsequently damaging the posterior surface of the cornea during the capsulorhexis procedure. It was found during experiments that we could only deploy the Helicotome 1.5 of its 2 turns within the eye before we could see contact between the blade and the cornea, which indicates that the distance from the lens capsule to the posterior of the cornea is approximately 2.6 mm (75% of the overall fully deployed blade height of 3.5 mm). Hence, the overall height of the helical blade in its fully deployed state must be reduced to provide enough clearance such that the blade does not contact the posterior of the cornea.

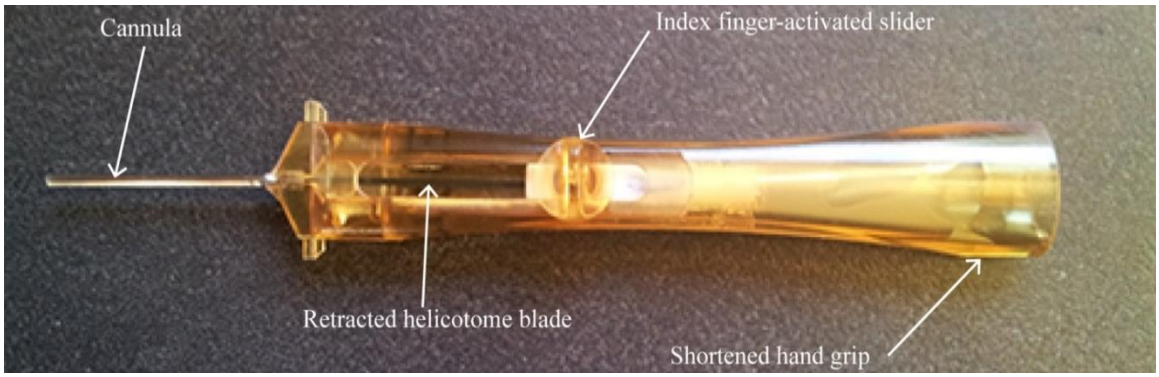

Figure 8.10: Final design of the Helicotome incorporating user-specified ergonomic needs.

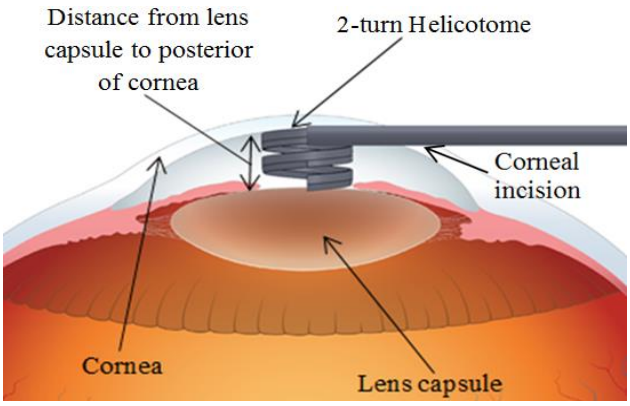

Figure 8.11: Helicotome blade deployed between the posterior surface of the cornea and the lens capsule. Image modified from [58].

8.3 Discussion of the Helicotome Results

The Helicotome blade performs with a 100% success rate with respect to cut diameter, circularity, outer-fiber strain, cannula fit within the corneal incision, the ability of the blade to fit within cannula, radius of curvature of the blade edge, included primary angle, and procedure duration. The Helicotome meets the design specifications for all of those categories, as discussed in Section 8.2. However, this prototype fails to satisfy the specification for cut completion angle, yielding a success rate of 70%, where five of the 17 excisions resulted in tears; and the Helicotome is unable to be deployed within the anterior

chamber of the eye without contacting the posterior of the cornea. This signifies that further design changes are required to make the Helicotome compatible for human-use procedures, and to improve the performance of the Helicotome with regard to the completion of cuts performed with the device.

8.4 Proposed Solution to Helicotome Failure

Because the Helicotome fails to deploy above the anterior lens capsule without contacting the posterior surface of the cornea, we have reduced the helical portion of the blade from two rotations to 1.5 rotations, while simultaneously decreasing the helix pitch from 1.25 mm for the 2-turn design, to 0.8 mm for the 1.5-turn design to reduce the height of the deployed helical blade from 3.5 mm to 2 mm, resulting in a clearance of approximately 0.6 mm between the blade and the posterior of the cornea. The height of 2 mm results from the decision to reduce the helix to 1.5 turns and minimize the pitch. The pitch cannot be further reduced, as different layers of the helix cannot occupy the same space at the same time. Figure 8.12 shows the relative difference in blade height between the two designs after insertion into the corneal incision. Figure 8.12 A shows the lens capsule and surrounding tissue, Fig. 8.12 B shows the insertion of the 1.5-turn Helicotome blade into the corneal incision, and Fig. 8.12 C shows the insertion of the 2-turn Helicotome blade into the corneal incision.

The 1.5-turn Helicotome blades are designed and fabricated from the same materials and using the same processes as the 2-turn Helicotome blades and, thus, the same design verification requirements apply, including cut diameter, cut completion angle, circularity, outer-fiber strain, cannula diameter, blade height, radius of curvature of the

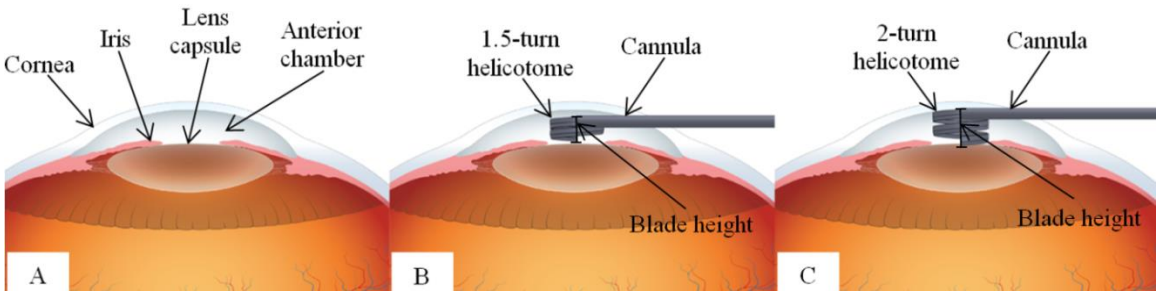

Figure 8.12: Helicotome prototype designs. (A) lens capsule and surrounding tissue. (B) 1.5-turn Helicotome entering corneal incision. (C) 2-turn Helicotome entering corneal incision. Image modified from [58].

blade edge, included primary angle, and procedure duration. Table 8.15 shows cannula outer and inner diameter, blade height, blade thickness, and outer-fiber strain for the 1.5-turn Helicotome blades. Table 8.15 shows that the 1.5-turn Helicotome exhibits a 100% success rate with respect to outer-fiber strain, cannula outer diameter, and blade height.

The radius of curvature of the blade edge is determined using an SEM as described in Section 8.1.7. Figure 8.13 displays an SEM image of the distal portion of a 1.5-turn Helicotome blade. Figure 8.14 illustrates the location of the SEM measurements at 0°, 90°, 180°, and 270° along the circular path of each blade. These locations are chosen to verify that the blade meets the specification for radius of curvature of the blade edge over the full 360° of the blade path. Table 8.16 shows the SEM radius-of-curvature measurements of all 1.5-turn Helicotome devices at 0°, 90°, 180°, and 270° along the circular path of each blade. Table 8.16 shows that all 14 1.5-turn Helicotome blades satisfy the requirement for radius of curvature of the blade edge, resulting in a 100% success rate. Therefore, the blades are appropriate for use in experimental trials. Blades one through twelve were used in bovine capsulorhexis experiments and blades 13 and 14 were used in human-cadaver capsulorhexis experiments.

Table 8.15: Cannula outer and inner diameter, blade height, blade thickness, and outer-fiber strain for the 1.5-turn Helicotome blades.

Blade#	Cannula OD [mm]	Cannula ID [mm]	Blade height [mm]	Blade thickness [mm]	Outer-fiber strain [%]
1	1.46	1.21	0.84	0.16	3.2
2	1.46	1.21	0.84	0.16	3.2
3	1.46	1.22	0.84	0.16	3.2
4	1.45	1.22	0.84	0.16	3.2
5	1.46	1.21	0.84	0.16	3.2
6	1.46	1.21	0.84	0.16	3.2
7	1.46	1.21	0.85	0.16	3.2
8	1.45	1.21	0.84	0.16	3.2
9	1.46	1.21	0.84	0.16	3.2
10	1.46	1.21	0.84	0.16	3.2
11	1.46	1.21	0.84	0.16	3.2
12	1.46	1.21	0.84	0.16	3.2
13	1.46	1.21	0.84	0.16	3.2
14	1.46	1.22	0.84	0.16	3.2

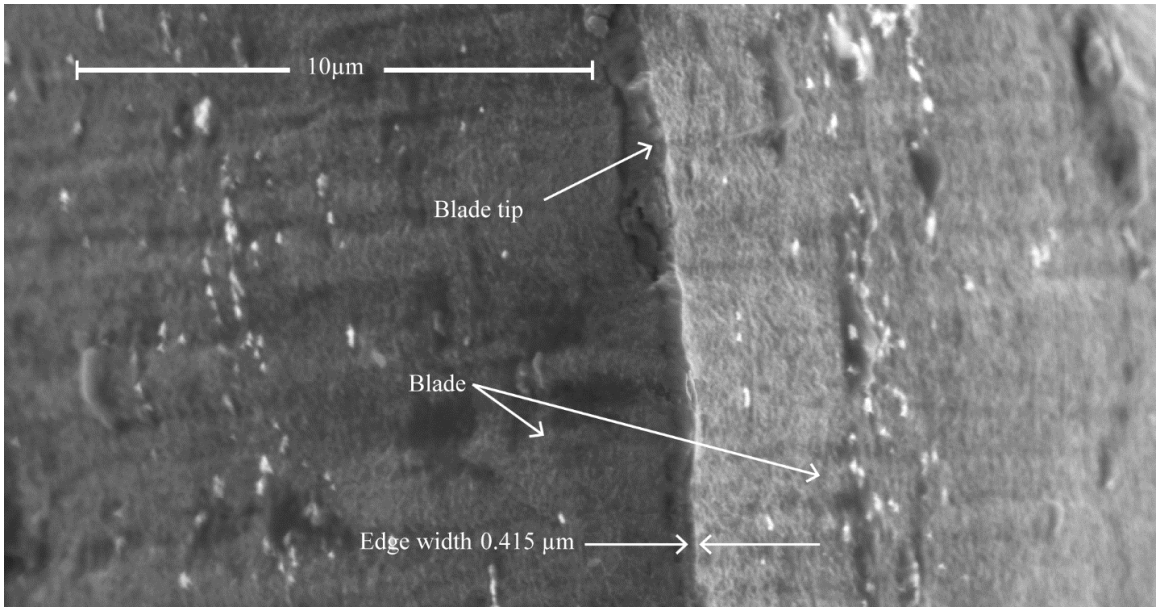

Figure 8.13: SEM image of a Helicotome blade tip. The measured edge width, where edge width is 2x the radius of curvature.

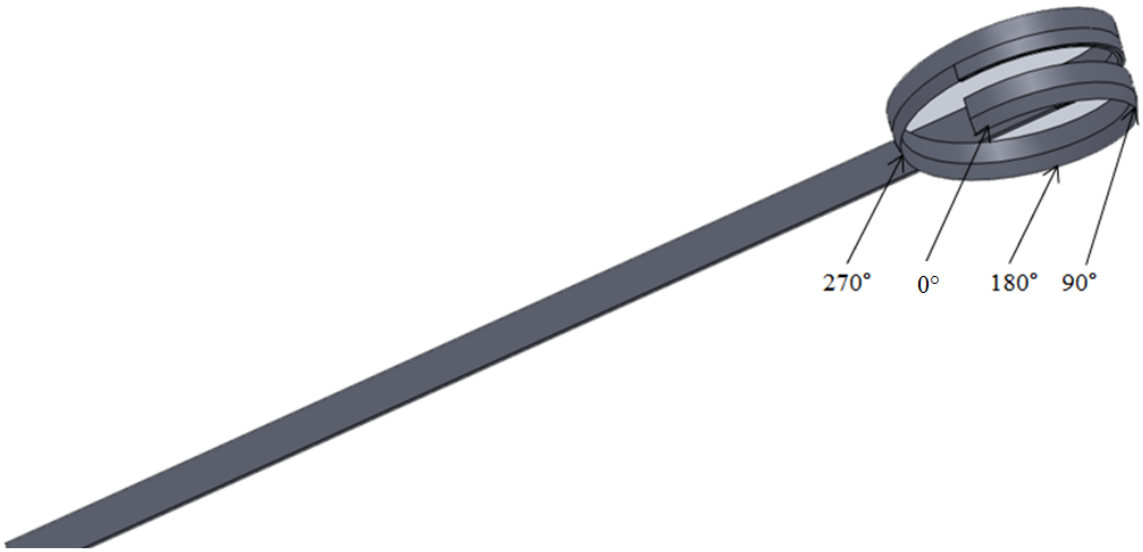

Figure 8.14: 1.5-turn Helicotome blade showing the location of SEM image measurements performed to determine the radius of curvature of the blade along its 360° circular path.

Table 8.16: Radius-of-curvature measurements at 90°, 180°, 270°, and 360° along the circular path of each blade of the 1.5-turn Helicotome device.

Blade #	**Radius of curvature measurement 0° [µm]**	**Radius of curvature measurement 90° [µm]**	**Radius of curvature measurement 180° [µm]**	**Radius of curvature measurement 270° [µm]**
1	0.13	0.41	0.21	0.37
2	0.38	0.43	0.22	0.73
3	0.33	0.30	0.27	0.91
4	0.15	0.61	0.19	0.85
5	0.43	0.38	0.21	0.26
6	0.25	0.20	0.48	0.37
7	0.47	0.26	0.33	0.55
8	0.30	0.65	0.24	0.22
9	0.17	0.18	0.31	1.04
10	0.12	0.17	0.20	0.23
11	0.17	0.21	0.21	0.41
12	0.20	0.31	0.51	0.16
13	0.21	0.20	0.32	0.34
14	0.28	0.32	0.19	0.51

Table 8.17 reports the cut diameter, procedure duration and cut completion for the 1.5-turn Helicotome for 14 capsulorhexis procedures. Table 8.18 shows the excision area, minimum bounding diameter, minimum bounding circle area, and circularity for the 1.5-turn Helicotome. The results indicate the need for another redesign of the Helicotome. The 1.5-turn blades failed to cut, or fully excise, the lens capsule in any of the experiments. This newer design enables the Helicotome to deploy above the anterior lens capsule without contacting the cornea, but prevents the blade from creating an incision in any of the experiments. The failure of the 1.5-turn iteration is believed to be inherent to the configuration of the 1.5-turn blade, specifically the point along the helix where the maximum amount of cutting force is applied. The distal edge of the blade is the first portion of the blade to come into contact with the lens capsule, and is most likely where the blade is initiating a cut in the lens capsule. Figure 8.15 shows the point of application of force relative to the distal edge of the 2-turn blade (Fig 8.15 A), and the 1.5-turn blade (Fig. 8.15 B). The distal edge of the 2-turn blade is directly beneath the cannula, i.e., the point of application of force, whereas the distal edge of the 1.5-turn blade is on the opposite side of the helix, laterally offset to the point of application of force by the 5 mm helix diameter. Rather than utilizing the full application of force, a portion of the force is lost due to the moment created when the distal edge of the blade is offset from the point of application of force. This results in the blade rolling out of plane to the lens capsule and distributing the applied load across more of the blade, rather than the full force being applied near the distal edge of the blade.

Table 8.17: Cut diameter, procedure duration, and cut completion angle for the 1.5-turn Helicotome.

Blade #	Cut diameter [mm]	Procedure duration [s]	Cut completion angle [º]
1	*	*	0
2	*	*	0
3	*	*	0
4	*	*	0
5	*	*	0
6	*	*	0
7	*	*	0
8	*	*	0
9	*	*	0
10	*	*	0
11	*	*	0
12	*	*	0
13	*	*	0
14	*	*	0

**No cut was made, so no data for the cut exists.*

Table 8.18: Excision area, minimum bounding diameter, minimum bounding circle area, and circularity for the 1.5-turn Helicotome.

Blade #	Excision area [mm^2]	Minimum bounding diameter [mm]	Minimum bounding circle area [mm^2]	Circularity
1	*	*	*	*
2	*	*	*	*
3	*	*	*	*
4	*	*	*	*
5	*	*	*	*
6	*	*	*	*
7	*	*	*	*
8	*	*	*	*
9	*	*	*	*
10	*	*	*	*
11	*	*	*	*
12	*	*	*	*
13	*	*	*	*
14	*	*	*	*

**No cut was made, so no data for the cut exists.*

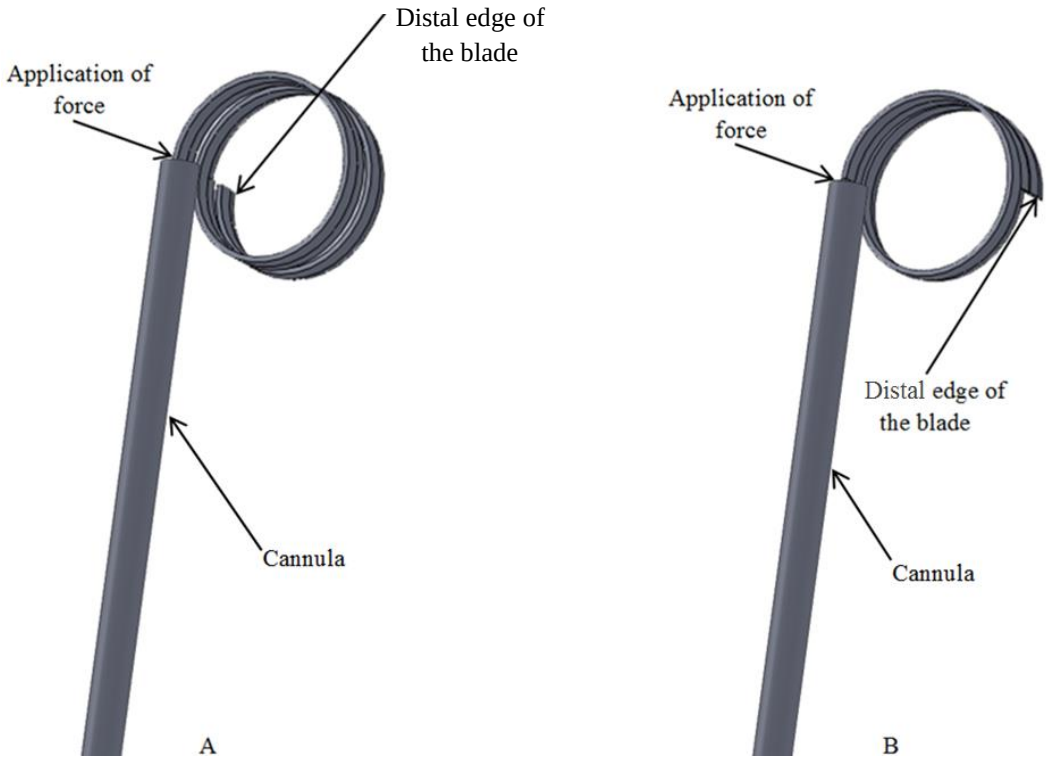

Figure 8.15: Point of application of force relative to the distal edge of the 2-turn blade (A), and the 1.5-turn blade (B).

8.5 Discussion

The 1.5-turn and 2-turn Helicotome blades are produced using identical materials and manufacturing processes. We observe no difference in the outer-fiber strain, cannula diameter, blade height, and included primary angle verification metrics for either blade design. All of the 1.5-turn Helicotomes were verified for radius of curvature of blade edge, as opposed to the verification of only one blade from the 2-turn Helicotome experimental batch. Consequently, we do not believe there is any correlation between the success or failure of the two blade designs in terms of those verification metrics.

There are three physical differences between the two designs. The first is the additional 180° of blade incorporated in the 2-turn Helicotome, which equates to an additional 8 mm of blade. The second is the difference in helical pitch between the two,

which is 1.25 mm for the 2-turn blade versus 0.8 mm for the 1.5-turn blade. Finally, the location of the distal edge of the blade, which is directly under the point of application of force for the 2-turn blade and offset from the point of application of force by the 5 mm diameter of the helix for the 1.5-turn blade. In spite of the similarities, the 2-turn Helicotome blades produce lens capsule excisions in all 20 experiments performed with them, whereas the 1.5-turn Helicotome blades were unable to produce any lens capsule excisions in the 14 experiments performed with them.

8.6 References

[56] "21 CFR 820.30 – Design controls," 2012, from http://www.gpo.gov/fdsys/granule/CFR-2012-title21-vol8/CFR-2012-title21-vol8-sec820-30/content-detail.html

[57] Friedman, N.J., Palanker, D.V., Schuele, G., Anderson, D., Marcellino, G., Seibel, B.S., Batlle, J., Feliz, R., Talamo, J.H., Blumenkranz, M.S., and Culbertson, W.W., 2011, "Femtosecond Laser Capsulotomy," Journal of Cataract Refractive Surgery, **37**, pp. 1189-98.

[58] "Vision Insights," 2013, from http://128.248.91.60/visioninsights/?page_id=1044

CHAPTER 9

CONCLUSIONS AND FUTURE WORK

9.1 Thesis Summary and Conclusions

Cataracts are the most common visual impairment and account for approximately 42% of all blindness worldwide. Cataract extraction requires three critical steps: (1) accessing the cataract-afflicted lens, (2) removing the cataract from the eye, and (3) implanting the new, artificial intraocular lens in place of the cataract. The current methods used in cataract removal surgeries are not optimal in terms of accessibility and patient outcomes. The need for a safer, more effective, less expensive, and more accessible cataract removal method is of interest to the ophthalmological community.

Capsulorhexis, which is the removal of the anterior lens capsule, is a tedious and intricate procedure, and perhaps the most critical step of the cataract removal surgery. Developing a disposable, manually operated, handheld cutting device specifically designed to produce a circular incision in the lens capsule of the eye could create a paradigm shift in the capsulorhexis portion of cataract surgery, providing quality and reproducibility comparable to laser-assisted surgery, while maintaining the efficiency and cost of standard surgery.

The solution proposed in this thesis, a novel device referred to as the Helicotome, comprises a handheld deployment tool, a superelastic shape-memory-alloy blade formed

into a helical shape, a manual actuator to deploy and retract the blade, and a cannula through which the blade is deployed and retracted. This design, which utilizes both the shape-memory and superelastic properties of Nitinol, enables a 5 mm diameter circular blade to be inserted, deployed, retracted, and removed through a 2 to 3 mm corneal wound. One motivation for the creation of the Helicotome is to make the capsulorhexis easier to perform, reducing the time required to perform the capsulorhexis. Because the capsulorhexis is currently one of the most difficult portions of a cataract surgery, another motivation for the creation of the Helicotome is to enable less-skilled surgeons to perform the procedure with outcomes similar to their more-skilled colleagues.

Verification testing and device validation of Helicotome prototypes show that the Helicotome is capable of producing a 360° circular cut in the anterior lens capsule while reducing procedure duration. A Nitinol blade that fits within a 1.45 mm diameter cannula was made as sharp as surgical blades currently used in practice, and deployed from the cannula without incurring plastic deformation. The tool, which was ergonomically designed based on surgeon feedback, is easily actuated with the index finger.

Since the lens capsule experiences a tensile stress due to intraocular pressure, the 5 mm diameter blade may produce a circular excision that is slightly larger when the remaining lens capsule finds a new elastic equilibrium. This could lead to an excised area that is too large for implanting the artificial lens. The opening needs to be sufficiently large for the lens to fit, but small enough to contain the lens and not compromise the structural integrity of the lens capsule. According to personal communication with Dr. Balamurali Ambati, a capsulorhexis should be between 4 mm and 6 mm in diameter.

Due to the geometry of the current successful prototype, which deploys two full

turns of the helical superelastic blade, the helix is too large to fit within the anterior chamber of the eye without contacting the posterior of the cornea. The research team attempted to resolve this problem by minimizing the helical pitch and reducing the helix to 1.5 turns. Although this solution produced a blade that could be deployed within the anterior chamber without contacting the posterior of the cornea, it was not successful in cutting the lens capsule.

9.2 Recommendations and Future Work

Future work on the Helicotome should consist of four primary tasks: (1) scaling down, (2) handle redesign, (3) cannula optimization, and (4) process refinement and control.

9.2.1 Scaling Down

The Nitinol blade should be scaled down to adequately fit within the anterior chamber of the eye. This can be done by reducing the Nitinol blade height from 0.8 mm to approximately 0.5 mm while maintaining the current 5° helix angle. This modification will enable two full turns for the helix to fit within the anterior chamber, such that the distal end of the fully deployed blade is directly beneath the tip of the cannula. An alternate design that should also be considered is a helical blade that is between 1 and 1.25 full turns, such that the overall height of the helix is only approximately half that of the current successful prototype, but the distal end of the fully deployed blade is still close to being beneath the tip of the cannula.

The Nitinol blade should also be scaled down to reduce the diameter of the resulting

capsulorhexis. This can be done by reducing the Nitinol ribbon thickness from 0.16 mm to approximately 0.10 mm to facilitate a smaller helix diameter. At this thickness, a 3.5 mm diameter helix could be achieved while adhering to elastic outer-fiber strain constraints, which would result in a 4 to 5 mm diameter capsulorhexis. This reduction in helix diameter will have the additional benefit of helping the deployed helical blade fit within the anterior chamber of the eye, due to the domed curvature of the cornea.

9.2.2 Handle Redesign

The body of the tool should be redesigned to emulate the current device without having to retrofit a Malyugin-Ring Injector. A similar slider, knob, and cannula would provide adequate functionality, and a redesigned injection-molded handle would further improve ergonomics and stability.

9.2.3 Cannula Optimization

The cannula-blade interaction should be optimized to provide maximum blade stability in terms of resistance to twisting, while preserving its sharpness during storage and use. A Teflon insert within the cannula could prevent undesired contact of the blade with the cannula wall, provide guidance during deployment of the blade, and prevent the blade from twisting within the cannula. This would result in application of the cutting force orthogonal to the lens tissue. Alternatively, machining or extruding a cannula with a customized noncircular bore could be a feasible solution for mass production.

9.2.4 Process Refinement and Control

The Helicotome manufacturing process should be refined and standardized to provide repeatable results through process qualification. Limiting human interaction within the process through automation will increase the repeatability and reproducibility of the manufacturing process. Multistage, centerless, wet grinding, using reel-to-reel Nitinol ribbon, could streamline the sharpening process. The Nitinol ribbon could seamlessly transfer from one grit stone to another (e.g., 200-grit to 1000-grit to 4000-grit to a leather honing wheel), and the grinding time could be precisely controlled.

The shape-set process could also be improved upon. The sharpened blades could be loaded into fixtures and shape-set in batches. The same superelastic Nitinol with a transition temperature of 10°C should be used. Rather than using an air furnace, the blades should be shape-set in a molten sodium bath at 530°C to 540°C for 10 to 15 minutes. This would facilitate a more complete shape-set while accurately controlling the transition temperature and minimizing contamination and oxidation of the Nitinol blades. The blades would then be cold-water quenched, removed from their fixtures and trimmed to their final shape as is currently done.

APPENDIX A

CAPSULORHEXIS IMAGES

Figure A.1: Lens capsule excision from bovine capsulorhexis experiments corresponding to Helicotome blade # 1.

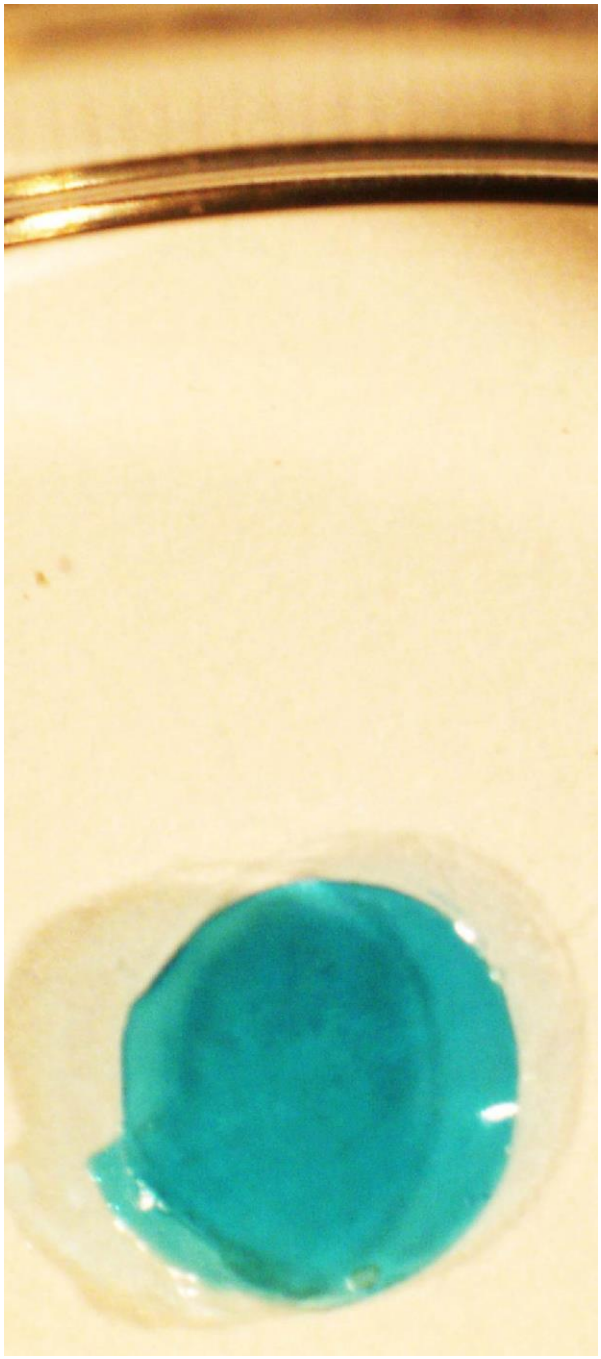

Figure A.2: Lens capsule excision from bovine capsulorhexis experiments corresponding to Helicotome blade # 2.

Figure A.3: Lens capsule excision from bovine capsulorhexis experiments corresponding to Helicotome blade # 3.

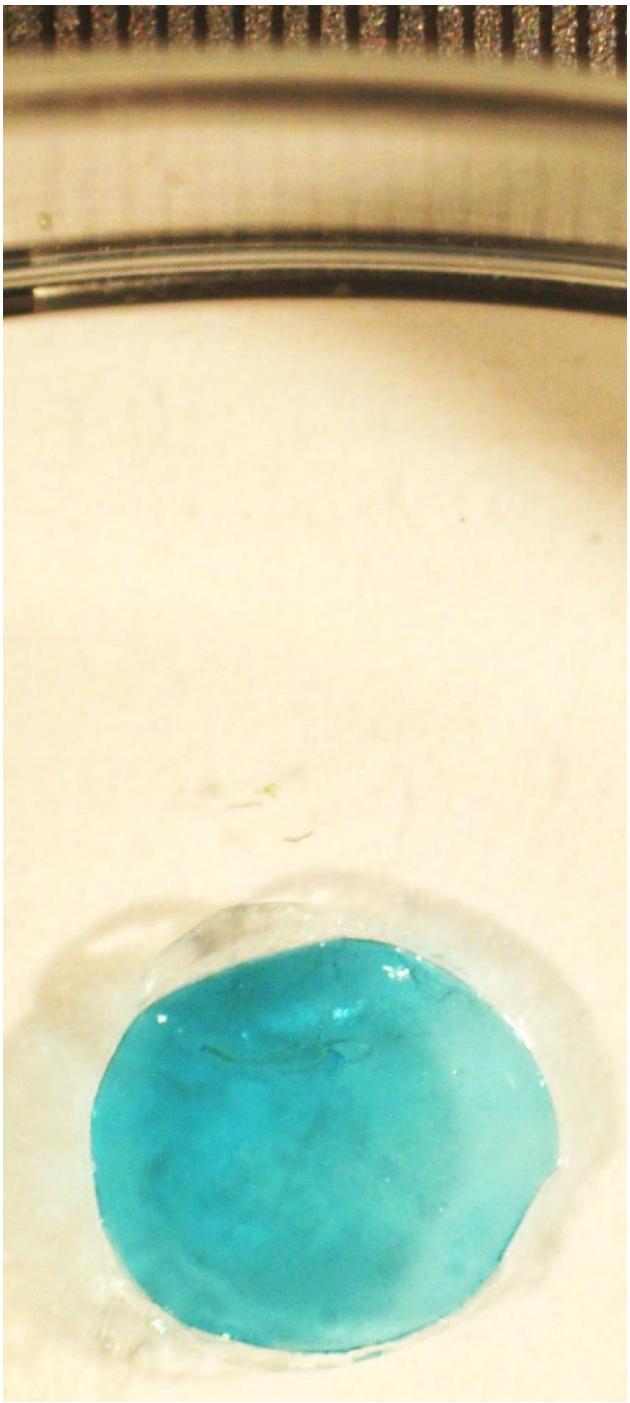

Figure A.4: Lens capsule excision from bovine capsulorhexis experiments corresponding to Helicotome blade # 4.

Figure A.5: Lens capsule excision from bovine capsulorhexis experiments corresponding to Helicotome blade # 5.

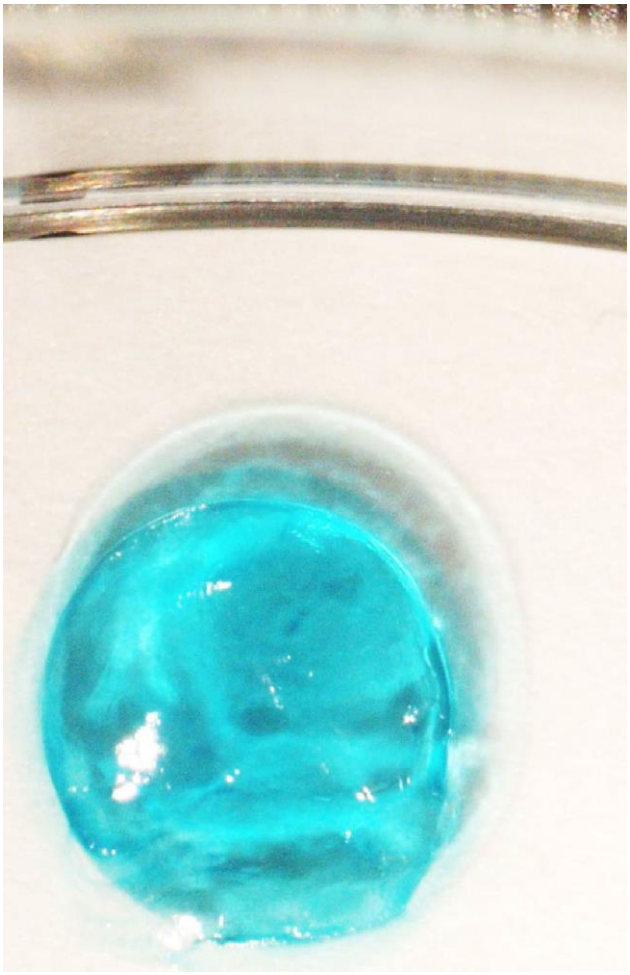

Figure A.6: Lens capsule excision from bovine capsulorhexis experiments corresponding to Helicotome blade # 6.

Figure A.7: Lens capsule excision from bovine capsulorhexis Experiments corresponding to Helicotome blade # 7.

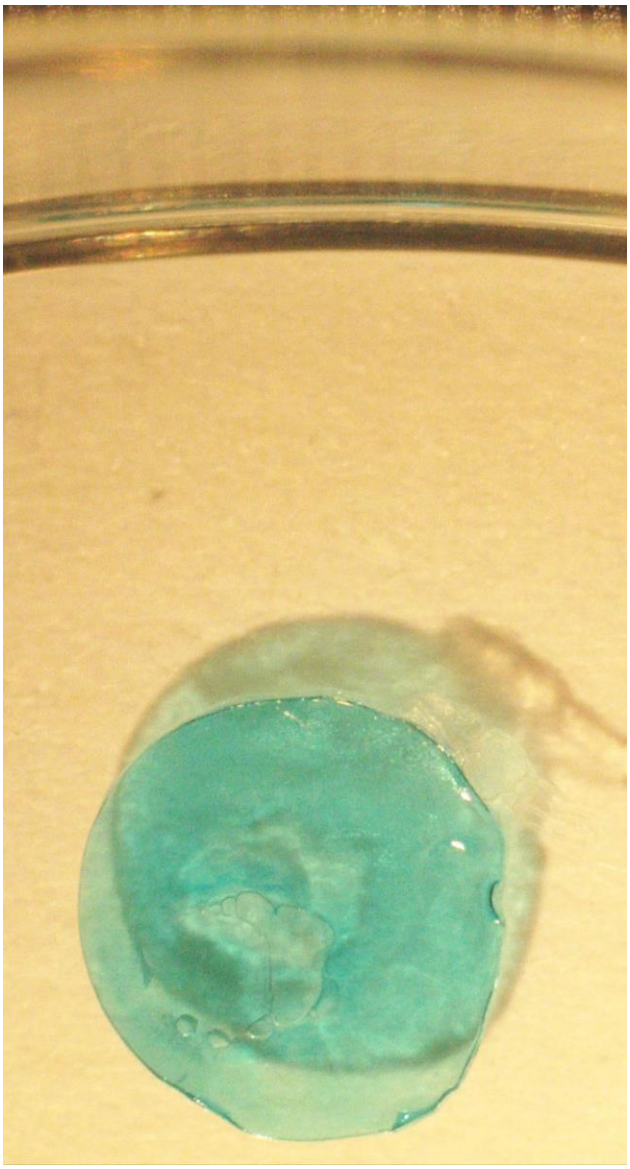

Figure A.8: Lens capsule excision from bovine capsulorhexis Experiments corresponding to Helicotome blade # 8.

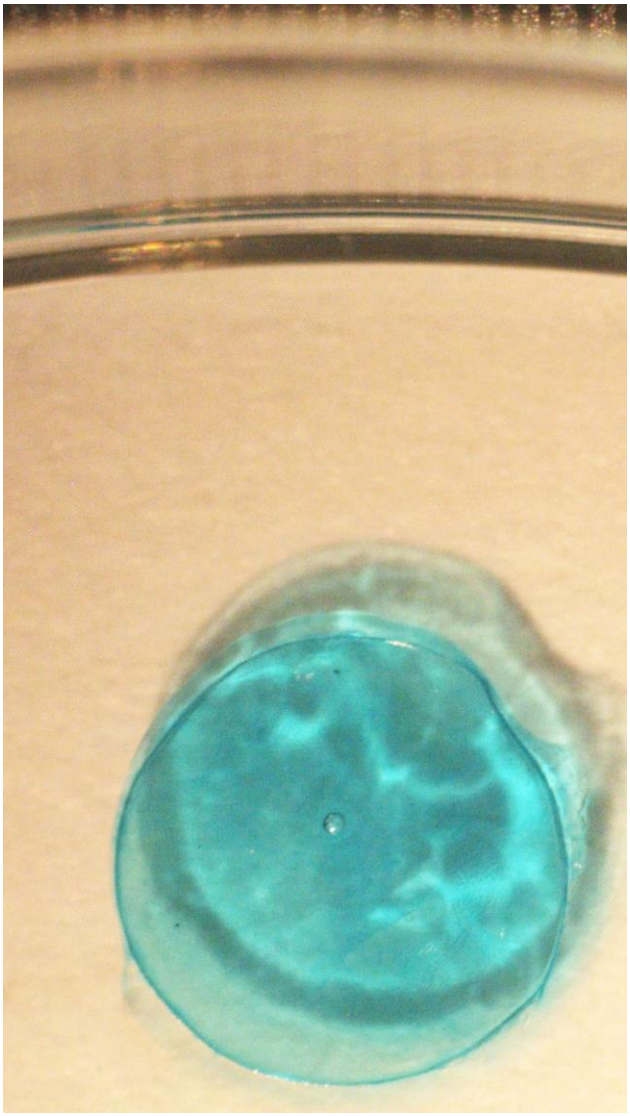

Figure A.9: Lens capsule excision from bovine capsulorhexis experiments corresponding to Helicotome blade # 9.

Figure A.10: Lens capsule excision from bovine capsulorhexis experiments corresponding to Helicotome blade # 10.

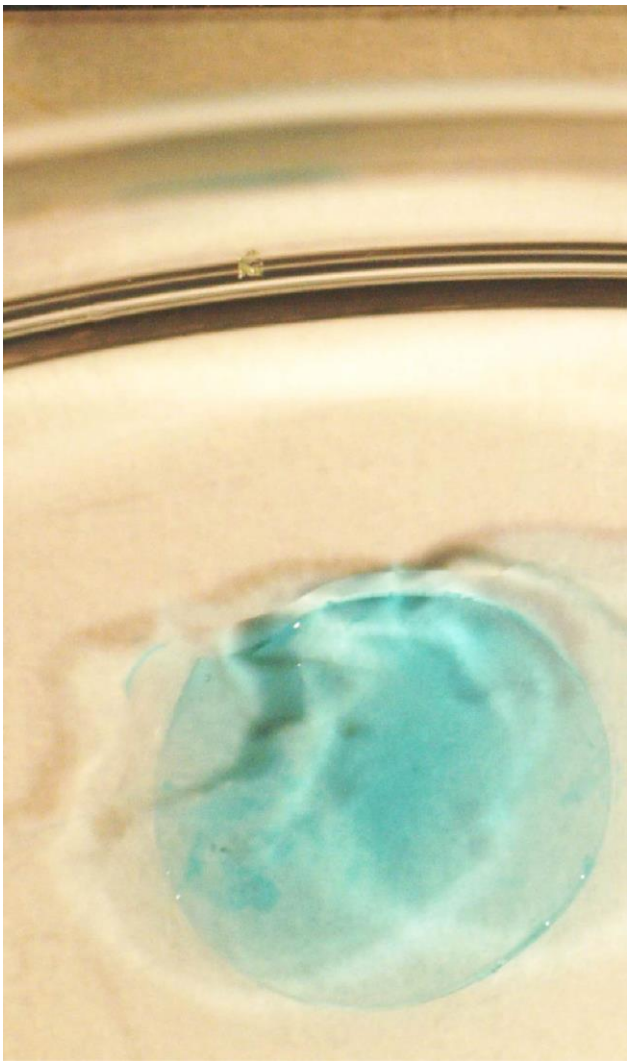

Figure A.11: Lens capsule excision from bovine capsulorhexis experiments corresponding to Helicotome blade # 11.

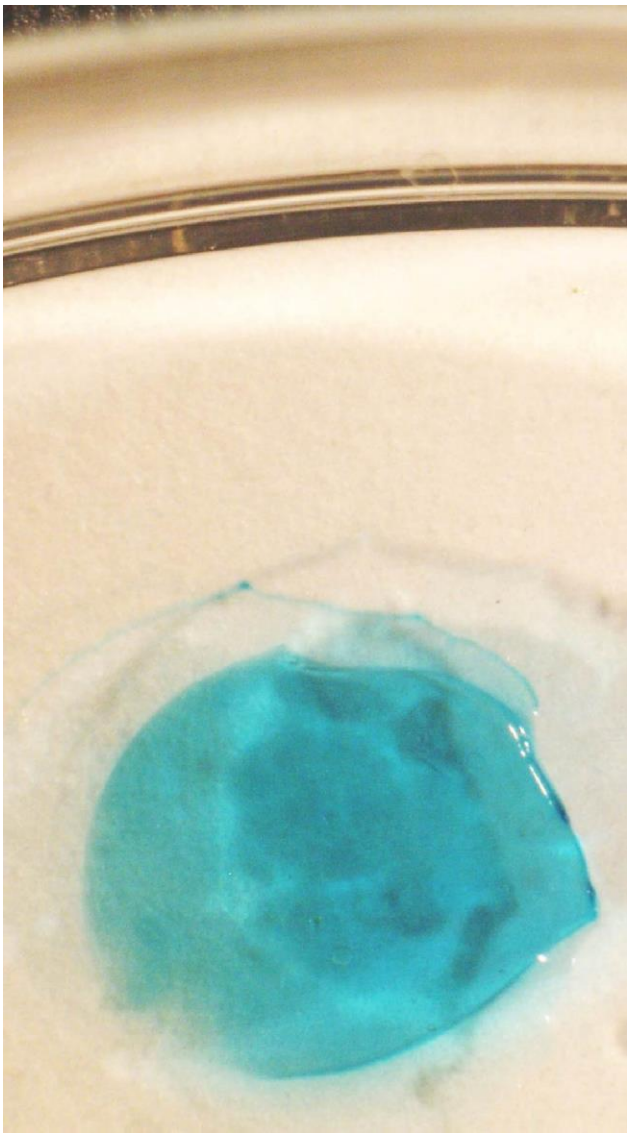

Figure A.12: Lens capsule excision from bovine capsulorhexis experiments corresponding to Helicotome blade # 12.

Figure A.13: Lens capsule excision from bovine capsulorhexis experiments corresponding to Helicotome blade # 13.

Figure A.14: Lens capsule excision from bovine capsulorhexis experiments corresponding to Helicotome blade # 14.

Figure A.15: Lens capsule excision from bovine capsulorhexis experiments corresponding to Helicotome blade # 15.

Figure A.16: Lens capsule excision from bovine capsulorhexis experiments corresponding to Helicotome blade # 16.

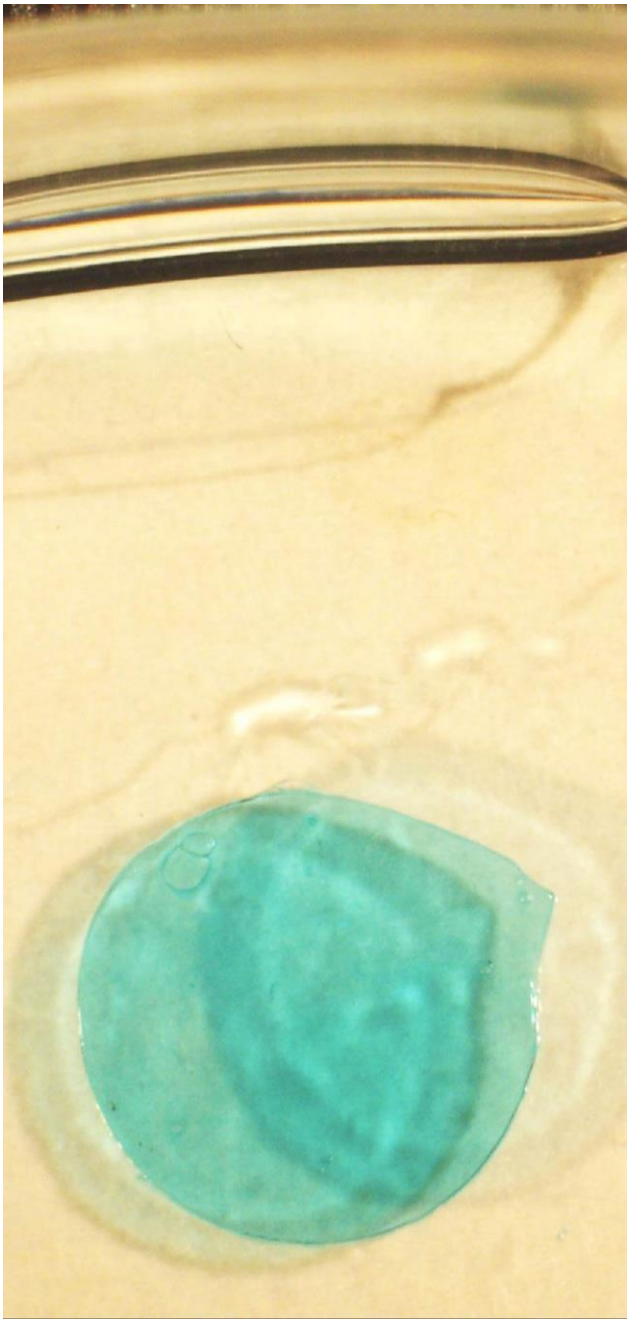

Figure A.17: Lens capsule excision from bovine capsulorhexis experiments corresponding to Helicotome blade # 17.

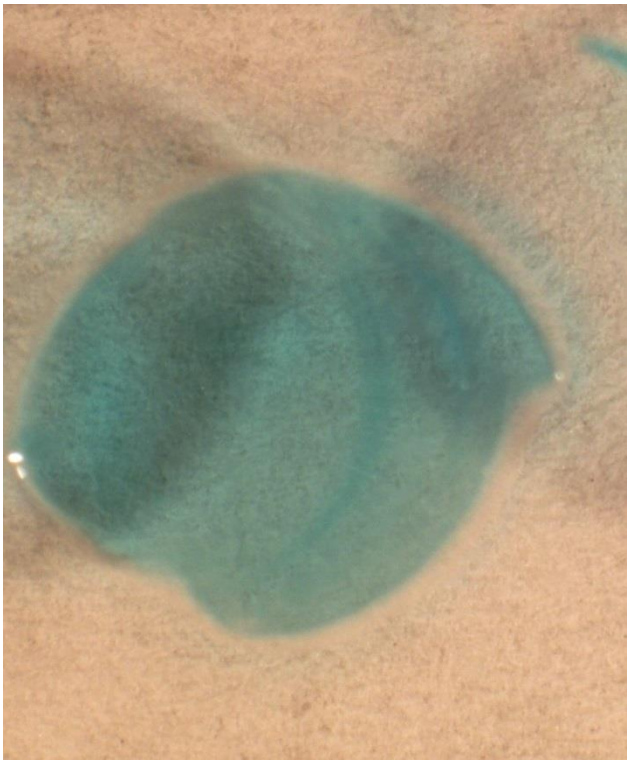

Figure A.18: Lens capsule excision from human capsulorhexis experiments corresponding to Helicotome blade # 1.

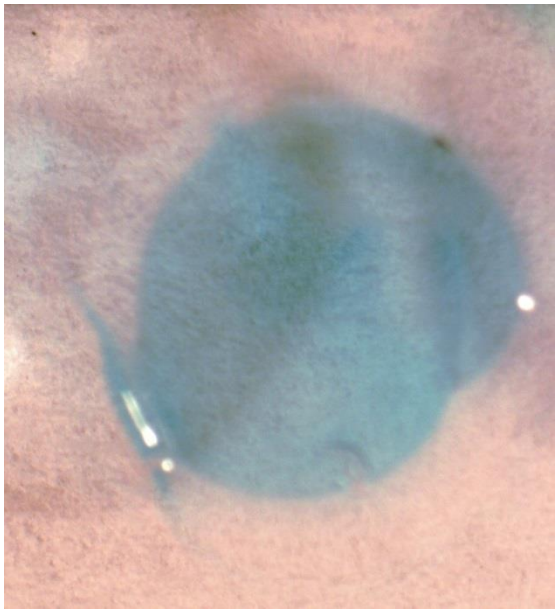

Figure A.19: Lens capsule excision from human capsulorhexis experiments corresponding to Helicotome blade # 2.

APPENDIX B

SHAPE-SET FIXTURES

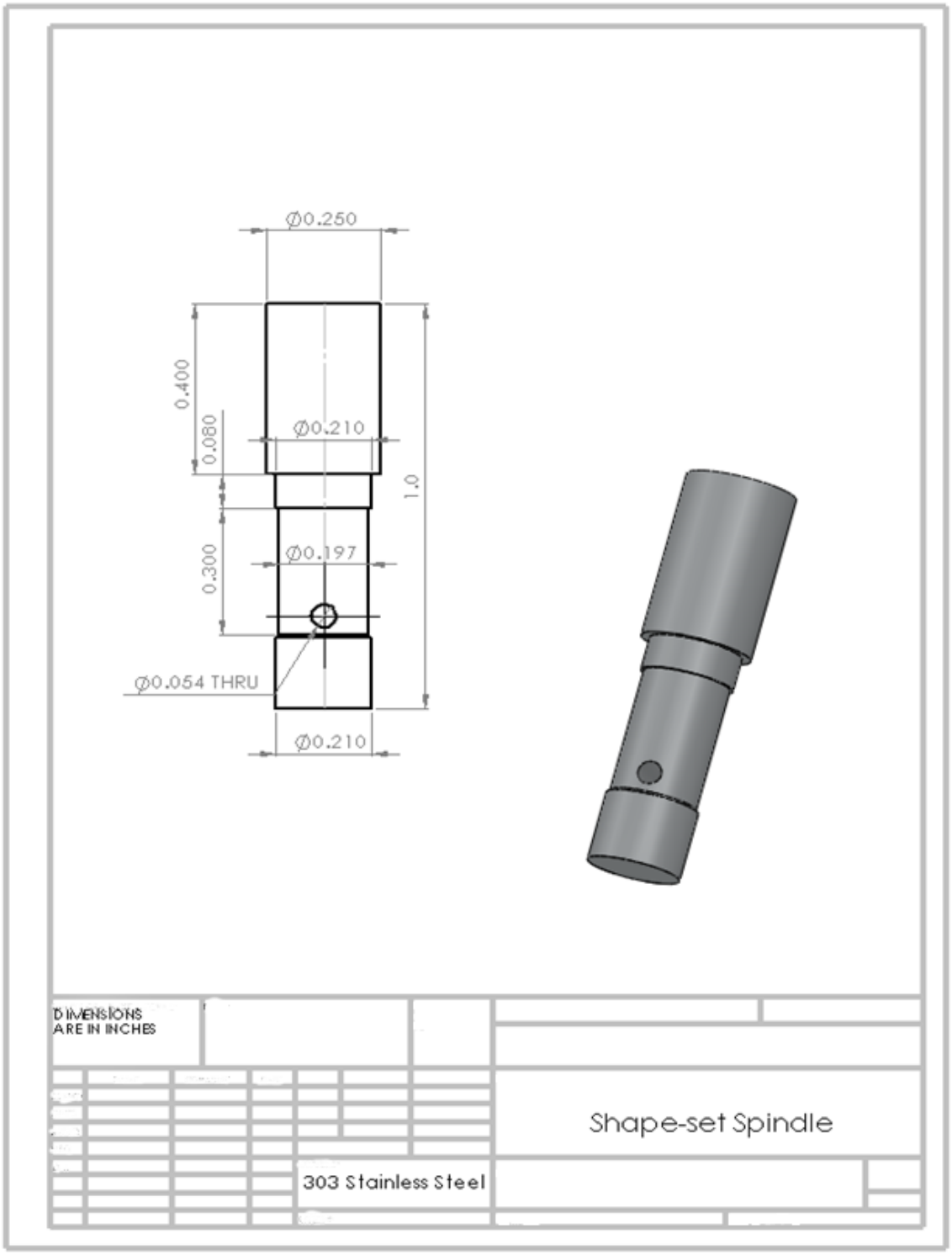

Figure B.1: Shape-set spindle drawing.

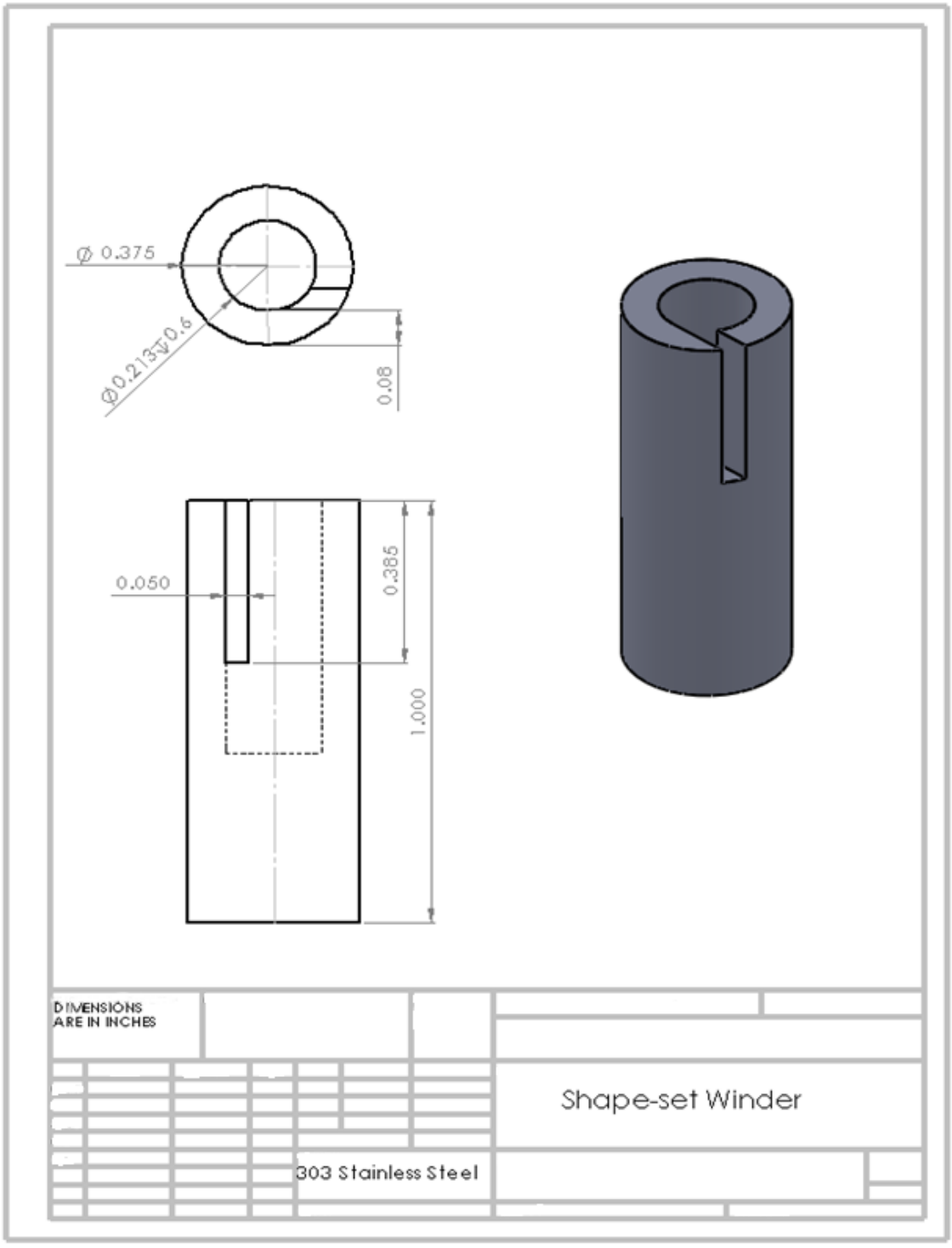

Figure B.2: Shape-set winder drawing.

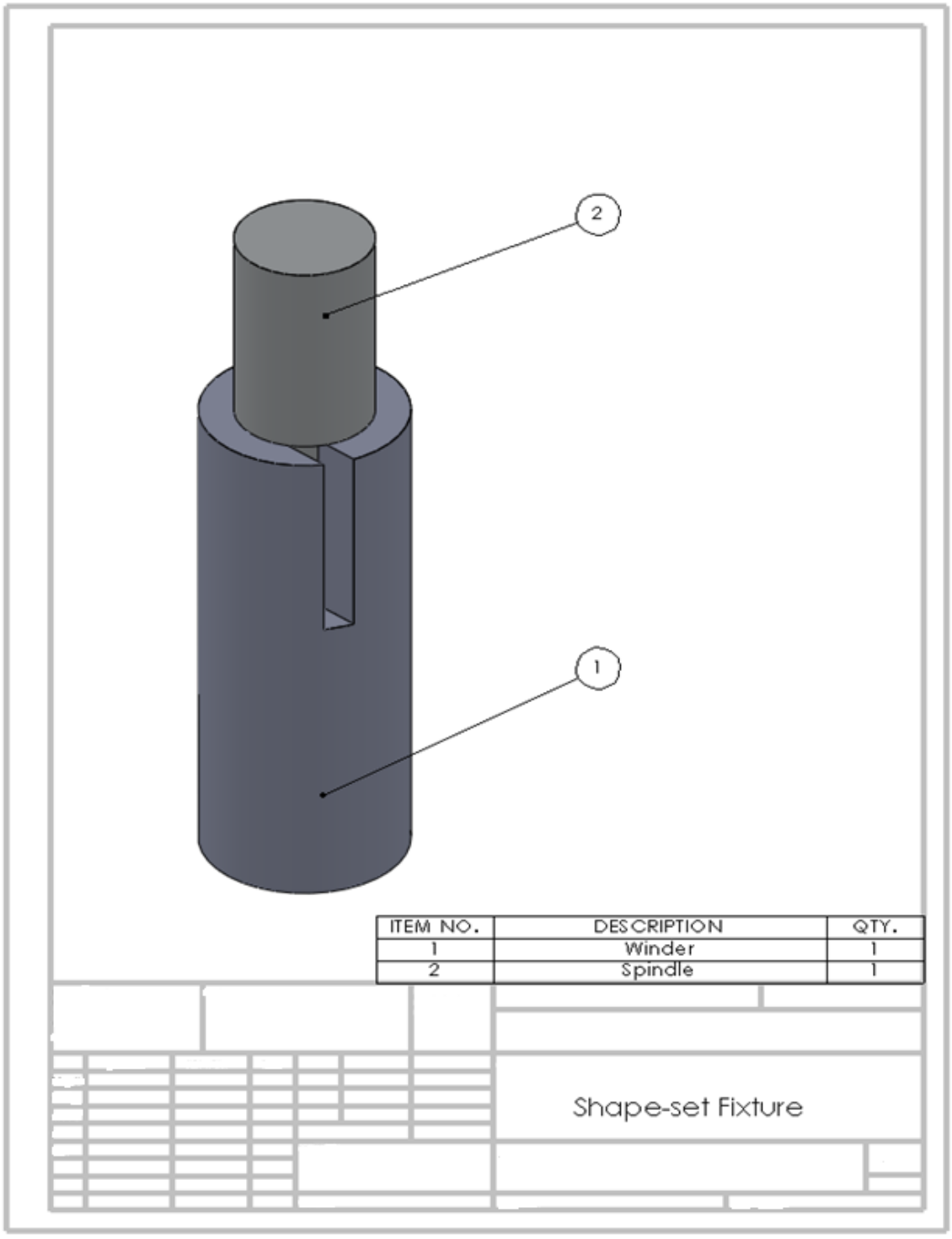

Figure B.3: Shape-set fixture drawing.

APPENDIX C

MATLAB CODE USED FOR IMAGE PROCESSING

```
%%
% This code imports an image of an excised lens capsule, converts it to a
% black and white binary image, and calculates the area of the excision.
% This is used to calculate a "cut diameter" by approximating the excision
% as a circle. Next, it detects the edge of the excision and determines the
% diameter of the minimum bounding circle by calculating the maximum
% distance between all points on the edge. The area of the minimum bounding
% circle is then calculated from this diameter. The circularity of the
% excised lens capsule is calculated by taking the normalized area ratio,
% which is the excision area divided by the minimum bounding circle area.

clear,clc
close all
pic = 16;                                % Variable image number
file = [num2str(pic),'.jpg'];            % Sets the filename based on the image number
I = imread(file);                        % Reads in the file
i(:,:) = I(:,:,1);                       % Takes the first layer of the image
B = im2bw(i);                            % Converts to a binary black and white image
figure(1);imshow(B)                      % Displays the binary image
[x,y] = size(B);
total_area = x*y;
scale = 16/64;                           % Scaled image width [in]
pix = y/scale;                           % New resolution [pixels/in]
excised_area = total_area - bwarea(B);   % Calculate excision area [pixels]
area_in = excised_area/(pix^2);          % Calculate excision area [in^2]
Excision_area = area_in*(25.4^2);        % Calculate excision area [mm^2]
Cut_Diameter = sqrt(4*Excision_area/pi); % Calculate cut diameter [mm]
BW = edge(B, 'sobel');                   % Sobel edge detection
figure(2); imshow(BW)                    % Display edge
hold on
count = 1;
for j = 1:x;                             % Determine position of pixels comprising excision
   for k = 1:y;
     if BW(j,k)
        pos(count,:) = [k,j];
        count = count + 1;
     end
   end
end

for q = 1:length(pos)                    % Calculate distance between all pixels
   for r = 1:length(pos)
      dist(q,r) = sqrt(((pos(q,1)-pos(r,1))^2)+((pos(q,2)-pos(r,2))^2));
   end
end
[Y, I] = max(max(dist));                 % Find pixels farthest apart
[YY, II] = max(dist(I,:));
                                         % Calculate diameter of minimum bounding circle
DIST = sqrt(((pos(I,1)-pos(II,1))^2)+((pos(I,2)-pos(II,2))^2));
Bound_D = DIST/pix*25.4;                 % Convert diameter to mm
Disk_area = pi/4*(Bound_D^2);            % Calculate area of minimum bounding circle
Circularity = Excision_area/Disk_area;   % Calculate circularity
                                         % Display edge with minimum bounding circle diameter.
figure(2); line([pos(I,1) pos(II,1)],[pos(I,2) pos(II,2)])

% End of program
```